

Electronic Thesis and Dissertation Repository

8-3-2022 1:30 PM

Soil Amplification and Peak Frequencies from Thousands of Passive Seismic Measurements Across Metro Vancouver, British Columbia, Canada

Aamna A. Sirohey, *The University of Western Ontario*

Supervisor: Molnar, Sheri E, *The University of Western Ontario*

A thesis submitted in partial fulfillment of the requirements for the Master of Science degree in Geophysics

© Aamna A. Sirohey 2022

Follow this and additional works at: <https://ir.lib.uwo.ca/etd>

Recommended Citation

Sirohey, Aamna A., "Soil Amplification and Peak Frequencies from Thousands of Passive Seismic Measurements Across Metro Vancouver, British Columbia, Canada" (2022). *Electronic Thesis and Dissertation Repository*. 8810.

<https://ir.lib.uwo.ca/etd/8810>

This Dissertation/Thesis is brought to you for free and open access by Scholarship@Western. It has been accepted for inclusion in Electronic Thesis and Dissertation Repository by an authorized administrator of Scholarship@Western. For more information, please contact wlsadmin@uwo.ca.

Abstract

Seismic site effects arise from local geologic and topographic conditions, and modify incident earthquake ground motions at a site. Understanding variability in seismic site conditions is necessary for accurate assessment of seismic hazard. The microtremor horizontal to vertical spectral ratio (mHVSR) method is a cost-effective and non-invasive method to measure the site's filtering effect in terms of an amplification frequency spectrum. Using a large, compiled database of mHVSR measurements from the Metropolitan Vancouver area, the impact of acquisition and processing parameter choices on the computed mHVSR is investigated. A robust processing algorithm is developed to batch process high-quantity mHVSR datasets. Products related to seismic microzonation hazard mapping, such as a regional map of the site fundamental frequency and the suite of unique mHVSR amplification spectra in the region are provided. This thesis exemplifies the practicality of using the mHVSR method for seismic site characterization.

Keywords

mHVSR, site effects, site amplification, site characterization, site period, microzonation, big data, Vs30, earthquake site response

Summary for Lay Audience

The ground shaking resulting from an earthquake can vary significantly between two proximal sites for the same earthquake. This variability is a result of variations in the local geologic and topographic conditions at a site, which act as a filter for the input ground motion and can modify characteristics of the incident motion such as amplitude, frequency, and duration. It is important to develop an understanding of how these site conditions vary throughout a region, and how incident earthquake motions are affected by these variable conditions so that the distribution of seismic hazard in an area can be accurately assessed. The microtremor horizontal to vertical spectral ratio (mHVSR) method has applications in providing estimates of parameters that are related to the ground motion modification experienced at a site. The method involves recording omnipresent microtremors using a three-component seismometer. Using a large database of single station microtremor measurements from the Metropolitan (Metro) Vancouver area, experimental setup and data processing decisions were studied to investigate their impact on the processed mHVSR result. A framework of suggestions is presented to aid future practitioners in carrying out effective surveys, as well as a novel processing algorithm, particularly well-suited for processing large datasets. The mHVSR database from Metro Vancouver was processed using this novel algorithm, and the processed results were used to extract parameters and create maps and other tools to aid in understanding the variability of site response in the region.

Co-Authorship Statement

This thesis contains only the original research contributions conducted by the author under supervision of Dr. Sheri Molnar with supervisory committee support by Dr. Hadi Ghofrani and informative discussions with Jamal Assaf (PhD Candidate). Original contributions include compilation of an mHVSR database of over 2,000 locations for Metro Vancouver, algorithms developed to achieve systematic mHVSR computation, and mapped products for application in seismic site characterization/hazard mapping. The written literature review and background information of the mHVSR method in section 2.3 is published within:

Molnar, S., Sirohey, A., Assaf, J., Bard, P. Y., Castellaro, S., Cornou, C., ... & Yong, A. (2022). A review of the microtremor horizontal-to-vertical spectral ratio (MHVSR) method. *Journal of Seismology*, 1-33.

Chapter 3 is drafted for publication in *Geophysical Journal International*. Chapter 4 is drafted for publication in *Geophysical Research Letters*. Chapter 5 is drafted for publication in *Nature Geoscience*.

Acknowledgments

Before anyone else, I thank you, God.

Throughout the completion of this work my father and mother have provided support and tough love as required. My siblings have provided me with laughter and distraction. To all of them, I am grateful.

Without Dr. Sheri Molnar's unwavering confidence in me, and her insistence that I be able to complete this work, even in the face of many obstacles, it would not have been possible. Thank you, Sheri.

Table of Contents

Abstract.....	ii
Summary for Lay Audience.....	iii
Co-Authorship Statement.....	iv
Acknowledgments	v
Table of Contents	vi
List of Tables.....	ix
Chapter 1	1
1 Introduction	1
1.1 Site Response Indicator Variables	5
1.2 Seismic Microzonation.....	11
1.3 Thesis Motivation	13
1.4 Organization of Work	14
1.5 References	14
Chapter 2.....	20
2 Geology and Previous Site Effects Studies of Metro Vancouver.....	20
2.1 Geology of Metro Vancouver.....	20
2.1.1 Physiographic Regions	21
2.1.2 Regional Geology and Tectonic Setting.....	21
2.1.3 Glaciations	22
2.1.4 Stratigraphy.....	23
2.2 Microtremor Horizontal to Vertical Spectral Ratio	24
2.3 Previous Site Effects Studies.....	27
2.4 References	33
Chapter 3.....	43

3	Impact of Experimental and Processing Choices on mHVSR Results	43
3.1	Introduction	43
3.2	mHVSR Database	47
3.3	Impact of Experimental Factors on mHVSR.....	51
3.3.1	Instrument Type	51
3.3.2	Sensor-Ground Coupling and Measurement Surface	58
3.4	Impact of mHVSR Processing Parameters.....	60
3.4.1	Existing mHVSR Processing Software	64
3.4.2	Field Data Acquisition and Preliminary Data QC.....	67
3.4.3	Processing Parameter Sensitivity Analysis.....	70
3.4.4	Optimal Time Window Selection.....	71
3.4.5	Proposed mHVSR Batch Processing Methodology	76
3.5	Discussions	77
3.6	References	81
	Chapter 4.....	91
4	Preliminary Interpretation and Development of mHVSR Database.....	91
4.1	Picking Peaks in mHVSR Measurements	94
4.1.1	Peak Picking and Ranking Algorithm	99
4.1.2	Development of f_{OHV} Map	106
4.1.3	Interpretation of mHVSR Peaks.....	111
4.2	Proposed mHVSR Database Structure.....	115
4.3	Discussions	118
4.4	References	120
	Chapter 5.....	128
5	Representative mHVSR Curves for Metro Vancouver Region.....	128
5.1	Metro Vancouver Geology	130

5.2	Theoretical Basis of mHVSF	133
5.2.1	Short investigation into Theoretical Site Response in the Fraser River Delta.....	134
5.3	Clustering mHVSF Curves	138
5.4	Discussion.....	144
5.5	References	146
6	Conclusions	151
7	Curriculum Vitae	155

List of Tables

Table 1-1. Seismic site classification of the NBCC (2005, 2010, 2015) and CHBDC (2015). 6	6
Table 1-2. Summary of slope ranges for subdivided site classes based on V_{S30} ranges. Adapted from Wald and Allen (2007).	6
Table 1-3. Detailed site classification scheme based on T_0 (from Pitilakis <i>et al.</i> , 2018).	9
Table 2-1. Summary of earthquake events recorded in Metro Vancouver region.	31
Table 3-1. Summary of mHVSr field campaigns occurring between 2002 and 2021.	49
Table 3-2. Input parameters for HVSRPy.....	77
Table 4-1. Comparison of original SESAME criteria (Bard <i>et al.</i> , 2008) vs. modified criteria proposed by Wang (2020).....	95
Table 4-2. Parameters used as input to peak picking algorithm.....	100
Table 4-3. Model coefficients a and b of f_{0HV} -depth relationships for various sedimentary basins across the world. Adapted from Rugar & Gosar (2020).	114
Table 5-1. Model parameter ranges for rock types in Fraser River delta. Adapted from Assaf <i>et al.</i> (2022).	134
Table 5-2. Parameters used as input to forward model SH-transfer function of two-layer model overlying half-space through rattle.m.	137

List of Figures

Figure 1-1. Amplification phenomena (Hunter and Crow, 2015).....	2
Figure 1-2. Site amplification plot from the Earthquakes Canada website (https://earthquakescanada.nrcan.gc.ca/hazard-alea/interpolat/nbc2020-cnb2020-en.php). Amplification is different for 0.2 sec and 2.0 sec period (shown). Dashed lines show 2015 NBCC site class-based method, and solid lines show 2020 NBCC direct V_{S30} method.	7
Figure 2-1. (a) Simplified geology map of Metro Vancouver based on age of sediments. (b) Geologic cross-section along line A-A' (modified from Rogers <i>et al.</i> , 1998). Figure modified from Molnar <i>et al.</i> (2020).....	20
Figure 2-2. Six generic V_s profiles developed by Kim (2019) for the Fraser River Delta. Adapted from Kim (2019).	30
Figure 3-1. Locations of mHVSr measurements (black circles) acquired throughout the Metro Vancouver region. Background GSC surficial geology mapping (Armstrong 1979, 1980) is shown coloured according to geologic unit listed in the Legend.	50
Figure 3-2. Response to velocity for inertial sensors. Adapted from Ackerly <i>et al.</i> (2014)...	52
Figure 3-3. Comparison of mHVSr at six Metro Vancouver sites from co-located microtremor recordings using a broadband seismometer and older (TEP generation) and newer (TE3) generation short period seismometers. The middle panel of the bottom row has the results from two different broadband seismometers displayed.	54
Figure 3-4. Comparison of co-located measurements obtained using both the newer and older generation short-period Tromino® seismometer.	56
Figure 3-5. Comparison of mHVSr computed using co-located, contemporaneous measurements with different gain settings using the newer generation Tromino® seismometer.....	57
Figure 3-6. Comparison of mHVSr calculated from single-station microtremor measurements using a Tromino® short-period seismometer (RMD16) and a Pinnocchio	

velocity transducer (RI54). Measurements were obtained in the Fraser River delta. Dashed lines show upper and lower bound.	58
Figure 3-7. Comparison of co-located measurements made on both natural (i.e., soil/dirt and man-made (artificial) surfaces).....	60
Figure 3-8. Example of mHVSr calculated from all time windows, time windows identified as having low level signal and time windows identified as having high level signal. Adapted from Mihaylov <i>et al.</i> (2016).....	62
Figure 3-9. Comparison of mHVSr calculating using three different software, same parameters and same measurement.	67
Figure 3-10. Four examples of the Fourier amplitude data for each component of recorded ground motion. Top left: example of good quality data with a geologic peak at ~1-2 Hz evident due to the ‘eye-shape’, top right: example where data is noisy on all three components, bottom right: example where data for two components, h2 and v, are good quality, and one component is not functioning properly, bottom right: example where data at low frequencies (<1Hz) is corrupted by noise.	69
Figure 3-11. Coefficient of Variation (COV) computed on a point-by-point basis for each site (gray line) included in the analysis.....	71
Figure 3-12. Results from HVSRPy in which frequency domain window rejection algorithm is successful in removing time windows which produce anomalous results in the frequency domain.	73
Figure 3-13. Results from HVSRPy for which frequency domain window rejection algorithm is not successful in terms of removing time windows that produce anomalous frequency response.....	74
Figure 3-14. Results from proposed clustering-based window selection algorithm for 16 sites. Green windows are from the user-selected most self-consistent cluster, red traces are from other clusters identified.....	76
Figure 4-1. Example output of IRIS HVSR toolbox. Adapted from Bahavar <i>et al.</i> (2020)..	97

Figure 4-2. Examples of proposed peak picking algorithm applied to mHVSR curves at 12 sites. Only the mHVSR curves for the user-selected optimal cluster are considered. Blue crosses are peaks determined from the 90% and 10% quartile curves, green crosses are peaks determined from the average curve. Shaded blue region shows standard deviation of $f_{\#HV}$, and horizontal lines denote peak broadness measures (half- and quarter-width). The optimal Gaussian curve fit to the average mHVSR is also displayed.103

Figure 4-3. Fourier spectra shown for the same 12 sites in Figure 4-2 are shown with the location of $f_{\#HV}$ (vertical dashed line) and its shaded standard deviation. Fourier spectra for each component are shown and for all time windows; not only windows included in the user-defined optimal cluster.105

Figure 4-4. Map of sites for which an estimate of f_{0HV} was obtained from the mHVSR, symbology based on value of f_{0HV}109

Figure 4-5. Interpolated f_{0HV} map, estimated from f_{0HV} values extracted from mHVSR measurements.110

Figure 4-6. f_{0HV} values for different classes of surficial geology.111

Figure 4-7. Examples of depth vs f_{0HV} relationships developed for seven regions. Adapted from Assaf *et al.* (2022), the two relations specific to the Fraser River delta using mHVSR data of this study are referred to as “This study” in the legend.115

Figure 5-1. Contours of interpreted depth to Tertiary sedimentary bedrock in the Fraser River Delta. Contours from Britton *et al.* (1995).132

Figure 5-2. Results of forward modelling the 1-D SH transfer function for different thicknesses of post-glacial sediments considering material properties of the sediments in the FR delta.135

Figure 5-3. Amplification spectrum of empirical mHVSR response (green line) compared to the theoretical SH wave transfer function (blue line) predicted from the 1-D model (soil column and V_s depth profile are shown) for the six sites in the FR delta.138

Figure 5-4. Groups of valid clusters identified from K-means clustering of more than 2000 mHVSR curves. Colored according to which representative curve they were assigned to in Figure 5-5.....141

Figure 5-5. Three standard mHVSR response types defined for the Metro Vancouver region through cluster analysis. Solid line is the mean and grey dashed lines are 10th and 90th percentile.....142

Figure 5-6. Map demonstrating spatial distribution of measurements included in each cluster. Background map is of simplified surficial geology, same as Figure 5-1.143

Figure 5-7. Surficial geologic conditions of ~2000 mHVSRs categorized by clustered mHVSR response type.....144

Preface

“It doesn’t matter how beautiful your theory is, it doesn’t matter how smart you are. If it doesn't agree with experiment, it’s wrong.”

-Richard Feynman

Chapter 1

1 Introduction

The ground shaking resulting from an earthquake can be strongly influenced by local geologic and topographic conditions (Wood 1908, Baratta 1910). The seismic motions experienced at the surface can be amplified or deamplified depending on the site of interest's surface and subsurface topography, soil strata (elastic material properties or moduli, thickness), dynamic nonlinear behaviour of the soil strata, as well as the frequency content and duration of the incident motions. Therefore, when predicting the regional variation of earthquake ground shaking for seismic (micro)zonation hazard mapping, it is necessary to consider seismic properties of the local site conditions. Defining zones that are likely to experience similar levels of ground motion is challenging due to the variability of geologic materials within a region or urban area, as well as earth structures that result from weathering, erosion, deposition, and other near-surface geologic phenomena.

Seismic site effects arise from the local geologic and topographic conditions at a site, and modify the amplitude, duration, and frequency content of incident ground motions. (Figure 1-1). These physical phenomena occur due to mechanical properties of the soil column, the presence of heterogeneities and discontinuities, as well as the geometry of shallower layers and the existence of topographic irregularities both in the basement rock and at the ground surface (Panzeria *et al.*, 2013). Stratigraphic soil column effects (A and B in Figure 1-1) are understood as the modifications affecting a seismic motion that propagates (near-surface) vertically inside a deposit having a flat free surface, horizontal layers, and negligible lateral heterogeneities; known as one-dimensional (1D) site effects (Panzeria *et al.*, 2013). Kramer (1996) provided an analysis of wave propagation in which he considered a sediment deposit overlying bedrock and demonstrated that the amount of reflected energy in the deposit increases with the seismic impedance (product of velocity and mass density) contrast between the sediments and bedrock, this is referred to as impedance-based amplification and is quantified according to,

$$A_{imp} = \sqrt{\frac{\rho_2 V s_2}{\rho_1 V s_1}} \quad \text{equation 1-1}$$

where ρ_1 is the density of the sediments, ρ_2 is the density of the bedrock, V_{s1} is the shear-wave velocity of the sediments, and V_{s2} is the shear-wave velocity of the rock. Resonance-based amplification, illustrated in Figure 1-1- A, occurs at specific frequencies (f_n), related to the stiffness and thickness of sedimentary layers,

$$f_n = \frac{V_{s_{ave}}}{4h} (2n + 1), n = 0,1,2,3 \dots \quad \text{equation 1-2}$$

where $V_{s_{ave}}$ is the average shear-wave velocity of the sedimentary layer, and h is the thickness of the sedimentary layer. In addition, 2D and 3D earthquake site effects manifest due to lateral geologic variability (C and D in Figure 1-1).

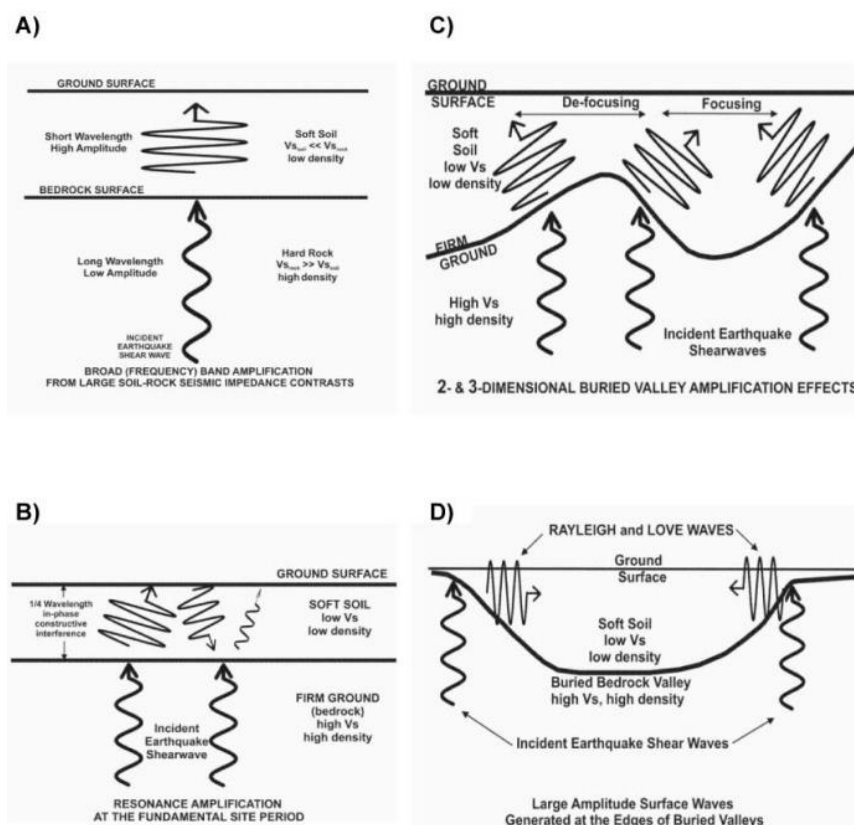


Figure 1-1. Amplification phenomena (Hunter and Crow, 2015)

There are several methodologies used to assess the local seismic site response. Generally, this assessment is in the form of an amplification spectrum which can be used to quantify

the amplification of seismic motion expected at each frequency due to the local conditions at a site. The methods can broadly be grouped into numerical or theoretical, and empirical techniques. Numerical 1D site response methods use computer codes that simulate wave propagation vertically upward through a soil column, from bedrock (input ground motion) to the free surface (Panzera *et al.*, 2013). Such codes involve modelling of the dynamic behaviour of soils by adopting linear, equivalent-linear or non-linear models (e.g., SHAKE, Schnabel *et al.*, 1972, DESDRA, Lee & Finn, 1978, EERA, Bardet *et al.*, 2000). Numerical 2D and 3D wave propagation codes also exist (e.g., FLAC2D, Itasca, 2013). Empirical methods allow evaluation of seismic site response using recordings (time series) of seismic signals generated by earthquakes, artificial seismic sources, or microtremors (ambient vibrations, seismic noise). They implicitly consider all site effects.

The surface ground motion at a site can be thought of as the convolution of earthquake source, path, and site effects. Empirical site response methods attempt to deconvolve the site effects observed at a site from the source and path effects. The surface to bedrock (soil base) spectral ratio method involves measuring incident seismic ground motions at the interface between the sediment overburden and engineering bedrock, as well as at the surface, and computing the ratio between the spectra of horizontal ground motions at each of these locations. The ground motions at the soil base are removed from the surface recording and thereby only shaking differences between soil base and surface remain, i.e., the 1D site amplification or soil filter (transfer function). This method is limited in applicability due to cost of an instrumented borehole array with two three-component geophones at a minimum.

Borcherdt (1970) proposed the Standard Spectral Ratio (SSR) technique which involves calculating the spectral ratio between simultaneously recorded horizontal ground motions at a soil site, and a nearby reference rock site. The reference site is assumed to be free from site effects (hence the choice of bedrock) and affected by the same source and path effects (hence “nearby”). A general rule of thumb to ascertain the appropriateness of a reference site is that the distance between sensors should be significantly less than epicentral distance. The challenge with implementing this method lies in proper choice of the reference site; outcropping rock is most convenient for seismometer installation although

not guaranteed to be free of site effects (e.g., Steidl *et al.* 1996) since outcropping rock tends to be of higher elevation (topographic effects) and weathered, jointed or fractured (impedance effects). Strong-motion instruments that had a set trigger threshold also presented another challenge of this technique since earthquake shaking at the reference rock site may not be sufficient to trigger the instrument and provide the reference recording. This challenge is waning as technology has advanced and become less costly, e.g., continuous and digital network monitoring. The lowest frequency peak of the SSR amplification spectrum is as a measure of f_0 as expressed in equation 1-2

The earthquake horizontal to vertical spectral ratio (eHVSR) removes the requirement for a reference site (Lermo and Chavez-Garcia 1993). It assumes that the vertical component of motion is not affected by the local geological conditions (does not contain shear motions), which in practice does not always hold true (Panzera *et al.*, 2013), i.e. can contain radial shear and Rayleigh wave motion (Lermo and Chavez-Garcia 1993, Theodulidis *et al.* 1996, Raptakis *et al.* 1998, Parolai *et al.* 2000, Bonilla *et al.* 2002). The fundamental peak frequency from the eHVSR (f_{0HV}) has been shown to be consistent with earthquake SSRs (f_0) but is less reliable for estimating the site amplification (surface-to-soil-base or soil-to-rock) (e.g., Lermo & Chavez-Garcia, 1993, Field & Jacob, 1995, Lachet *et al.* 1996, Theodulidis *et al.*, 1996, Bonilla *et al.*, 1997, Riepl *et al.*, 1998).

The microtremor horizontal to vertical spectral ratio (mHVSR) technique, popularized by Nakamura (1989), uses microtremor (passive seismic, seismic noise, ambient vibrations) as the signal instead of earthquake motions. Traditionally, the term microtremor was restricted to higher frequency (> 1 Hz) background seismic noise generated by more local human-generated sources (e.g., traffic, construction, daily activities) and the term microseisms was restricted to lower frequency (< 1 Hz) seismic noise generated by natural activities (e.g., ocean waves, wind). The term microtremor is used here as a general term for all frequencies of background seismic noise. The mHVSR method was first applied within Canada in 2003 at strong motion stations in Victoria, British Columbia to compare with eHVSR and SSRs of the 2001 **M** 6.8 Nisqually earthquake (Molnar and Cassidy 2006). The mHVSR method involves use of a single three-component seismometer to record ambient vibrations at a site for ~15-60 minutes (on average). The time series data is

then treated, converted to the frequency domain, and the ratio between the merged horizontal components and vertical component provide the site mHVSr amplification function, from which $f_{\#HV}$ may be extracted. Although a complete understanding of the physics of the microtremor wavefield is still lacking, the method has been shown to consistently provide reliable estimates of f_{0HV} consistent with the fundamental peak frequency from eHVSrs and SSRs (e.g., Lermo & Chavez-Garcia, 1994, Bard, 1999), despite large variations in the mHVSr amplification due to temporal variance in the microtremor signal amplitude combined with user-defined choices of instrumentation, sensor coupling, etc. (described in more detail in Chapter 3; e.g., Cara *et al.*, 2003).

1.1 Site Response Indicator Variables

In early GMMs earthquake recording sites were binned or sorted into simple site condition categories as either rock or soil (e.g., Si & Midorikawa, 1999), before being explicitly characterized according to a piecewise six category site classification scheme (Atkinson and Boore 2003), until being used a continuous site term proxy (e.g., Boore *et al.*, 2008). The six category site classification scheme, proposed by NEHRP and adopted by the NBCC in 2005, is provided in Table 1-1. Borchardt (1994) proposed use of an in situ and quantitative measure of seismic site conditions: the time-averaged (harmonic mean) Vs of the upper 30 meters, V_{S30} . V_{S30} has become the standard site term used in development of GMMs. It has been demonstrated that V_{S30} is a useful parameter to predict local impedance-based site amplification, especially when it is accurately measured (Borchardt 1994, Castellaro *et al.* 2008, Chiou *et al.* 2008, Gallipoli *et al.* 2009, Lee and Trifunac 2010, Derras *et al.* 2016). Direct measurement of in situ V_{S30} is expensive, and as such, Wald & Allen (2007) and Allen & Wald (2009) proposed to use topographic slope from digital elevation models derived from remote sensing to give a first order estimation of site classes based on V_{S30} (Table 1-2). Because ground motion amplification is dependent on the frequency of motion on soft soil, the amplification factor associated with a given V_{S30} derived site class, or a particular value of V_{S30} is frequency dependent (example provided in Figure 1-2).

Table 1-1. Seismic site classification of the NBCC (2005, 2010, 2015) and CHBDC (2015).

Site Class	Soil Profile Name	Average properties in Top 30 m		
		Shear wave velocity V_s (m/s)	Standard Penetration Resistance, N_{60}	Soil Undrained Shear Strength, s_u kPa
A	Hard rock	$V_s > 1500$	Not applicable	
B	Rock	$760 < V_s \leq 1500$	Not applicable	
C	Very dense soil and soft rock	$360 < V_s \leq 760$	$N_{60} > 50$	$s_u > 100$
D	Stiff soil	$180 < V_s \leq 760$	$15 \leq N_{60} \leq 50$	$50 < s_u \leq 100$
E	Soft soil	$V_s \leq 180$	$N_{60} < 15$	$s_u < 50$
E	Soft soil	Any profile with more than 3 m of soil with the following characteristics: <ul style="list-style-type: none"> • Plastic index $PI > 20$ • Moisture content $w \geq 40\%$ • Undrained shear strength, $s_u < 25$ kPa 		
F	Other	Site specific evaluation required		

Table 1-2. Summary of slope ranges for subdivided site classes based on V_{s30} ranges. Adapted from Wald and Allen (2007).

Class	V_{s30} range (m/s)	Slope range (m/m) – (active tectonic)	Slope range (m/m) – (stable continent)
E	<180	<1.0E-4	<2.0E-5
D	180-240	1.0E-4 – 2.2E-3	2.0E-5 – 2.0E-3
	240-300	2.2E-3 – 6.3E-3	2.0E-3 – 4.0E-3
	300-360	6.3E-3 – 0.018	4.0E-3 – 7.2E-3
C	360-490	0.018 – 0.050	7.2E-3 – 0.013
	490-620	0.050 – 0.10	0.013 – 0.018
	620-760	0.10 – 0.138	0.018 – 0.025
B	>760	>0.138	>0.025

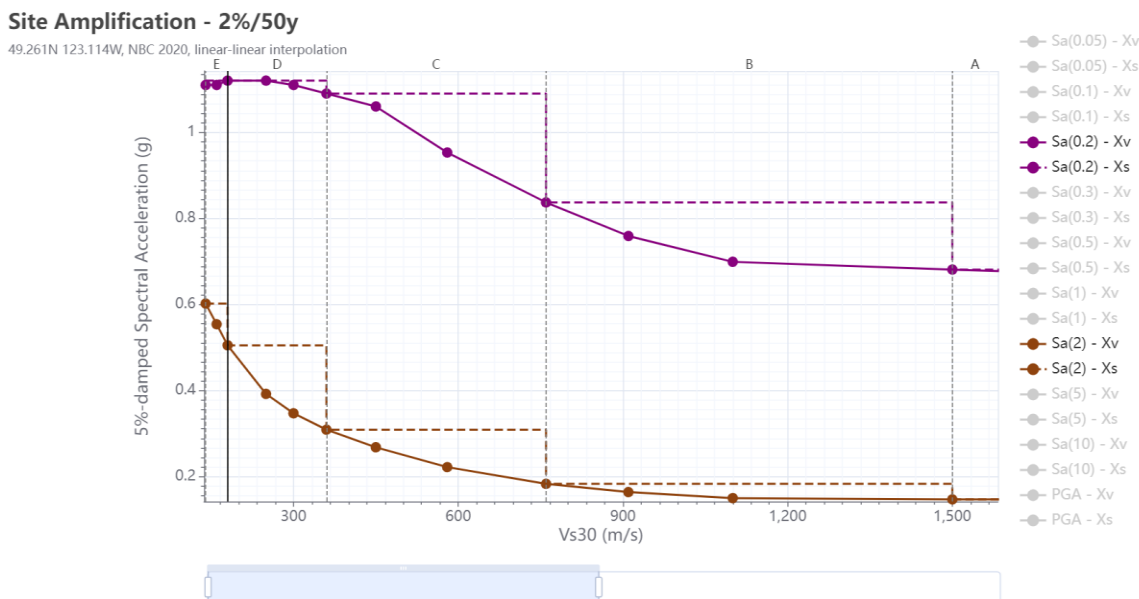


Figure 1-2. Site amplification plot from the Earthquakes Canada website (<https://earthquakescanada.nrcan.gc.ca/hazard-alea/interpolat/nbc2020-cnbc2020-en.php>). Amplification is different for 0.2 sec and 2.0 sec period (shown). Dashed lines show 2015 NBCC site class-based method, and solid lines show 2020 NBCC direct V_{S30} method.

There are two ways in which V_{S30} is commonly used to predict seismic design ground motions in the NBCC. The first involves using it as the V_{S30} value to assign site class and then amplification (foundation) factors are used to adjust the site class C reference uniform hazard spectrum (UHS) to derive the site-specific UHS (e.g., dashed lines in Figure 1-2). This method was used in the 2005, 2010 and 2015 NBCC. The second method explicitly utilizes the V_{S30} value within the GMM, either in the mathematical expression (e.g., solid lines in Figure 1-2), or through utilization of look-up tables that provide the ground-motion estimate for different periods of motion, for different seismic events at varying epicentral distances. This method is permitted in the 2020 NBCC if in situ V_{S30} is known/obtained.

Although V_{S30} is commonly used as the site term variable in GMMs, and is quite effective in certain geologic conditions, in many glaciated regions, it is common to have a unit of soil sediment underlain by a much stiffer bedrock leading to sharp impedance contrasts (Hashash *et al.* 2019). Resonance-based amplification is important or can be the controlling

amplification at f_0 and higher-order modes for high impedance contrast sites. The use of V_{S30} on its own does not capture resonance-based amplification. Recently, use of f_0 as an additional site term variable has been considered in the development of GMMs (e.g., Hassani and Atkinson 2016a) and in site classification for earthquake design codes (e.g., Pitilakis *et al.* 2018). Recent studies have shown that incorporating f_0 as an additional site proxy can further reduce uncertainties in GMMs (Hassani & Atkinson, 2016a, 2016b; Zhu *et al.*, 2019). Hassani & Atkinson (2017) found that a site-effects model using the combination of V_{S30} and f_0 can be applied in California, but the contribution of f_0 is reduced compared to Central/Eastern North America (CENA). In other words, in CENA, f_0 plays a more significant role in predicting ground motions.

The use of f_0 as a site classification metric, instead of or combined with V_{S30} , has been proposed. Zhao *et al.* (2006) developed a five category site classification scheme (I-V) using site period obtained from eHVSR of 5% damped response spectra in Japan. di Alessandro *et al.* (2012) modified Zhao's (2006) proposed scheme by adding two more classification categories (I-VII) for multi-peak response based on earthquake HVSRs in Italy. Pitilakis *et al.* (2018) presented a new classification scheme for Eurocode 8 to introduce site fundamental period as a main parameter and further sub-divide the original NEHRP six site class categories. Their proposed classification scheme is presented in Table 1-3.

Table 1-3. Detailed site classification scheme based on T_0 (from Pitilakis *et al.*, 2018).

Site class	Description	T_0	Remarks	
A	Rock formations	$\leq 0.2s$	Hard rock $V_{s,av} > 1500$ m/s	
	Slightly weathered/ segmented rock formations (thickness of weathered layer $< 5.0m$)		Rock like formations: $V_{s,av}$ or $V_{s,30} \geq 800$ m/s	
	Geologic formations resembling rock formations in their mechanical properties and their composition (e.g. conglomerates)		Surface weathered layer (if any with $H < 5m$): $V_{s,av} \geq 300$ m/s	
B	Soft rock formations	$0.1-0.3s$ $\leq 0.3s$	$V_{s,av}$: 350-600 m/s	
	Formations which resemble to soft rock in their mechanical properties (e.g. stiff marls)			
	Very dense sand-gravels		$V_{s,30}$: 400-760m/s	B1
	Hard and very stiff clays		N-SPT > 50	
B	H $<30m$		$S_u > 150$ kPa	
	Soil formations of very dense sand –sand gravel and/or very stiff/ to hard clay, of homogenous nature, whose mechanical properties increase with depth	$0.3-0.6s$ $\leq 0.6s$	$V_{s,av}$: 400-550 m/s $V_{s,30}$: 350-500m/s N-SPT > 50	B2
	30m $<H<120m$		$S_u > 150$ kPa	
C	Soil formations of dense sand –sand gravel and/or stiff clay, of great thickness ($> 60.0m$), whose mechanical properties and strength are constant and/or increase with depth	$0.6-1.0s$ $\leq 1.0s$	$V_{s,av}$: 400-600 m/s $V_{s,30}$: 350-450 m/s N -SPT > 50 $S_u > 150$ kPa $\leq 1.0s$	C1
	H $>60m$			
	Soil formations of medium dense sand – sand gravel and/or medium stiffness clay (PI > 15 , fines percentage $> 30\%$)	$0.3-0.7s$ $\leq 0.8s$	$V_{s,av}$: 250-450 m/s $V_{s,30}$: 250-400 m/s N -SPT > 20	C2
C	20m $<H< 60m$		150 kPa $> S_u > 70$ kPa $V_{s,av}$: 300-500 m/s	
	Like C2 but with great thickness	$0.7-1.4s$ $\leq 1.4s$	$V_{s,30}$: 200-350 m/s N -SPT > 20	C3
	H $>60m$		150 kPa $> S_u > 70$ kPa	

	Recent soil deposits of substantial thickness (up to 60m), with the prevailing formations being soft clays or/ and clays with a thickness $h > 3.0\text{m}$, of high plasticity index ($PI > 20-30$), high water content ($W > 40\%$) and low values of strength parameters ($S_u < 25\text{ kPa}$)	$\leq 1.4\text{s}$	
D	Recent soil deposits of substantial thickness (up to 60m), with prevailing loose sandy to sandy-silty formations with a substantial fines percentage (not to be considered susceptible to liquefaction)	$\leq 1.4\text{s}$	$V_{s,av}$: 200-400 m/s $V_{s,30}$: 150-300 m/s N-SPT < 20 $S_u < 70\text{ kPa}$
	Soil formations of great overall thickness ($> 60.0\text{m}$), interrupted by layers of soft soils of a small thickness (5 – 15m), up to the depth of $\sim 40\text{m}$, within soils (sandy and/or clayey, category C) of evidently greater strength, with $V_{s,at} \geq 300\text{ m/s}$	1.4-3.0s $\leq 3.0\text{s}$	
E	Surface soil formations of small thickness (5 - 20m), small strength and stiffness, likely to be classified as category C and D according to its geotechnical properties, which overlie category A formations ($V_{s,av} \geq 800\text{ m/s}$)	0.1-0.5s $\leq 0.5\text{s}$	$V_{s,av}$: 160- 300 m/s
X	Loose fine sandy-silty soils beneath the water table, susceptible to liquefaction (unless a special study proves no such danger, or if the soil's mechanical properties are improved)		
	Soils near obvious tectonic faults		
	Steep slopes covered with loose deposits		
	Loose granular or soft silty-clayey soils, provided they have been proven to be hazardous in terms of dynamic compaction or loss of strength.		
	Recent loose landfills Soils with a very high percentage in organic material		
	Special soils requiring site-specific evaluations		

Derras *et al.* (2017) investigated the performance of various site condition proxies by deriving GMMs with single and pairs of these proxies and assessing the performance of the proxies to reduce ground-motion aleatory variability and evaluate how they capture non-linear site effects. They demonstrated that at very short periods ($T < 0.05\text{ s}$), none of the commonly used proxies provided good results on their own in terms of the stated objectives; using pairs of proxies provided improved results. V_{s30} and f_0 provide the best results at short-to-intermediate periods, whereas f_0 and the depth at which V_s is 800 m/s

(H_{800}) provide best results at longer periods. The pair of f_0 and topographic slope exhibits good performance over the whole period range.

Héloïse *et al.* (2012) compared the misfits of five single site proxies V_{s_z} (shear-wave velocity to a depth z , $z = 5, 10, 20,$ and 30 m) and T_0 and four site proxy pairs (e.g., V_{s_z} and T_0) in modelling KiK-net surface-to-borehole amplification. T_0 and ($T_0, V_{s_{30}}$) were found to be the best proxy pair. Régnier *et al.* (2014) concluded that, in addition to $V_{s_{30}}$, T_0 could reduce site-to-site variability of KiK-net sites in deep sedimentary basins. At longer periods, and for deeper sites, T_0 does a better job for characterizing site effects than $V_{s_{30}}$ (e.g., Luzi *et al.*, 2011, McVerry, 2011, Stambouli *et al.*, 2017). No single proxy performs best at all oscillator frequencies, because of the period-dependency of site amplification. Thus, a schema based on a combination of metrics is most appropriate.

1.2 Seismic Microzonation

Due to heterogeneous seismic behaviour, it is necessary to understand how incident ground motions are impacted by local soil characteristics to mitigate seismic risk and enhance safety. This is accomplished through seismic microzonation (SM). Seismic microzonation is a general term referring to the defining of seismic microzones, most often spatially as a 2D plan map but also includes development of 3D subsurface models, which can be depicted as distinct zones (polygons) that differ in seismic hazard level or via spatial interpolation (e.g., geostatistical kriging) with a continuous hazard scale.

Seed & Idriss (1969) studied ground motions from the 1957 San Francisco earthquake. Their results demonstrated that over only a few hundred meters, the same earthquake caused significantly different ground motions dependent on the thickness and characteristics of the near-surface soil profile. Similar observations have been made for many other earthquakes (e.g., Mexico City 1968, 1985, 2017; Kobe, 1992; Izmit, 1999). The purpose of SM is to study phenomena such as ground motion amplification, liquefaction, and slope instability to better inform those in charge of planning or implementing projects in a geographic area of the seismic risk.

SM mapping (SMM) seeks to identify lateral and vertical heterogeneities in geological and geophysical properties within a region to convey the variable seismic response (Hartzell *et al.* 1997, Panzera *et al.* 2017). A detailed geologic mapping, coupled with knowledge of V_s and f_0 can be useful to accomplish SMM. For the zones established by SM, 1D (or 2D/3D) amplification functions and site-specific response spectra can be computed to determine the zone's seismic hazard level.

SM studies require collection and organized storage of subsurface in situ “geo” data. Geologic, geomorphic, geophysical, and geotechnical data are required. Geodata sought and compiled during a SM study are variable in terms of in situ measures (e.g., material type, V_s , cone tip resistance), in situ methods (e.g., invasive to non-invasive), their access (e.g., online repositories, proprietary reports, or acquired during the SM study), and their format (e.g., paper copies, digital file). The density of data sufficient for a given SM study depends on the homogeneity of geological, geotechnical, and geophysical conditions.

There are three levels of SMM established by the ICMS 2008; the higher the level, the greater the quality and quantity of geodata and the greater the quality of seismic hazard analyses performed with the geodata. Level 1 SM map products typically depict only variation in site conditions related to the seismic hazard (termed as seismic hazard susceptibility), and are thereby independent of the seismic demand (input ground motions). SM susceptibility map products related to earthquake shaking (amplification) include mapping of the spatial variability in V_{s30} , f_0 , NBC site class, or soil thickness, i.e., any of measures used as site term variables in GMMs. In contrast, Level III SM map products depict variation in predicted seismic hazard (ground motions, amplification) and thereby involve performing seismic hazard analyses or calculations that depend on inputs of the seismic demand and Level I-II SM susceptibility mapping.

The use of non-invasive seismic methods and particularly the mHVSR method to define seismic microzones has proliferated over the last several decades (Bour *et al.* 1998, Ansal *et al.* 2002, Tuladhar *et al.* 2004, Paudyal *et al.* 2012, Gosar 2017). Given the ease of data acquisition, and processing for microzonation, the use of microtremors, either through

computation of V_{S30} from inverted velocity profiles from surface wave dispersion curves or interpreting mHVSRS for f_0 , has grown significantly in the past several decades.

1.3 Thesis Motivation

The motivation for this thesis is to present a replicable procedure to process three-component microtremor data to compute the mHVSRS at a site, particularly in the case of large databases (100's to 1000's). In addition, a first attempt was made to demonstrate the use of mHVSRS data to accomplish seismic microzonation in the Metro Vancouver region. To date, the mHVSRS method has been widely applied, however, due to a lack of standardization of acquisition and processing parameters as well as uncertainty regarding the physical basis of the mHVSRS, its full potential use for characterization of seismic site effects has not been realized.

Through analysis of thousands of single-station microtremor measurements acquired throughout the Metro Vancouver region over the past two decades, this work aims to first investigate the impact of experimental conditions on the calculated mHVSRS, and then to develop a processing methodology that is able to handle batch processing of large microtremor-recording datasets and is robust in its identification of mHVSRS peak frequencies ($f_{\#HV}$, where # is 0, 1, 2 in this study) with little user input. The developed processing methodology will then be applied to the full suite of microtremor measurements available across the Metro Vancouver region, and a mHVSRS database, developed considering the full spectrum of potential applications of the end-user, as well as an interpolated f_{0HV} map, will be produced. Finally, both qualitative and quantitative interpretation of individual mHVSRS measurements is accomplished to exemplify the seismic site condition information that can be extracted from an mHVSRS at a single site. A total of nine mHVSRS response types are identified for the Metro Vancouver region which are simplified to three types for spatial mapping to communicate the distribution of typical amplification spectra throughout the region.

1.4 Organization of Work

This thesis is comprised of six chapters which review the use of mHVSr to aid in seismic microzonation and site effect assessment in the Metro Vancouver region.

In Chapter 2, a description of the geology in Metro Vancouver is provided. Applications of the mHVSr method and a review of previous seismic microzonation and site effect studies in the Metro Vancouver region are also included.

In Chapter 3, single station microtremor data acquired from 2002-2021 is used to investigate the impact of experimental conditions on processed mHVSrs, to provide a set of guidelines to aid practitioners during data acquisition and mHVSr calculation. A robust processing algorithm, that is suited for batch processing large datasets, is developed based on knowledge gained from experimental trials with three existing mHVSr processing softwares.

In Chapter 4, a peak picking methodology, suited for mHVSr measurements with multiple peaks is presented. An interpolated map of f_{0HV} for Metro Vancouver is presented. A brief interpretation of typical mHVSr measurements in the Metro Vancouver area is provided, as well as some additional information regarding challenges interpreting mHVSr measurements that demonstrate multiple peaks or broad peaks. Finally, the proposed mHVSr database structure is introduced.

In Chapter 5, cluster analyses are performed on the mHVSr data to define zones in the Metro Vancouver region that have mHVSr responses of similar morphology and thus may experience similar seismic behavior. A brief investigation into forward modelling of the mHVSr based on assumptions about the underlying wavefield is completed.

Chapter 6 presents the overall thesis findings.

1.5 References

- Allen, T., & Wald, D. (2009). On the Use of High-Resolution Topographic Data as a Proxy for Seismic Site Conditions (VS30). *Bulletin of The Seismological Society of America*, 99, 935–943. <https://doi.org/10.1785/0120080255>

- Ansal, A. M., Iyisan, R., & Güllü, H. (2002). Microtremor Measurements for the Microzonation of Dinar. *Earthquake Microzoning*, 2525–2541. https://doi.org/10.1007/978-3-0348-8177-7_15
- Atkinson, G. M., & Boore, D. M. (2003). Empirical Ground-Motion Relations for Subduction-Zone Earthquakes and Their Application to Cascadia and Other Regions. *Bulletin of the Seismological Society of America*, 93(4), 1703–1729. <https://doi.org/10.1785/0120020156>
- Baratta, M. (1910). ... *La catastrofe sismica Calabro messinese (28 dicembre 1908)*.
- Bard, P.-Y. (1999). Microtremor measurements: A tool for site effect estimation? *The Effects of Surface Geology on Seismic Motion*, 3, 1251–1279.
- Bardet, J.-P., Ichii, K., & Lin, C. (2000). *EERA—A Computer Program for Equivalent-linear Earthquake site Response Analyses of Layered Soil Deposits*.
- Bonilla, L. F., Steidl, J. H., Gariel, J. C., & Archuleta, R. J. (2002). Borehole Response Studies at the Garner Valley Downhole Array, Southern California. *Bulletin of the Seismological Society of America*, 92(8), 3165–3179. <https://doi.org/10.1785/0120010235>
- Bonilla, L. F., Steidl, J. H., Lindley, G. T., Tumarkin, A. G., & Archuleta, R. J. (1997). Site amplification in the San Fernando Valley, California: Variability of site-effect estimation using the S-wave, coda, and H/V methods. *Bulletin of the Seismological Society of America*, 87(3), 710–730. <https://doi.org/10.1785/BSSA0870030710>
- Boore, D. M., Stewart, J. P., Seyhan, E., & Atkinson, G. M. (2014). NGA-West2 Equations for Predicting PGA, PGV, and 5% Damped PSA for Shallow Crustal Earthquakes. *Earthquake Spectra*, 30(3), 1057–1085. <https://doi.org/10.1193/070113eqs184m>
- Borcherdt, R. (1970). Effects of local geology on ground motion near San Francisco Bay. *Bulletin of the Seismological Society of America*, 60.
- Borcherdt, R. (1994). Estimates of Site-Dependent Response Spectra for Design (Methodology and Justification). *Earthquake Spectra*, 10(4), 617–653. <https://doi.org/10.1193/1.1585791>
- Boudghene Stambouli, A., Zendagui, D., Bard, P. Y., & Derras, B. (2017). Deriving amplification factors from simple site parameters using generalized regression neural networks: Implications for relevant site proxies. *Earth, Planets and Space*, 69(1). <https://doi.org/10.1186/S40623-017-0686-3>
- Bour, M., Fouissac, D., Dominique, P., & Martin, C. (1998). On the use of microtremor recordings in seismic microzonation. *Soil Dynamics and Earthquake Engineering*, 17(7–8), 465–474. [https://doi.org/10.1016/S0267-7261\(98\)00014-1](https://doi.org/10.1016/S0267-7261(98)00014-1)

- Cara, F., di Giulio, G., & Rovelli, A. (2003). A Study on Seismic Noise Variations at Colfiorito, Central Italy: Implications for the Use of H/V Spectral Ratios. *Geophysical Research Letters*, 30(18). <https://doi.org/10.1029/2003GL017807>
- Castellaro, S., Mulargia, F., & Rossi, P. (2008). Vs30: Proxy for Seismic Amplification? *Seismological Research Letters*, 79, 540–543. <https://doi.org/10.1785/gssrl.79.4.540>
- Chiou, B., Darragh, R., Gregor, N., & Silva, W. (2008). NGA Project Strong-Motion Database. *Earthquake Spectra*, 24(1), 23–44. <https://doi.org/10.1193/1.2894831>
- Derras, B., Bard, P. Y., & Cotton, F. (2017). VS30, slope, H800 and f0: Performance of various site-condition proxies in reducing ground-motion aleatory variability and predicting nonlinear site response 4. *Seismology. Earth, Planets and Space*, 69(1), 1–21. <https://doi.org/10.1186/S40623-017-0718-Z/FIGURES/13>
- Derras, B., Bard, P.-Y., & Cotton, F. (2016). Site-Conditions Proxies, Ground-Motion Variability and Data-Driven GMPEs: Insights from NGA-West 2 and RESORCE Data Sets. *Earthquake Spectra*, 32. <https://doi.org/10.1193/060215EQS082M>
- di Alessandro, C., Bonilla, L. F., Boore, D. M., Rovelli, A., & Scotti, O. (2012). Predominant-Period Site Classification for Response Spectra Prediction Equations in Italy. *Bulletin of the Seismological Society of America*, 102(2), 680–695. <https://doi.org/10.1785/0120110084>
- Field, E. H., & Jacob, K. H. (1995). A comparison and test of various site-response estimation techniques, including three that are not reference-site dependent. *Bulletin of the Seismological Society of America*, 85(4), 1127–1143. <https://doi.org/10.1785/BSSA0850041127>
- Gallipoli, M. R., Mucciarelli, M., & Vona, M. (2009). Empirical estimate of fundamental frequencies and damping for Italian buildings. *Earthquake Engineering and Structural Dynamics*, 38(8), 973–988. <https://doi.org/10.1002/EQE.878>
- Gosar, A. (2017). Study on the applicability of the microtremor HVSR method to support seismic microzonation in the town of Idrija (W Slovenia). *Natural Hazards and Earth System Sciences*, 17(6), 925–937. <https://doi.org/10.5194/NHESS-17-925-2017>
- Hartzell, S., Cranswick, E., Frankel, A., Carver, D., & Meremonte, M. (1997). Variability of site response in the Los Angeles urban area. *Bulletin of the Seismological Society of America*, 87, 1377–1400.
- Hashash, Y., Ilhan, O., Harmon, J., Parker, G., Stewart, J., Rathje, E., Campbell, K., & Silva, W. (2019). Nonlinear Site Amplification Model for Ergodic Seismic Hazard Analysis in Central and Eastern North America. *Earthquake Spectra*, 36. <https://doi.org/10.1177/8755293019878193>

- Hassani, B., & Atkinson, G. (2017). Site-Effects Model for Central and Eastern North America Based on Peak Frequency and Average Shear-Wave Velocity. *Bulletin of the Seismological Society of America*, 108. <https://doi.org/10.1785/0120170061>
- Hassani, B., & Atkinson, G. M. (2016a). Applicability of the Site Fundamental Frequency as a V_{s30} Proxy for Central and Eastern North America. *Bulletin of the Seismological Society of America*, 106(2), 653–664. <https://doi.org/10.1785/0120150259>
- Hassani, B., & Atkinson, G. M. (2016b). Site-Effects Model for Central and Eastern North America Based on Peak Frequency. *Bulletin of the Seismological Society of America*, 106(5), 2197–2213. <https://doi.org/10.1785/0120160049>
- Héloïse, C., Bard, P. Y., Duval, A. M., & Bertrand, E. (2012). Site effect assessment using KiK-net data: Part 2—Site amplification prediction equation based on f_0 and V_{sz} . *Bulletin of Earthquake Engineering*, 10(2), 451-489.
- Hunter, J. A. M., & Crow, H. L. (2015). *Shear wave velocity measurement guidelines for Canadian seismic site characterization in soil and rock*. Natural Resources Canada.
- Itasca, F. L. A. C. Version 7.00, 2013. *A Computer Program for Seismic Response Analysis for Soil Deposits, Tutorial and User Manual of the FLAC*. Itasca Consulting Group, Minneapolis, MN.
- Kramer, S. L. (1996). *Geotechnical earthquake engineering*.
- Lachet, C., Hatzfeld, D., Bard, P.-Y., Theodulidis, N., Papaioannou, C., & Savvaidis, A. (1996). Site effects and microzonation in the city of Thessaloniki (Greece) comparison of different approaches. *Bulletin of the Seismological Society of America*, 86(6), 1692–1703.
- Lee, & Finn. (1978). *DESRA-2: Dynamic effective stress response analysis of soil deposits with energy transmitting boundary including assessment of liquefaction potential*. <https://ci.nii.ac.jp/naid/10013393501/>
- Lee, V., & Trifunac, M. (2010). Should average shear-wave velocity in the top 30 m of soil be used to describe seismic amplification? *Soil Dynamics and Earthquake Engineering*, 30, 1250–1258. <https://doi.org/10.1016/j.soildyn.2010.05.007>
- Lermo, J., & Chavez-Garcia, F. J. (1993). Site effect evaluation using spectral ratios with only one station. *Bulletin of the Seismological Society of America*, 83(5), 1574–1594. <https://doi.org/10.1785/BSSA0830051574>
- Lermo Samaniego, J., & J Chavez- Garcia, F. (1994). Are microtremors useful in site response evaluation? *Bulletin of the Seismological Society of America*, 84, 1350–1364.
- Luzi, L., Puglia, R., Pacor, F., Gallipoli, M. R., Bindi, D., & Mucciarelli, M. (2011). Proposal for a soil classification based on parameters alternative or complementary to $V_{s,30}$. *Bulletin of Earthquake Engineering* 2011 9:6, 9(6), 1877–1898. <https://doi.org/10.1007/S10518-011-9274-2>

- McVerry GH. (2011). Site-effect terms as continuous functions of site period and Vs30. *Ninth Pacific Conference on Earthquake Engineering*.
- Nakamura, Y. (1989). A method for dynamic characteristics estimation of subsurface using microtremor on the ground surfac. *Quarterly Report of RTRI (Railway Technical Research Institute) (Japan)*, 30.
- Panzer, F., D'Amico, S., Burjanek, J., & Pischiutta, M. (2017). Advance in seismic site response: Usual practices and innovative methods. *Physics and Chemistry of the Earth Parts A/B/C*, 98, 1–2. <https://doi.org/10.1016/j.pce.2017.04.005>
- Parolai, S., Bindi, D., the, P. A.-B. of, & 2000, undefined. (2000). Application of the generalized inversion technique (GIT) to a microzonation study: numerical simulations and comparison with different site-estimation techniques. *Bulletin of the Seismological Society of America*, 90, 286–297.
- Paudyal, Y. R., Bhandary, N. P., & Yatabe, R. (2012). Seismic Microzonation of Densely Populated Area of Kathmandu Valley of Nepal using Microtremor Observations. *Journal of Earthquake Engineering*, 16(8), 1208–1229. <https://doi.org/10.1080/13632469.2012.693242>
- Pitilakis, K., Riga, E., Anastasiadis, A., Fotopoulou, S., & Karafagka, S. (2018). Towards the revision of EC8: Proposal for an alternative site classification scheme and associated intensity dependent spectral amplification factors. *Soil Dynamics and Earthquake Engineering*, 126. <https://doi.org/10.1016/j.soildyn.2018.03.030>
- Raptakis, D., Theodulidis, N., & Pitilakis, K. (1998). Data analysis of the euroseistest strong motion array in Volvi (Greece): Standard and horizontal-to-vertical spectral ratio techniques. *Earthquake Spectra*, 14(1), 203–224. <https://doi.org/10.1193/1.1585996>
- Régnier, J., Bonilla, L. F., Bertrand, E., & Semblat, J. F. (2014). Influence of the VS Profiles beyond 30 m Depth on Linear Site Effects: Assessment from the KiK-net DataInfluence of the VS Profiles beyond 30 m Depth on Linear Site Effects. *Bulletin of the Seismological Society of America*, 104(5), 2337–2348. <https://doi.org/10.1785/0120140018>
- Riepl, J., Bard, P.-Y., Hatzfeld, D., Papaioannou, C., & Nechtschein, S. (1998). Detailed evaluation of site-response estimation methods across and along the sedimentary valley of volvi (EURO-SEISTEST). *Bulletin of the Seismological Society of America*, 88(2), 488–502. <https://doi.org/10.1785/BSSA0880020488>
- Schnabel, P., Lysmer, J., & Seed, H. (1972). *SHAKE—a computer program for earthquake response analysis of horizontally layered sites*.
- Seed, H. B., & Idriss, I. M. (1969). Influence of Soil Conditions on Ground Motions During Earthquakes. *Journal of the Soil Mechanics and Foundations Division*, 95(1), 99–137. <https://doi.org/10.1061/JSFEAQ.0001260>

- Si, H., & Midorikawa, S. (1999). New attenuation relationships for peak ground acceleration and velocity considering effects of fault type and site conditions. *Journal of Structural and Construction Engineering (Transactions of AIJ)*, 64(523), 63–70. https://doi.org/10.3130/aijs.64.63_2
- Theodulidis, N., Bard, P. Y., Archuleta, R., & Bouchon, M. (1996). Horizontal-to-vertical spectral ratio and geological conditions: The case of Garner Valley Downhole Array in southern California. *Bulletin of the Seismological Society of America*, 86(2), 306–319. <https://doi.org/10.1785/BSSA0860020306>
- Tuladhar, R., Yamazaki, F., Warnitchai, P., & Saita, J. (2004). Seismic microzonation of the greater Bangkok area using microtremor observations. *Earthquake Engineering & Structural Dynamics*, 33(2), 211–225. <https://doi.org/10.1002/EQE.345>
- Wald, D., & Allen, T. (2007). Topographic Slope as a Proxy for Seismic Site Conditions and Amplification. *Bulletin of the Seismological Society of America*, 97, 1379–1395. <https://doi.org/10.1785/0120060267>
- Wood, H. O. (1908). *Distribution of apparent intensity in San Francisco, in the California earthquake of April 18, 1906.*
- Zhao, J. X., Irikura, K., Zhang, J., Fukushima, Y., Somerville, P. G., Asano, A., Ohno, Y., Oouchi, T., Takahashi, T., & Ogawa, H. (2006). An Empirical Site-Classification Method for Strong-Motion Stations in Japan Using h/v Response Spectral Ratio. *Bulletin of the Seismological Society of America*, 96(3), 914–925. <https://doi.org/10.1785/0120050124>
- Zhu, C., Pilz, M., & Cotton, F. (2019). Which is a better proxy, site period or depth to bedrock, in modelling linear site response in addition to the average shear-wave velocity? *Bulletin of Earthquake Engineering* 2019 18:3, 18(3), 797–820. <https://doi.org/10.1007/S10518-019-00738-6>

Chapter 2

2 Geology and Previous Site Effects Studies of Metro Vancouver

This thesis begins with a summary of the important geologic units and their mapping in Metro Vancouver since knowledge of the geologic and geotechnical properties of sediments is important to understand how the local site conditions will modify the amplitude and frequency content of incident seismic waves (Seed *et al.* 1976). Previous seismic site effect studies in Metro Vancouver are then summarized.

2.1 Geology of Metro Vancouver

The following section will summarize existing knowledge regarding the geology of Metro Vancouver. The geology map of the Metro Vancouver is presented in Figure 2-1.

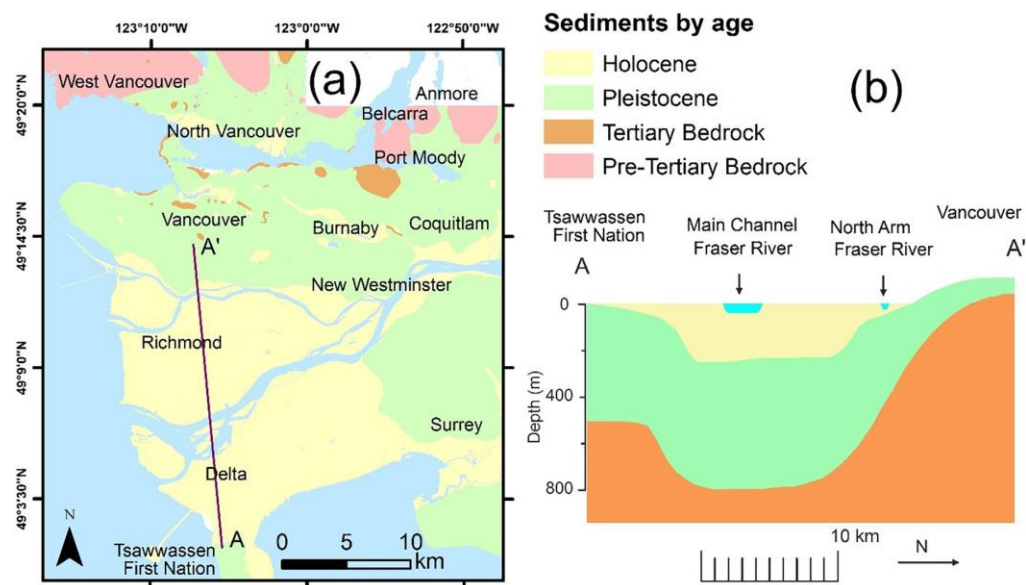


Figure 2-1. (a) Simplified geology map of Metro Vancouver based on age of sediments. (b) Geologic cross-section along line A-A' (modified from Rogers *et al.*, 1998). Figure modified from Molnar *et al.* (2020).

2.1.1 Physiographic Regions

The Metro Vancouver region is composed of two distinct geographical areas, namely, the Coast Mountains along the North Shore and the Georgia Basin depression encompassing much of the city and extending south to the Canada-USA border (Armstrong, 1990).

The Georgia Basin consists of gently rolling and flat-topped uplands, separated by wide, flat-bottomed valleys. Prominent landmarks, such as Burnaby Mountain, Grant Hill, Silverdale Hill and further east, Sumas Mountain expose the oldest rock. These sedimentary rocks have been tilted from their initial horizontal deposition and are now slightly inclined to the south (Armstrong, 1990). Along the northern edge of the Georgia Basin depression they form a thin veneer over the granitic rocks of the Coast Mountains, however, they thicken to the south, and reach a maximum thickness of 4,400 m near the Canada-USA border (Armstrong, 1990).

2.1.2 Regional Geology and Tectonic Setting

60% of Canada's earthquakes occur along the coast of British Columbia (Natural Resources Canada, 2016). Southwest British Columbia is located at the northern end of the Cascadia subduction zone, where the oceanic Juan de Fuca Plate is being subducted beneath the western margin of the North American Plate (Rogers, 1998). Earthquakes occur in three distinct settings in this region:

- i) crustal earthquakes which occur in the continental crust of North America (max. moment magnitude, $M > 8$, typically occurring between 5 and 25 km depth),
- ii) in-slab earthquakes in the subducted Juan de Fuca Plate (max. $M \sim 7$, occur at 60-70 km depth below Southwestern BC),
- iii) and interface earthquakes, on the subduction interface (max. $M \sim 9$, Metro Vancouver is 150-200 km distant).

Southwest British Columbia is a region of complex deformation above a bend in the subducting plate below (Balfour *et al.* 2011).

The geology in Metro Vancouver is built upon late Cretaceous (99.6-65.5 mya) to early Tertiary (65.5-55.8 mya) south-dipping sedimentary rocks of the Georgia basin that overlie

Mesozoic plutonic rocks exposed in the Coast Mountains (Monger and Journeay, 1994). West of Vancouver, the Strait of Georgia conceals the boundary between the Coast Mountains and the mountains of Vancouver Island. South of Vancouver, the broad valley of the lower Fraser River is underlain by glacial and fluvial deposits, southeast of which lie the Cascade Ranges.

The present Georgia Basin is an erosional remnant and its configuration is largely the result of post-depositional deformation. Sedimentary rocks of the Georgia Basin comprise two main packages: the Upper Cretaceous/Late Tertiary Nanaimo Group exposed mainly on the east side of Vancouver Island and on the islands of Georgia Strait; and Paleocene/early Tertiary to Miocene (23.03-5.332 mya) sedimentary and extrusive igneous rocks exposed mainly in the Vancouver area and northwest of Washington State. The Nanaimo Group comprises a stratigraphic thickness of more than 4 km of Turonian (93.9-89.8 mya) to Maastrichtian (72.1-66 mya) age. The Tertiary (66-2.6 mya) rocks of the Georgia basin unconformably overlie sedimentary rocks of the Late Cretaceous Nanaimo Group (Roddick 1965, Mustard 1994).

The lowlands of the Metro Vancouver region are underlain by thick Quaternary (2.58 mya – present) sediments. Heterogeneous units of stratified drift from at least three different glaciations are separated by unconformities and in some local areas by non-glacial sediments (Clague, 1994).

2.1.3 Glaciations

A dominant force in shaping the landscape of Metro Vancouver has been glaciation. Three major periods of glaciation are recognized in the Vancouver area. During these periods, glaciers from the Coast Mountains and the Cascade Mountains formed large ice sheets which covered the Fraser Lowland and extended out into the Strait of Georgia. During these periods of glaciation, the bedrock surface, consisting of either Tertiary or Pre-Tertiary (>66 mya) rocks, was scoured, creating an irregular surface over which Quaternary sediments were deposited (Armstrong, 1990).

Southwest of the Coast Mountains, thick accumulations of proglacial sand (Quadra sand) were deposited around Vancouver, West Vancouver and North Vancouver. Proglacial deposits were overlain by till and gravelly ice-contact sediments (Vashon drift) (Armstrong, 1984).

At the end of the Fraser glaciation (~13,000 years ago), Capilano sediments (glaciomarine silt and clay) were deposited over the Vashon till unit. Thick glaciers did not override these Capilano sediments. The thickness of Capilano sediments in marine and glaciomarine depositional environments is ~15 m, thinning to 8 m in fluvial channels (Armstrong, 1984). Holocene (11,700 yrs to present) Salish sediments were deposited between 10 and 12 thousand years ago, and include alluvial fan, organic, lacustrine, coarse-grained alluvial and deltaic deposits of smaller rivers that formed in post-glacial time. The Fraser River, which developed after the ice left the lowlands approximately 8 to 10 thousand years ago, began depositing sands, silts, and clays forming the Holocene Fraser River delta (Armstrong, 1984).

2.1.4 Stratigraphy

The Metro Vancouver area consists mostly of Pleistocene (2.58 mya to 11,700 ya) glacial and interglacial sediments overlying Tertiary bedrock of the Georgia Basin. The Quaternary succession in south-coastal British Columbia consists of sediments deposited during several glaciations and intervening interglaciations (Clague, 1994). The thickness of Quaternary sediments overlying sedimentary bedrock is variable throughout the Metro Vancouver region, and understanding these geologic trends is important for accurate prediction of ground motion amplification.

Miocene sandstones and shales have a shear-wave velocity (V_s) of 2.0 to 3.5 km/s (Monahan and Levson, 2001). The depth to the bedrock surface varies from ~200 m, north of the Fraser River, to ~800 m near Ladner (Britton *et al.*, 1995).

Pleistocene sediments overlie Tertiary bedrock, and consist mostly of fine sands and interbedded silt of glacial and interglacial origin. Diamicton is less common. The Pleistocene succession beneath the Fraser delta is up to 500 m thick beneath the center of

the delta (Britton *et al.*, 1995) and displays complex changes in sediment type both vertically, at individual sites, and laterally between sites. The average Vs of Pleistocene sediments ranges between 0.4 and 1.1 km/s, with no known relationship between velocity and depth (Hunter & Christian, 2001).

In addition to the Pleistocene sediments are the thick unconsolidated Holocene (11,700 yrs to present) sediments comprising the Fraser River delta, south of Vancouver. The delta consists of silt and sand with thicknesses up to 300 m (Cassidy and Rogers, 2004). These Holocene silts and sands exhibit an average Vs between 200 and 300 m/s which increases with depth due to sedimentary loading (Hunter *et al.*, 1998). These deltaic sediments are subject to high amplification and liquefaction due to their significant thickness, relatively low seismic velocity, and presence of saturated channel sands (Monahan *et al.*, 1993, Hunter *et al.*, 1998, Jackson *et al.*, 2017, Javanbakht *et al.* 2021).

2.2 Microtremor Horizontal to Vertical Spectral Ratio

Microtremor (or ambient vibration) is defined as the constant vibration of the Earth's surface generated by a combination of low frequency ($< \sim 1$ Hz) natural microseisms, and higher frequency ($> \sim 1$ Hz) anthropogenic microtremors (Bonney-Claudet *et al.*, 2006). This background noise is a mixture of seismic wave phases, which contain information on the sources and transmission paths of the waves and subsurface structure (Okada and Suto, 2003). The use of microtremors was pioneered by Bertelli (1872) and then Omori (1909). Engineering applications were introduced by Gutenberg (1958) and Kanai & Tanaka (1961). Based on these developments, the single-station microtremor approach was developed in Japan by Nogoshi & Igarashi (1971) for characterizing site response, and later popularized by Nakamura (1989).

The mHVSR is an analysis technique that calculates the ratio of the horizontal-to-vertical Fourier amplitude spectra (FAS) derived from microtremor recordings at a site made with a tri-axial seismometer. Recently, mHVSR has gained popularity and use in Europe (SESAME project; Bard *et al.*, 2008), Canada (Hunter *et al.*, 2010; Molnar & Cassidy, 2006), New Zealand (Wotherspoon *et al.* 2015, Vantassel *et al.* 2018) and South America

(Pilz *et al.* 2009, Leyton *et al.* 2013). Its use in the United States is increasing (Teague *et al.* 2018, Stephenson *et al.* 2019).

Although there remains ambiguity with regards to the physical basis of the mHVSR, empirical evidence suggests that f_{0HV} occurs at, or close to, f_0 provided there is a sufficiently strong impedance contrast (Field and Jacob, 1993, Lermo and Chavez-Garcia, 1994, Bonilla *et al.* 1997, Bour *et al.* 1998, Bard 1999, Fäh *et al.* 2001, Wollery and Street 2002, Haghshenas *et al.* 2008). Whether the wavefield composition is primarily body, surface, or diffuse waves and/or combinations thereof is still largely debated (Lachet and Bard 1994, Fäh *et al.* 2001, Malischewsky and Scherbaum 2004, Bonnefoy-Claudet *et al.* 2008, Kawase *et al.* 2011). Studies of microtremors have demonstrated that the contribution of different wave types varies with frequency, from site to site, and that Love waves are often a dominant part of the microtremor wavefield (Yamamoto, 2000, Köhler *et al.*, 2007, Endrun, 2010). Therefore, no single analytical expression exists for all real-world conditions. A brief review of the various interpretations of the mHVSR is provided.

Nakamura (1989), in his pioneering interpretation of the mHVSR, assumed that the microtremor wavefield is primarily composed of S and Rayleigh waves. He postulated that the effects of Rayleigh waves are ‘eliminated’ by considering the spectral ratio. By assuming the H/V ratio at the sediment-bedrock interface is unity, and the vertical component motions do not undergo amplification within the near surface sediments, the mHVSR can be treated as proxy for the SH-wave transfer function. Nakamura (1989, 2000, 2008) has repeatedly asserted the correspondence between both the frequency, and relative amplitude of peaks in the mHVSR and those of the SH-wave transfer function. Although, confidence in the correspondence of the entire mHVSR curve and the SH-transfer function has abated. Methods have been developed to correct/calibrate the mHVSR and associated interpreted values to improve its correspondence with the site transfer function (e.g., Kawase *et al.*, 2018, 2019, Hassani *et al.*, 2019).

The most prevalent physical interpretation of the mHVSR is that the microtremor wavefield is primarily composed of surface waves. Nogoshi & Igarashi (1971) compared mHVSR curves with fundamental-mode Rayleigh wave ellipticity and concluded that the

fundamental model Rayleigh wave provides the main contribution to the microtremor wavefield. Under the Rayleigh wave ellipticity assumption, the peaks of an mHVSr are related to vanishing of the vertical component motion. Konno & Omachi (1998) demonstrated that the mHVSr peak can be explained by fundamental-mode Rayleigh wave ellipticity, or the Airy phase of the fundamental mode Love wave. They also found that if the proportion of Rayleigh to Love waves is a certain value, the amplitude of the mHVSr peak is close to the S-wave amplification factor. Although the peak of the mHVSr is close to the S-wave resonance frequency, the curve itself is closely related to the fundamental mode Rayleigh wave ellipticity (Konno and Omachi 1998, Arai and Tokimatsu 2000). This has been shown to be true not only when Rayleigh waves are dominant in the microtremor wavefield (e.g., Scherbaum *et al.*, 2003), but also in numerical studies that use full wavefield modelling of microtremors (Field & Jacob, 1993, Lachet & Bard, 1994, Lunedei & Albarello, 2010).

Lachet and Bard (1994) carried out a numerical simulation of the microtremor wavefield by arranging sources randomly within a circle of a given radius from a receiver. The results of their theoretical study indicate that the peak of the mHVSr corresponds well with the S-wave resonance frequency, as well as the peak of the fundamental model Rayleigh wave ellipticity. They suggested that the shape of the mHVSr is controlled by all seismic phases. Field and Jacob (1993) proposed a theoretical way to related the ambient vibration displacement power spectrum to the Green's function of the ground. Lunedei and Albarello (2010) extended this model to include all seismic phases.

Sánchez-Sesma *et al.* (2011) proposed that microtremors form a diffuse field containing all types of body (P and S) and surface waves (Love and Rayleigh) for which their associated illumination strengths stabilize in fixed proportions. Within the diffuse field assumption (DFA) multiple scattering and its equilibrating effects play a prominent role. The relative power of each seismic state that composes the illumination emerges from the principle of equipartition of energy. Theory asserts that within a diffuse elastic wave field the autocorrelation in the frequency domain (the power spectrum), at any point of the medium, is proportional to the imaginary part of the Green's function for source and receiver at the same point. As average autocorrelations are proportional to average

directional energy densities (DED) then, by following Arai & Tokimatsu (2004) one way to assess the mHVSr is the square root of the ratio of the DEDs. For a horizontally layered medium this approach is straightforward for data at the surface (Sánchez-Sesma *et al.* 2011, Kawase *et al.* 2015) and at depth (Lontsi *et al.* 2015). Lateral heterogeneity can be dealt with similarly but computing Green's functions become computationally expensive (Matsushima *et al.* 2014, 2017).

Despite complexity regarding the physics behind the mHVSr phenomenon, the use of mHVSr is growing worldwide. There exist many studies demonstrating agreement between results from mHVSr studies and those from other geophysical techniques and geological observations (e.g., Parolai *et al.*, 2002, Hinzen *et al.*, 2004, Hunter *et al.*, 2010, Macau *et al.*, 2014, Mohamed *et al.*, 2019). mHVSr studies are particularly valuable in low seismicity regions where detailed fundamental site period maps can be generated and used for urban planning purposes (e.g., Picozzi *et al.* 2009, Hunter *et al.*, 2010, Zor *et al.*, 2010, Kamarudin *et al.*, 2016). The method has become routine in quantifying the thickness of sedimentary cover (e.g., Seht & Wohlenberg, 1999, Smith *et al.*, 2013, Scheib *et al.*, 2016, Jakica, 2018, Pratt, 2018). Accurate conversion from frequency to depth depends on the reliability of information pertaining to the Vs structure in the region. The mHVSr method has also been applied for liquefaction hazard mapping (e.g., Beroya *et al.*, 2009; Castellaro *et al.*, 2015) and for engineering applications such as evaluation both building and soil response using microtremors (e.g., Oliveira & Navarro, 2009, Castellaro & Mulargia, 2010, Michel *et al.*, 2010, Chiauuzzi *et al.*, 2011, Salameh *et al.*, 2016). Combining techniques, such as mHVSr and multi-channel analysis of surface waves (MASW) (e.g., Gorstein & Ezersky, 2015) or ambient vibration array (e.g., Zor *et al.*, 2010) is particularly beneficial for evaluating earthquake site response in areas of low seismicity.

2.3 Previous Site Effects Studies

An existing soil hazard map of the Lower Mainland was generated for the BC school seismic retrofit program by Dr. Patrick Monahan (Taylor *et al.*, 2006) and is based on his compilation of subsurface geodata and mapped spatially using the surficial geologic maps published by the Geological Survey of Canada (Armstrong and Hicock, 1979, 1980,

Armstrong, 1980a, 1980b, Dunn and Ricketts, 1994). The regional distribution of soil hazard is broken down as follows:

- Site Classes A and B: pertain to bedrock, occur in mountains to the north and southeast of the Fraser Lowland,
- Site Class C: assigned to areas where older Pleistocene deposits occur within approximately 5 m of the surface, widespread in the upland areas including most of the cities of Vancouver, Burnaby and Surrey,
- Site Class D: assigned to a number of different settings, most of which are dominated by sediments that have not been overridden by glacial ice. These areas include: Capilano glaciomarine clays that are between 5 and 20 m thick; Capilano glaciomarine clays that have been demonstrably overridden by glacial ice in the east-central Fraser Lowland; Capilano glaciomarine, glaciofluvial and glaciodeltaic sands and gravels; deposits of smaller Holocene sand and gravel-rich deltas (e.g., Capilano delta); large Holocene alluvial deposits in the eastern part of the Fraser Lowland.

Hunter *et al.* (2002) developed a V_{s30} map for the FR delta area using a geodataset consisting of 115 S-wave refraction profiles, 88 seismic cone penetration testing (SCPT) logs, and 52 downhole V_s profiles compiled from decades of multi-method V_s profiling by the Geological Survey of Canada (Hunter *et al.* 1998). An amplification hazard map for the District of North Vancouver was developed largely from surficial and bedrock mapping supplemented by ambient vibration array (AVA) V_s profiling at 3 locations, 80 standard penetration tests (SPT), and 90 mHVSr site period measurements (Journey *et al.*, 2015).

Three-component, digital recordings of two earthquakes, the 1996 **M** 5.1 Duvall, Washington earthquake and the 1997 **M** 4.3 Georgia Strait earthquake provided insight into the seismic shaking in the Metro Vancouver area (Cassidy & Rogers, 1999). During the 1996 earthquake, seven strong motion stations were triggered, and 13 were triggered during the 1997 event. Both events produced weak ground motions in the Metro Vancouver area (0.2 – 2.4% g). The resultant spectral ratios demonstrate amplification over a relatively narrow frequency range on the FR delta (1.5 to 4 Hz) with peak amplification of 4-10 relative to competent bedrock for the thick soil delta center sites, and 7-11 for the delta

edge sites (Cassidy and Rogers, 1999). At high frequencies, little or no amplification, or even slight attenuation, is observed (Cassidy and Rogers, 2004).

Other studies have performed site response modelling to demonstrate whether the known ground profile generates the observed amplification. Harris *et al.* (1998) used two 300 m boreholes in the FR delta as models and predicted a significant 1D amplification at longer periods (3.5 to 5 s) in contrast to the observed amplification. Finn *et al.*, (2003) compared theoretical site response analysis in Fraser delta to the 1996 earthquake recordings. They concluded that 1D analysis predicted the recorded response only at deep sites, while neither 1D nor 2D theoretical response predicted the observed amplification at shallow, delta edge sites (Assaf *et al.*, 2018). Uthayakumar & Naesgaard (2004) used 1D equivalent-linear site response analysis to estimate the ground motion amplification at four sites in the Fraser River Delta. They scaled ground motions from California to match the design spectrum and considered input PGA values of 0.23 and 0.5 g. They considered the top of Pleistocene sediments as an elastic half-space and thus did not consider the impact of Pleistocene sediments in their analysis. Kim (2019) developed 6 generic Vs profiles for the Fraser River Delta based on the general Vs-depth relationship of Hunter and Christian (2001) (Figure 2-2). Using a suite of recorded ground motions that cover a range of intensity values and these soil profiles as input to both equivalent-linear and non-linear site response simulations, he clearly demonstrated the effect of Fraser River soil depth on ground motion amplification for certain spectral periods. He found that ground motions for long periods are substantially amplified in the center of the delta, while those for short periods are de-amplified when input rock motions are large.

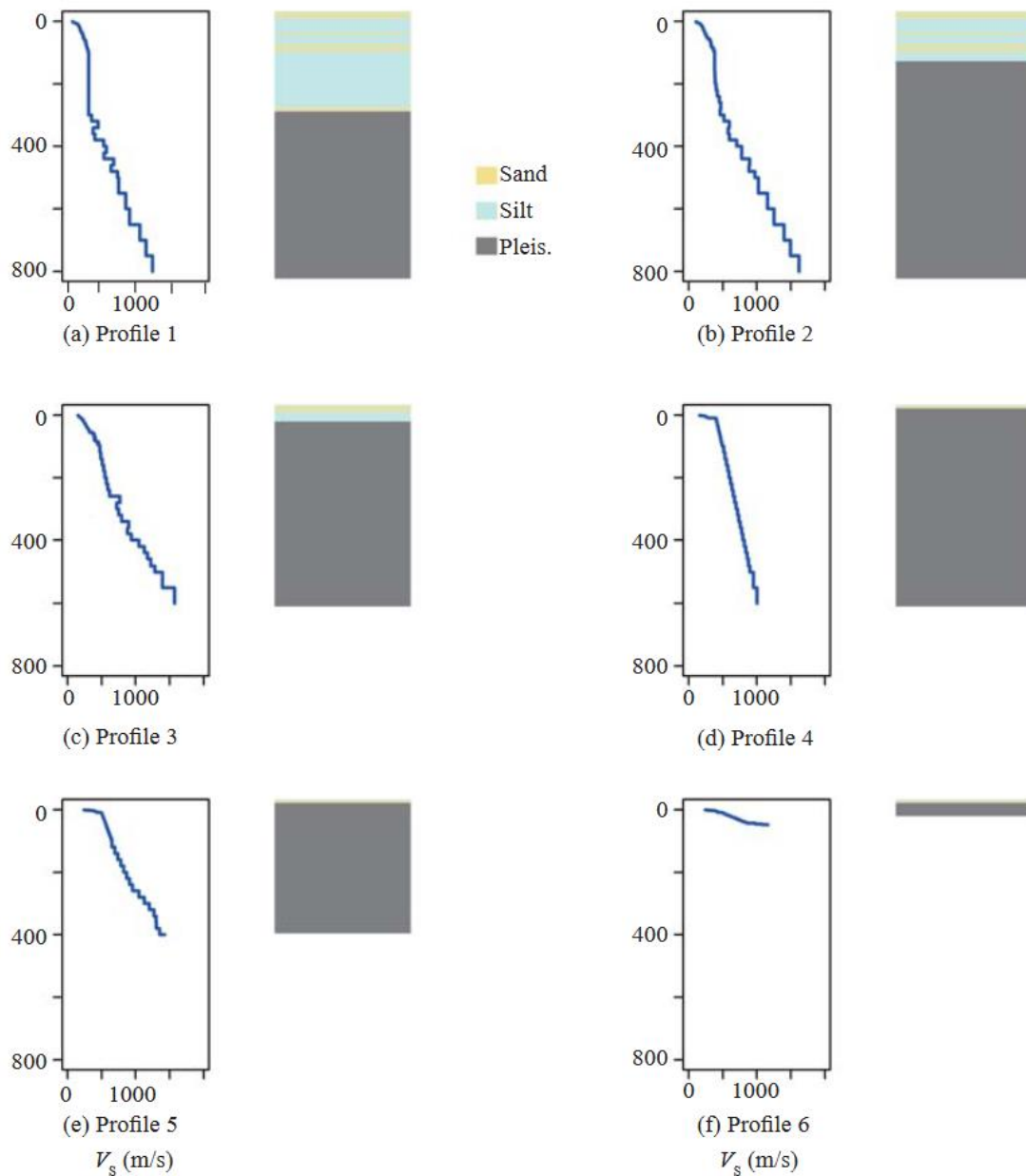


Figure 2-2. Six generic V_s profiles developed by Kim (2019) for the Fraser River Delta. Adapted from Kim (2019).

Trigger-based strong-motion accelerometers recorded 4 moderate earthquakes in Vancouver during the time period from 1976-2001 (Table 2-1) (Assaf *et al.*, 2018). In 2002, the Geological Survey of Canada installed 3-component Internet Accelerometers (IA) which record continuously. Acceleration time histories from three earthquakes have

been recorded in 2011, 2014 and 2015 by the IA network in Metro Vancouver. For all three earthquakes, a time window of 180 s was used to ensure the full energy of the S-wave is captured. Assaf *et al.* (2018, 2022) performed systematic eHVSR analysis of earthquake recordings in Metro Vancouver (Table 4) and major findings are summarized in the following.

Table 2-1. Summary of earthquake events recorded in Metro Vancouver region.

Earthquake	Year	Depth (km)	Moment Magnitude (M)	Distance* (km)
Offshore Vancouver	2015	60	4.7	~70
Vancouver Island	2014	10	6.6	~300
Vancouver Island	2011	22	6.3	~300
Nisqually, WA	2001	52	6.8	~220
Georgia Strait	1997	3	4.3	~40
Duvall, WA	1996	4	5.1	~180
Pender Island	1976	62	5.3	~50

*Distance is from downtown Vancouver to the earthquake's epicentre, rounded to nearest 10 km.

Assaf *et al.*'s (2018, 2022) observations from these earthquake ground motion records were that stations located on stiffer sediments exhibited the lowest amplification. The peak spectral amplitudes for all earthquakes, except for the 2011 and 2014 earthquakes, occur between 2 and 6 Hz. At frequencies greater than 8 Hz, rapid attenuation occurs. The 1996 earthquake spectra are amplified 2 to 4 times at soft soil sites relative to a stiff site (BND). High amplification of up to 10 is observed at both the center and edge of the delta for the 1997 earthquake. Spectral amplitudes of the 2015 earthquake show an amplification of about 2 to 3 at soil sites compared to a firm soil site (VNC22). The response at a delta edge site (MNY) consistently shows similar or higher spectral amplitudes compared to a site in

the middle of the delta, underlain by thick sediments (RMD09). This observation has been related to the large velocity contrast between glacial and post-glacial sediments at shallow depths near the edge of the delta where the two layers pinch out (Cassidy and Rogers, 1999; Rogers *et al.*, 1998).

Recordings of the 2011 and 2014 earthquakes ~300 km away from Vancouver were very weak with peak ground acceleration of 0.2%g (Assaf *et al.*, 2018). In contrast to the previously discussed earthquakes, the peak spectral amplitudes of the 2011 and 2014 earthquakes were between 0.2 and 0.4 Hz and attenuation occurred rapidly above ~1-2 Hz. These earthquakes have significant low frequency content due to their larger magnitude and the long distance travelled; the wavefield content is primarily surface waves. The peak amplification observed at a site in the middle of the delta (RMD09) is about 4 times that of the firm soil site (VNC22) for these earthquakes. This amplification at very low frequencies is consistent with the geology of deep soft sites at the center of the delta (e.g., Harris *et al.*, 1998, Cassidy and Rogers, 2004).

Acquisition of microtremor recordings for mHVSr analysis first occurred in Metro Vancouver in 2002 by the University of British Columbia (UBC) Earthquake Engineering Research Facility (EERF). mHVSr measurements from a subsequent 2004 field campaign by the UBC EERF and S. Molnar (Molnar, 2004; Onur *et al.*, 2004) demonstrate f_{0HV} around 0.2 Hz (5 sec) at sites with the thickest Holocene deposits. This suggests that at thick Fraser River delta sites, the response in the frequency band from 0.15 to 0.4 Hz may be important if an earthquake with substantial energy at these frequencies occurs, e.g., very large earthquakes that create long period surface waves that attenuate slower than body waves. One such possible earthquake that would affect Vancouver is a megathrust at the Cascadia subduction zone.

Molnar *et al.* (2013) show that for sites in the delta, peaks occur in the average mHVSr at 0.35, 1.0 and 4.0 Hz, consistent with eHVSrs from earthquakes recorded in 2004 and 2006. The low frequency (~0.3 Hz) is related to the thick accumulation of Holocene deltaic sediments. The thickest Holocene delta sediments exhibit mHVSr peaks around 0.2 Hz (5 s) (Onur *et al.*, 2004). Molnar (2014a,b) demonstrated that the ~5 km deep, late Cretaceous

Georgia basin, infilled with sedimentary rock and the Pleistocene glacial deposits, increases long period ground motions by an average of 3-4 in Greater Vancouver.

2.4 References

- Arai, H., & Tokimatsu, K. (2000). Effects of Rayleigh and Love waves on microtremor H/V spectra. *12th World Conference on Earthquake Engineering*.
- Arai, H., & Tokimatsu, K. (2004). S-wave velocity profiling by inversion of microtremor H/V spectrum. *Bulletin of the Seismological Society of America*, 94(1), 53-63.
- Armstrong, J. E. (1980a). *Surficial geology, Chilliwack (west half), West of Sixth Meridian, British Columbia*. <https://doi.org/10.4095/108877>
- Armstrong, J. E. (1980b). *Surficial geology, Mission, British Columbia*. <https://doi.org/10.4095/108875>
- Armstrong, J. E. (1984). *Environmental and engineering applications of the Surficial geology of the Fraser Lowland, British Columbia*. <https://doi.org/10.4095/119727>
- Armstrong, J. E. (1990). *Vancouver geology*. Cordilleran Section Geological Association of Canada.
- Armstrong, J. E., & Hicock, S. R. (1979). *Surficial geology, Vancouver, British Columbia*. <https://doi.org/10.4095/108876>
- Armstrong, J. E., & Hicock, S. R. (1980). *Surficial geology, New Westminster, West of Sixth Meridian, British Columbia*. <https://doi.org/10.4095/108874>
- Assaf, J., Molnar, S., & el Nagggar, H. M. (2018). *Comprehensive earthquake site amplification assessment for greater Vancouver*. GeoEdmonton.
- Assaf, J., Molnar, S., El Nagggar, M. H., & Sirohey, A. (2022). Seismic site characterization in Fraser River Delta in Metropolitan Vancouver. *Soil Dynamics and Earthquake Engineering*, 161, 107384.
- Assaf, J., Sirohey, A., Ghofrani, H., Molnar, S. (2022). Compilation and systematic processing of earthquake and microtremor HVSR amplification at Metro Vancouver strong-motion stations. *MVSMP Report 22-05*, 38 pg., ISSN 2816-6027
- Balfour, N. J., Cassidy, J. F., Dosso, S. E., & Mazzotti, S. (2011). Mapping crustal stress and strain in southwest British Columbia. *Journal of Geophysical Research: Solid Earth*, 116(B3).
- Bard, P.-Y. (1999). Microtremor measurements: A tool for site effect estimation? *The Effects of Surface Geology on Seismic Motion*, 3, 1251–1279.

- Bard, P.-Y., Acerra, C., Aguacil, G., Anastasiadis, A., Atakan, K., Azzara, R., Basili, R., Bertrand, E., Bettig, B., Blarel, F., Bonnefoy-Claudet, S., Paola, B., Borges, A., Sørensen, M., Bourjot, L., Cadet, H., Cara, F., Caserta, A., Chatelain, J.-L., & Zacharopoulos, S. (2008). Guidelines for the implementation of the H/V spectral ratio technique on ambient vibrations measurements, processing and interpretation. *Bulletin of Earthquake Engineering*, 6, 1–2.
- Beroya, M. A. A., Aydin, A., Tiglaio, R., & Lasala, M. (2009). Use of microtremor in liquefaction hazard mapping. *Engineering Geology*, 107(3–4), 140–153. <https://doi.org/10.1016/J.ENGGEOL.2009.05.009>
- Bertelli, T. (1872). *Osservazioni sui piccolo movimenti dei pendoli in relazione ad alcuni fenomeni meteorologiche*.
- Bonilla, L. F., Steidl, J. H., Lindley, G. T., Tumarkin, A. G., & Archuleta, R. J. (1997). Site amplification in the San Fernando Valley, California: Variability of site-effect estimation using the S-wave, coda, and H/V methods. *Bulletin of the Seismological Society of America*, 87(3), 710–730. <https://doi.org/10.1785/BSSA0870030710>
- Bonnefoy-Claudet, S., Cotton, F., & Bard, P. Y. (2006). The nature of noise wavefield and its applications for site effects studies: A literature review. *Earth-Science Reviews*, 79(3–4), 205–227. <https://doi.org/10.1016/J.EARSCIREV.2006.07.004>
- Bonnefoy-Claudet, S., Köhler, A., Cornou, C., Wathélet, M., & Bard, P. Y. (2008). Effects of Love Waves on Microtremor H/V Ratio. *Bulletin of the Seismological Society of America*, 98(1), 288–300. <https://doi.org/10.1785/0120070063>
- Bour, M., Fouissac, D., Dominique, P., & Martin, C. (1998). On the use of microtremor recordings in seismic microzonation. *Soil Dynamics and Earthquake Engineering*, 17(7–8), 465–474. [https://doi.org/10.1016/S0267-7261\(98\)00014-1](https://doi.org/10.1016/S0267-7261(98)00014-1)
- Britton, J., Harris, J., Hunter, J., & Luternauer, J. (1995). The bedrock surface beneath the Fraser River delta in British Columbia based on seismic measurements. *Current Research 1995-E, Geological Survey of Canada*, 83–89. <https://doi.org/10.4095/205191>
- Cassidy, J. F., & Rogers, G. C. (1999). Seismic site response in the greater Vancouver, British Columbia, area: spectral ratios from moderate earthquakes. *Canadian Geotechnical Journal*, 36(2), 195–209. <https://doi.org/10.1139/t98-096>
- Cassidy, J. F., & Rogers, G. C. (2004). Variation in ground shaking on the Fraser River delta (Greater Vancouver, Canada) from analysis of moderate earthquakes. *Thirteenth World Conference on Earthquake Engineering*.
- Castellaro, S., & Mulargia, F. (2010). How Far from a Building Does the Ground-Motion Free-Field Start? The Cases of Three Famous Towers and a Modern Building. *Bulletin of the Seismological Society of America*, 100(5A), 2080–2094. <https://doi.org/10.1785/0120090188>

- Castellaro, S., Panzeri, R., Mesiti, F., & Bertello, L. (2015). A surface seismic approach to liquefaction. *Soil Dynamics and Earthquake Engineering*, 77, 35–46. <https://doi.org/10.1016/J.SOILDYN.2015.04.023>
- Chiauzzi, L., Masi, A., Mucciarelli, M., Vona, M., Pacor, F., Cultrera, G., Gallovič, F., & Emolo, A. (2011). Building damage scenarios based on exploitation of Housner intensity derived from finite faults ground motion simulations. *Bulletin of Earthquake Engineering* 2011 10:2, 10(2), 517–545. <https://doi.org/10.1007/S10518-011-9309-8>
- Clague, J. J. (1994). Quaternary stratigraphy and history of south-coastal British Columbia. *Geology and geological hazards of the Vancouver region, southwestern British Columbia. Edited by JW Monger. Geological Survey of Canada, Bulletin, 481*, 181-192.
- Dunn, D., & Ricketts, B. (1994). *Surficial geology of Fraser Lowlands digitized from GSC Maps 1484A, 1485A, 1486A, and 1487A (92 G/1,2,3,6,7; 92 H/4)*. <https://doi.org/10.4095/194084>
- Fäh, D., Kind, F., & Giardini, D. (2001). A theoretical investigation of average HIV ratios. *Geophysical Journal International*, 145(2), 535–549. <https://doi.org/10.1046/J.0956-540X.2001.01406.X>
- Field, E., & Jacob, K. (1993). The theoretical response of sedimentary layers to ambient seismic noise. *Geophysical Research Letters*, 20(24), 2925–2928. <https://doi.org/10.1029/93GL03054>
- Finn, W. D. L., Zhai, E., Thavaraj, T., Hao, X.-S., & Ventura, C. E. (2003). 1-D and 2-D analyses of weak motion data in Fraser Delta from 1966 Duvall earthquake. *Soil Dynamics and Earthquake Engineering*, 23(4), 323–329. [https://doi.org/10.1016/S0267-7261\(02\)00207-5](https://doi.org/10.1016/S0267-7261(02)00207-5)
- Gorstein, M., & Ezersky, M. (2015). Combination of HVSR and MASW Methods to Obtain Shear Wave Velocity Model of Subsurface in Israel. *International Journal of Georesources and Environment - IJGE (Formerly Int'l J of Geohazards and Environment)*, 1(1), 1-1):20-41. <https://doi.org/10.15273/IJGE.2015.01.004>
- Gutenberg, B. (1958). Microseisms. *Advances in Geophysics*, 5(C), 53–92. [https://doi.org/10.1016/S0065-2687\(08\)60075-8](https://doi.org/10.1016/S0065-2687(08)60075-8)
- Haghshenas, E., Bard, P.-Y., Theodulidis, N., & Team, S. W. (2008). Empirical evaluation of microtremor H/V spectral ratio. *Bulletin of Earthquake Engineering*, 6(1), 75–108. <https://doi.org/10.1007/s10518-007-9058-x>
- Harris, J., Hunter, J., Luternauer, J. L., & Finn, L. (1998). Site amplification modelling of the Fraser delta, British Columbia. *Bulletin - Geological Survey of Canada*, 211–216.
- Hassani, B., Yong, A., Atkinson, G. M., Feng, T., & Meng, L. (2019). Comparison of Site Dominant Frequency from Earthquake and Microseismic Data in California. *Bulletin of*

the Seismological Society of America, 109(3), 1034–1040.
<https://doi.org/10.1785/0120180267>

Hinzen, K. G., Weber, B., & Scherbaum, F. (2004). On the resolution of H/V measurements to determine sediment thickness, a case study across a normal fault in the lower Rhine embayment, Germany. *Journal of Earthquake Engineering*, 8(6), 909–926.
<https://doi.org/10.1142/S136324690400178X>

Hunter, J. A., Benjumea, B., Harris, J. B., Miller, R. D., Pullan, S. E., Burns, R. A., & Good, R. L. (2002). Surface and downhole shear wave seismic methods for thick soil site investigations. *Soil Dynamics and Earthquake Engineering*, 22(9–12), 931–941.
[https://doi.org/10.1016/S0267-7261\(02\)00117-3](https://doi.org/10.1016/S0267-7261(02)00117-3)

Hunter, J. A., Burns, R. A., Good, R. L., & Pelletier, C. F. (1998). A compilation of shear wave velocities and geophysical logs in unconsolidated sediments of the Fraser River delta. In *Geological Survey of Canada, Open File 3622*.

Hunter, J. A., & Christian, H. A. (2001, March). Use of shear wave velocities to estimate thick soil amplification effects in the Fraser River delta, British Columbia. *Fourteenth EEGS Symposium on the Application of Geophysics to Engineering and Environmental Problems*.

Hunter, J., Crow, H., Brooks, G., Pyne, M., Motazedian, D., Lamontagne, M., Pugin, A., Pullan, S., Cartwright, T., Douma, M., Burns, R., Good, R., Kaheshi-Banab, K., Caron, R., Kolaj, M., Folahan, I., Dixon, L., Dion, K., Duxbury, A., & Muir, D. (2010). *Seismic site classification and site period mapping in the Ottawa area using geophysical methods*.

Jackson, F., Molnar, S., Ghofrani, H., Atkinson, G. M., Cassidy, J. F., & Assatourians, K. (2017). Ground motions of the December 2015 M 4.7 Vancouver Island earthquake: Attenuation and site response. *Bulletin of the Seismological Society of America*, 107(6), 2903–2916.

Jakica, S. (2018, May). *Using Passive Seismic to Estimate the Thickness of the Leonora Breakaways, Western Australia*.

Javanbakht, Alireza & Molnar, Sheri & Sadrekarimi, Abouzar & Adhikari, Sujun. (2021). Liquefaction severity maps in a probabilistic ground motion environment for Richmond, British Columbia, Canada.

Journey, J. M., Dercole, F., Mason, D., Westin, M., & Prieto, J. A. (2015). A profile of earthquake risk for the district of North Vancouver, British Columbia. In *Geological Survey of Canada, Open File 7677*.

Kamarudin, A. F., Daud, M. E., Ibrahim, Z., & Ibrahim, A. (2016). Sustainable Non-destructive Technique Ambient Vibrations for Ground Assessments. *Procedia - Social and Behavioral Sciences*, 216, 701–711. <https://doi.org/10.1016/J.SBSPRO.2015.12.064>

- Kanai, K., & Tanaka, T. (1961). On microtremor VIII. *Bulletin, Earthquake Institute*, 39, 97–114.
- Kawase, H., Matsushima, S., Satoh, T., & Sánchez-Sesma, F. J. (2015). Applicability of Theoretical Horizontal-to-Vertical Ratio of Microtremors Based on the Diffuse Field Concept to Previously Observed Data. *Bulletin of the Seismological Society of America*, 105(6), 3092–3103. <https://doi.org/10.1785/0120150134>
- Kawase, H., Mori, Y., & Nagashima, F. (2018). Difference of horizontal-to-vertical spectral ratios of observed earthquakes and microtremors and its application to S-wave velocity inversion based on the diffuse field concept. *Earth, Planets and Space*, 70(1), 1–32. <https://doi.org/10.1186/S40623-017-0766-4/TABLES/6>
- Kawase, H., Nagashima, F., Nakano, K., & Mori, Y. (2019). Direct evaluation of S-wave amplification factors from microtremor H/V ratios: Double empirical corrections to “Nakamura” method. *Soil Dynamics and Earthquake Engineering*, 126, 105067. <https://doi.org/10.1016/J.SOILDYN.2018.01.049>
- Kawase, H., Sánchez-Sesma, F. J., & Matsushima, S. (2011). The Optimal Use of Horizontal-to-Vertical Spectral Ratios of Earthquake Motions for Velocity Inversions Based on Diffuse-Field Theory for Plane Waves. *Bulletin of the Seismological Society of America*, 101(5), 2001–2014. <https://doi.org/10.1785/0120100263>
- Kim, B. (2019). Mapping of ground motion amplifications for the Fraser River delta in Greater Vancouver, Canada. *Earthquake Engineering and Engineering Vibration 2019* 18:4, 18(4), 703–717. <https://doi.org/10.1007/S11803-019-0531-8>
- Knapmeyer-Endrun, B. (2010). Love wave contribution to the ambient vibration H/V amplitude peak observed with array measurements. *Journal of Seismology*, 15, 443–472. <https://doi.org/10.1007/s10950-010-9191-x>
- Köhler, A., Ohrnberger, M., Scherbaum, F., Wathelet, M., & Cornou, C. (2007). Assessing the reliability of the modified three-component spatial autocorrelation technique. *Geophysical Journal International*, 168(2), 779–796.
- Konno, K., & Omachi, T. (1998). Ground-motion characteristics estimated from spectral ratio between horizontal and vertical components of microtremors. *Bulletin of the Seismological Society of America*, 88(1), 228–241.
- Lachet, C. D., & Bard, P.-Y. (1994). Numerical and Theoretical Investigations on the Possibilities and Limitations of Nakamura’s Technique. *Journal of Physics of the Earth*, 42, 377–397. <https://doi.org/10.4294/jpe1952.42.377>
- Lermo Samaniego, J., & J Chavez- Garcia, F. (1994). Are microtremors useful in site response evaluation? *Bulletin of the Seismological Society of America*, 84, 1350–1364.
- Leyton, F., Ruiz, S., Sepúlveda, S. A., Contreras, J. P., Rebolledo, S., & Astroza, M. (2013). Microtremors’ HVSR and its correlation with surface geology and damage observed after

- the 2010 Maule earthquake (Mw 8.8) at Talca and Curicó, Central Chile. *Engineering Geology*, 161, 26–33. <https://doi.org/10.1016/J.ENGGEOL.2013.04.009>
- Lontsi, A. M., Sánchez-Sesma, F. J., Molina-Villegas, J. C., Ohrnberger, M., & Krüger, F. (2015). Full microtremor H/V(z, f) inversion for shallow subsurface characterization. *Geophysical Journal International*, 202(1), 298–312. <https://doi.org/10.1093/GJI/GGV132>
- Lunedei, E., & Albarello, D. (2010). Theoretical HVSR curves from full wavefield modelling of ambient vibrations in a weakly dissipative layered Earth. *Geophysical Journal International*, 181(2), 1093–1108.
- Macau, A., Benjumea, B., Gabàs, A., Figueras, S., & Vilà, M. (2014). The Effect of Shallow Quaternary Deposits on the Shape of the H/V Spectral Ratio. *Surveys in Geophysics 2014 36:1*, 36(1), 185–208. <https://doi.org/10.1007/S10712-014-9305-Z>
- Malischewsky, P. G., & Scherbaum, F. (2004). Love's formula and H/V-ratio (ellipticity) of Rayleigh waves. *Wave Motion*, 40(1), 57–67. <https://doi.org/10.1016/J.WAVEMOTI.2003.12.015>
- Matsushima, S., Hirokawa, T., de Martin, F., Kawase, H., & Sánchez-Sesma, F. J. (2014). The Effect of Lateral Heterogeneity on Horizontal-to-Vertical Spectral Ratio of Microtremors Inferred from Observation and Synthetics. *Bulletin of the Seismological Society of America*, 104(1), 381–393. <https://doi.org/10.1785/0120120321>
- Matsushima, S., Kosaka, H., & Kawase, H. (2017). Directionally dependent horizontal-to-vertical spectral ratios of microtremors at Onahama, Fukushima, Japan. *Earth, Planets and Space*, 69(1), 1–12. <https://doi.org/10.1186/S40623-017-0680-9/FIGURES/15>
- Michel, C., Guéguen, P., el Arem, S., Mazars, J., & Kotronis, P. (2010). Full-scale dynamic response of an RC building under weak seismic motions using earthquake recordings, ambient vibrations and modelling. *Earthquake Engineering & Structural Dynamics*, 39(4), 419–441. <https://doi.org/10.1002/EQE.948>
- Mohamed, A. A., Helal, A. M. A., Mohamed, A. M. E., Shokry, M. M. F., & Ezzelarab, M. (2019). Effects of surface geology on the ground-motion at New Borg El-Arab City, Alexandria, Northern Egypt. <https://doi.org/10.1016/j.Nrjag.2015.11.005>, 5(1), 55–64. <https://doi.org/10.1016/J.NRJAG.2015.11.005>
- Molnar, S., & Cassidy, J. F. (2006). A Comparison of Site Response Techniques Using Weak-Motion Earthquakes and Microtremors. *Earthquake Spectra*, 22(1), 169–188. <https://doi.org/10.1193/1.2160525>
- Molnar, S., Cassidy, J., Olsen, K. B., Dosso, S. E., & J. He, (2014a). Earthquake Ground Motion and 3D Georgia Basin Amplification in Southwest British Columbia: Shallow Blind-Thrust Scenario Earthquakes. *Bulletin of the Seismological Society of America*, 104, 1. <https://doi.org/10.1785/0120130116>

- Molnar, S., Crow, H., Ventura, C. E., Finn, W. D. L., Stokes, T., Lapcevic, P., & Paradis, D. (2014b). Regional seismic hazard assessment for small urban centers in Western Canada. *10th National Conference in Earthquake Engineering*.
- Molnar, S., Dosso, S. E., & Cassidy, J. F. (2013). Uncertainty of linear earthquake site amplification via Bayesian inversion of surface seismic data. *Earthquake site amplification uncertainty. Geophysics, 78*(3), WB37–WB48. <https://doi.org/10.1190/GEO2012-0345.1>
- Monahan, P. A., & Levson, V. M. (2001). Development of a shear-wave velocity model of the near-surface deposits of southwestern British Columbia, Canada. *Fourth International Conference on Recent Advances in Geotechnical Earthquake Engineering*.
- Monahan, P. A., Luternauer, J. L., & Barrie, J. V. (1993). A delta plain sheet sand in the Fraser River delta, British Columbia, Canada. *Quaternary International, 20*(C), 27–38. [https://doi.org/10.1016/1040-6182\(93\)90034-D](https://doi.org/10.1016/1040-6182(93)90034-D)
- Monger, J. W. H., & Journeay, J. M. (1994). *Guide to the geology and tectonic evolution of the southern Coast Mountains*. <https://doi.org/10.4095/194829>
- Mustard, P. S. (1994). *The Upper Cretaceous Nanaimo Group, Georgia Basin*. <https://doi.org/10.4095/203246>
- Nakamura, Y. (1989). A method for dynamic characteristics estimation of subsurface using microtremor on the ground surface. *Quarterly Report of RTRI (Railway Technical Research Institute) (Japan), 30*.
- Nakamura, Y. (2000). Clear identification of fundamental idea of Nakamura's technique and its applications. *12th World Conference on Earthquake Engineering*.
- Nakamura, Y. (2008). On the H/V spectrum. *14th World Conference on Earthquake Engineering, 12–17*.
- Nogoshi, M., & Igarashi, T. (1971). On the Amplitude Characteristics of Microtremor (Part 2). *Journal of the Seismological Society of Japan, 24*, 26–40. https://doi.org/10.4294/zisin1948.24.1_26
- Natural Resources Canada. (2016). Earthquake Hazards and Risks. Retrieved July 7, 2022, from http://www.earthquakescanada.ca/hazard-alea/earthquake_hazards_risks.pdf
- Okada, H., & Suto, K. (2003). *The microtremor survey method*. Society of Exploration Geophysicists.
- Oliveira, C. S., & Navarro, M. (2009). Fundamental periods of vibration of RC buildings in Portugal from in-situ experimental and numerical techniques. *Bulletin of Earthquake Engineering 2009 8:3, 8*(3), 609–642. <https://doi.org/10.1007/S10518-009-9162-1>

- Omori, F. (1909). Preliminary report on the Messina-Reggio earthquake of Dec. 28, 1908. *Bulletin of the Imperial Earthquake Investigation Committee*, 3(2), 37–45. <https://ci.nii.ac.jp/naid/110006606486/>
- Onur, T., Molnar, S., Cassidy, J., Ventura, C., & Hao, K. X. S. (2004). Estimating site periods in Vancouver and Victoria, British Columbia using microtremor measurements and SHAKE analyses. *Canadian Geotechnical Conference, Quebec City, Quebec*, 24–27.
- Parolai, S., Bormann, P., & Milkereit, C. (2002). New Relationships between Vs, Thickness of Sediments, and Resonance Frequency Calculated by the H/V Ratio of Seismic Noise for the Cologne Area (Germany). *Bulletin of the Seismological Society of America*, 92(6), 2521–2527. <https://doi.org/10.1785/0120010248>
- Picozzi, M., Parolai, S., Bindi, D., & Strollo, A. (2009). Characterization of shallow geology by high-frequency seismic noise tomography. *Geophysical Journal International*, 176(1), 164–174.
- Pilz, M., Parolai, S., Leyton, F., Campos, J., & Zschau, J. (2009). A comparison of site response techniques using earthquake data and ambient seismic noise analysis in the large urban areas of Santiago de Chile. *Geophysical Journal International*, 178(2), 713–728.
- Pratt, T. L. (2018). Characterizing and Imaging Sedimentary Strata Using Depth-Converted Spectral Ratios: An Example from the Atlantic Coastal Plain of the Eastern United States. *Bulletin of the Seismological Society of America*, 108(5A), 2801–2815. <https://doi.org/10.1785/0120180046>
- Roddick, J. A. (1965). *Vancouver North, Coquitlam, and Pitt Lake map Areas, British Columbia With Special Emphasis On the Evolution of the Plutonic Rocks*. <https://doi.org/10.4095/100559>
- Rogers, G. C. (1998). *Earthquakes and earthquake hazard in the Vancouver area*. <https://doi.org/10.4095/210034>
- Salameh, C., Guillier, B., Harb, J., Cornou, C., Bard, P. Y., Voisin, C., & Mariscal, A. (2016). Seismic response of Beirut (Lebanon) buildings: instrumental results from ambient vibrations. *Bulletin of Earthquake Engineering* 2016 14:10, 14(10), 2705–2730. <https://doi.org/10.1007/S10518-016-9920-9>
- Sánchez-Sesma, F. J., Rodríguez, M., Iturrarán-Viveros, U., Luzón, F., Campillo, M., Margerin, L., García-Jerez, A., Suarez, M., Santoyo, M. A., & Rodríguez-Castellanos, A. (2011). A theory for microtremor H/V spectral ratio: application for a layered medium. *Geophysical Journal International*, 186(1), 221–225. <https://doi.org/10.1111/J.1365-246X.2011.05064.X>
- Scheib, A., Morris, P., Murdie, R., & Delle Piane, C. (2016). A passive seismic approach to estimating the thickness of sedimentary cover on the Nullarbor Plain, Western Australia. <Http://Dx.Doi.Org/10.1080/08120099.2016.1233455>, 63(5), 583–598. <https://doi.org/10.1080/08120099.2016.1233455>

- Scherbaum, F., Hinzen, K. G., & Ohrnberger, M. (2003). Determination of shallow shear wave velocity profiles in the Cologne, Germany area using ambient vibrations. *Geophysical Journal International*, 152(3), 597–612.
- Seed, H. B., Ugas, C., & Lysmer, J. (1976). Site-dependent spectra for earthquake-resistant design. *Bulletin of the Seismological Society of America*, 66(1), 221–243. <https://doi.org/10.1785/BSSA0660010221>
- Seht, M. I. von, & Wohlenberg, J. (1999). Microtremor measurements used to map thickness of soft sediments. *Bulletin of the Seismological Society of America*, 89(1), 250–259. <https://doi.org/10.1785/BSSA0890010250>
- Smith, N. R. A., Reading, A. M., Asten, M. W., & Funk, C. W. (2013). Constraining depth to basement for mineral exploration using microtremor: A demonstration study from remote inland Australia Using microtremor for mineral exploration. *Geophysics*, 78(5), B227–B242. <https://doi.org/10.1190/GEO2012-0449.1>
- Stephenson, W. J., Odum, J. K., Asten, M. W., & Frankel, A. D. (2019). Shear-Wave Velocity in the Seattle Basin to 2 km Depth Characterized with the krSPAC Microtremor Array Method: Insights for Urban Basin-Scale Imaging. *Seismological Research Letters*, 90(3), 1230–1242. <https://doi.org/10.1785/0220180194>
- Teague, D. P., Cox, B. R., & Rathje, E. M. (2018). Measured vs. predicted site response at the Garner Valley Downhole Array considering shear wave velocity uncertainty from borehole and surface wave methods. *Soil Dynamics and Earthquake Engineering*, 113, 339–355. <https://doi.org/10.1016/J.SOILDYN.2018.05.031>
- Uthayakumar, U. M., & Naesgaard, E. (2004). Ground response analysis for seismic design in Fraser River Delta, British Columbia. *13th World Conference on Earthquake Engineering*, 1–6.
- Vantassel, J., Cox, B., Wotherspoon, L., & Stolte, A. (2018). Mapping Depth to Bedrock, Shear Stiffness, and Fundamental Site Period at CentrePort, Wellington, Using Surface-Wave Methods: Implications for Local Seismic Site Amplification. *Bulletin of the Seismological Society of America*, 108. <https://doi.org/10.1785/0120170287>
- Wollery, W. W., & Street, R. (2002). 3D near-surface soil response from H/V ambient-noise ratios. *Soil Dynamics and Earthquake Engineering*, 22(9–12), 865–876. [https://doi.org/10.1016/S0267-7261\(02\)00109-4](https://doi.org/10.1016/S0267-7261(02)00109-4)
- Wotherspoon, L., Bradley, B., Thomson, E., Hills, A., Jeong, S., Wood, C., & Cox, B. (2015, April). *Development of deep V S profiles and site periods for the Canterbury region*.
- Yamamoto, H. (2000). Yamamoto, H. (2000). Estimation of shallow S-wave velocity structures from phase velocities of Love- and Rayleigh-waves in microtremors. *12th World Conference on Earthquake Engineering*.

Zor, E., Özalaybey, S., Karaaslan, A., Tapirdamaz, M. C., Özalaybey, S. Ç., Tarancioğlu, A., & Erkan, B. (2010). Shear wave velocity structure of the Izmit Bay area (Turkey) estimated from active-passive array surface wave and single-station microtremor methods. *Geophysical Journal International*, 182(3), 1603–1618.

Chapter 3

3 Impact of Experimental and Processing Choices on mHVSr Results

Minimizing the influence of acquisition and processing choices on the resulting mHVSr amplification spectrum is important for mHVSr interpretation. The objective of this chapter is to review existing literature to summarize the existing recommendations for the experimental setup and processing of mHVSr data, then to use a large database of more than 5000 single-station mHVSr measurements acquired since the early 2000s in the Metro Vancouver region to reassess these choices/parameters and ultimately provide a recommended workflow for acquisition and processing mHVSr data to ensure mHVSrs are obtained using a standardized procedure and can be replicated by any practitioner.

3.1 Introduction

The earthquake shaking experienced at a site is the convolution of source, path, and local site effects. One aspect of local site effects is 1D site amplification, which refers to the increase in the amplitude of seismic waves as they pass through soil layers close to the Earth's surface (Safak, 2001). The increase in amplitude towards surface is a result of decreasing seismic impedance (Z), defined as the product of the mass density (ρ) and wave propagation velocity (V_s) of the surficial layers compared to deeper layers,

$$Z = V_s \times \rho. \quad \text{equation 3-1}$$

In addition, resonance-based amplification will occur at select frequencies (1/period) due to the seismic site conditions,

$$f_n = (2n+1)(V_{s_{ave}}/4h), \text{ for } n=0, 1, 2, \text{ etc.} \quad \text{equation 3-2}$$

where $V_{s_{ave}}$ is the average shear-wave velocity of the layer overlying bedrock and h is soil layer thickness. Other factors that influence earthquake shaking locally include wave focusing, rupture directivity, basin geometry, and topography.

To understand differences in site conditions that result in variations in site effects, the standard spectral ratio (SSR) method was introduced by Borchardt (1970). The method involves using spectral ratios calculated by taking the ratio of the Fourier amplitude spectrum (FAS) of a ground motion record at a soil site to that of a reference (i.e., a rock) site's record. In general, the method is valid if the distance between the two sites is much smaller than the epicentral distance, so one can assume the differences in observed ground motion are only due to local site effects. This method has several limitations including difficulties in finding a suitable reference site and the scarcity of good quality ground motion records; particularly in regions which experience low-to-intermediate seismicity (Archuleta *et al.*, 1992, Lachet & Bard, 1994, Field & Jacob, 1995). The spectral ratio between borehole and surface sensors (e.g., Kitagawa *et al.*, 1988, Satoh *et al.*, 1995, Steidl *et al.*, 1996, Bonilla *et al.*, 2002) overcomes the issues of having a suitable nearby reference site, however, this method has difficulties in terms of eliminating the effects of reflected waves contained in the observed borehole seismograms (Steidl *et al.* 1996, Tao and Rathje 2020) and can be more expensive.

The receiver function technique was introduced by Langston (1977, 1979). Originally it was pitched as a technique to determine crustal velocity structure from S-wave conversion of teleseismic, steeply incident P-waves. The method was adapted for use with earthquake ground motion records to study site effects and led to the development of the eHVSR method (e.g., Lermo and Chavez-Garcia, 1993). The fundamental assumption of the method is that the vertical component of motion is not influenced by local structure and soil conditions, whereas the horizontal components contain the P-to-S conversions due to local geological layering (Strollo, 2010). Field & Jacob (1995) showed that the earthquake HVSR ratios (eHVSR) for S-waves reveal the overall frequency dependence of site response. This does not hold true for P-waves. Although this technique addresses the issue of not having a suitable reference site, it does not address the issue of absence of ground motion data in low-to-moderate seismicity regions, nor the fact that the assumption of the vertical component being unaffected by site effects is not universally applicable.

The Metro Vancouver region is one of the most seismically active regions in Canada. The geology of Metro Vancouver also varies significantly. The general stratigraphic profile is

of softer, post-glacial deposits overlying stiffer, glacial deposits overlying Early Cretaceous sedimentary bedrock of the Georgia sedimentary basin. Early Cretaceous sedimentary rocks are exposed in sea cliffs and along steep slopes of the Fraser Lowland and older plutonic granitic rocks outcrop in the North Shore mountains. Pleistocene (glacial) sediments are present at surface in the uplands across Burnaby and Vancouver. Proglacial Quadra sand deposits are found around Vancouver, West and North Vancouver. These proglacial deposits were covered by glacial till and gravelly ice-contact sediments of the Pleistocene epoch (Armstrong, 1990). These Quaternary sediments of three major glaciations covered the irregular, glacier-eroded bedrock. South of Vancouver, the Holocene Fraser River (FR) delta is a lowland region with deltaic silts and sands up to 300 m thick (Roger, 1998). Quaternary sediments have a maximum thickness of 800-1000 m in the central FR delta beneath Ladner (Hunter *et al.*, 1998). The unconformities between these sedimentary packages give rise to significant impedance contrasts, yielding the mHVSr method as a useful tool for seismic site characterization and seismic microzonation mapping in the region.

The quantity of strong-motion instrumentation in Metro Vancouver has increased from < 10 trigger-based accelerometers in the 1970's to ~100 accelerometers operating currently (Cassidy *et al.* 2019). The Geologic Survey of Canada through the Pacific Geoscience Center has maintained an urban Strong Motion Network in BC since 2003 (Kaya *et al.*, 2017). The Canadian National Seismograph Network maintains a network of permanent high gain (short period and broadband) weak motion and low gain strong motion stations in Canada, including in British Columbia (NRCAN, 1975). However, earthquake recordings within Metro Vancouver (Assaf *et al.* 2022) are weak in terms of amplitude (highest recorded PGA of 0.55 g) and quantity (~10 earthquakes have generated useable recordings), complicating the process of studying earthquake site effects.

Based on the work of Kanai & Tanaka (1961) and Nogoshi and Igarashi (1971), Nakamura (1989) popularized the microtremor horizontal to vertical ratio (mHVSr) method. The method itself requires a single tri-axial ground motion sensor. The ground motion records are processed, transformed into the frequency domain, and a ratio of the horizontal to vertical component spectra is calculated. As with the eHVSr, the fundamental assumption

of the mHVSR method is that the vertical component is free of site effects. The method has several advantages over both the SSR and eHVSR methods, due to its ease of implementation as well as its universal applicability in that, its use is not limited to available earthquake records, seismic microtremors are ubiquitous. During the past several decades, the method has been used extensively for seismic microzonation as well as site effect studies (e.g., Chávez-García & Bard, 1994, Guéguen *et al.*, 2000, Duval *et al.*, 2001, Alfaro *et al.*, 2002, Guillier *et al.*, 2004, Panou *et al.*, 2005, Chatelain *et al.*, 2008, Bensalem *et al.*, 2010, Hellel *et al.*, 2010).

The SH-wave transfer function, or site amplification spectrum, quantifies frequency-dependent 1D seismic site effects. The transfer function also provides the SH-wave resonant frequency of the soil column (f_0) and its corresponding amplification factor (A_0). The f_0 measure is increasingly being used as a site term parameter in ground motion models (GMMs) and seismic site classification in building codes. Theoretically, for a simple model comprised of a single, laterally homogenous layer overlying a half-space, f_0 is

$$f_0 = \frac{V_{save}}{4h}, \quad \text{equation 3-3}$$

where V_{save} is the soil layer's average shear wave velocity, and h is the thickness of the overlying layer (Haskell, 1960). Although the site effects measured by the mHVSR amplification spectrum are related to the full 3D geology, as well as possible topographic effects, most often when interpreting an mHVSR measurement it is assumed that the resultant measurement primarily reflects the impedance structure of the subsurface.

The SESAME guidelines (Bard *et al.*, 2004) provide recommendations on suitable equipment and deployment and acquisition selections, as well as processing parameter choices and basic interpretation of the mHVSR. Many studies (Bard, 1999; Lachet & Bard, 1994; Lermo & Chavez- Garcia, 1994) have shown that for sites with a strong impedance contrast, the peak frequency interpreted from the mHVSR closely corresponds to f_0 at a site determined from eHVSR or SSR, whereas the mHVSR amplification had less correlation with eHVSR and SSR. As such, the major information extracted from an mHVSR measurement is an estimate of f_0 (i.e., f_{0HV}) at a site. Due to ambiguity regarding the wavefield composition of microtremors, as well as uncertainty regarding whether the

vertical component motion is truly free from site effects, A_0 cannot be reliably extracted from an mHVSr (Lachet & Bard, 1994, Fäh *et al.*, 2001, Malischewsky & Scherbaum, 2004, Bonnefoy-Claudet *et al.*, 2008, Sánchez-Sesma *et al.*, 2011). In contrast, mHVSrs provide a reliable measure of f_0 and A_0 for most sites across Canada due to multiple glaciations that have generated strong seismic impedance contrasts (see Molnar *et al.* 2020 and references therein).

3.2 mHVSr Database

From 2002 until 2021, several mHVSr field campaigns were completed to acquire single station microtremor measurements throughout the Metro Vancouver region. Microtremor measurements were first obtained in May and June 2002 at 48 Canadian Urban Seismic Program (CUSP) proposed strong motion sites by the UBC EERF at 1 km spacing in an area spanning 6 by 8 km (Onur *et al.*, 2004). The hardware used for the microtremor measurements consisted of two horizontal and one vertical velocity transducers, an amplifier, an analog-to-digital converter and a computer for 5-minutes duration data acquisition. These measurements are not included in the present work because the digital data files were not accessible. In 2004, 20 of the southernmost CUSP sites on the FR delta were revisited by S. Molnar for the UBC EERF with a three-component broadband seismometer to confirm the presence of a low frequency peak. During the 2004 campaign, microtremors were recorded for at least 30 minutes. An Orion seismic recorder and a Guralp CMG-40T sensor were used. The original data are in Seismic Analysis Code (SAC) format.

Between 2009 and 2011, microtremor testing was accomplished by the UBC EERF in North Vancouver, the District of North Vancouver, Vancouver City, West Vancouver, and Richmond. Testing was performed using three Pinocchio Data Systems three-component velocity transducers. Whenever possible, measurements were accomplished on concrete or asphalt to ease sensor installation. During the summer of 2012, microtremor testing was completed throughout Metro Vancouver, directed by S. Molnar as a postdoctoral fellow at the UBC EERF, as a continuation to the testing campaign from 2009 to 2011. Measurements were obtained along a 500 by 700 m grid, using three-component Tromino® short-period seismometers (<http://moho.world/en/>) (TEP Engineering version,

referred to as ‘old’ Tromino®). Whenever possible, two Trominos were placed side by side on different surfaces at a site, e.g., sidewalk concrete vs. dirt with grass removed.

As part of a multi-year seismic microzonation project (2017-2024), microtremor measurements were acquired throughout Metro Vancouver during the summers of 2018 to 2021 by the University of Western Ontario’s Good Vibrations and Excitations laboratory at a nominal grid spacing of 600 m. Most measurements were obtained with Tromino® seismometers (TE3 version, referred to as ‘new’ Tromino® as well as the older TEP version). Guralp CMP-40T broadband sensors combined with a Nanometrics Taurus digitizer were employed at select locations to validate low frequency peaks obtained using Tromino® seismometers. In addition to the single-station measurements, passive microtremor array measurements were acquired using the same Tromino seismometers at 117 sites during the 2018 to 2021 summer field campaigns. At each array site approximately 28 single-station microtremor measurements were obtained, typically in circular array geometries with 30 m maximum radius.

A total of more than 5000 individual microtremor measurements from the described campaigns (Table 3-1) are assembled into a database for mHVSr analysis. More than 2000 unique mHVSr locations are shown in Figure 3-1; array sites with multiple recordings are shown by a single location. Given the variability in instrumentation and experimental setup over time, the compiled microtremor database provides an opportunity to investigate the impact of processing and acquisition parameters on the final mHVSr.

Table 3-1. Summary of mHVSr field campaigns occurring between 2002 and 2021.

Year	Area	Seismic sensor	Duration & Sampling Rate	Approx. grid resolution	Number of sites	Digital data avail.
2002	Southern Vancouver & Richmond	1-Hz velocity transducers	5-min @ 100 Hz	1000 x 1000 m	48	N
2004	Richmond	Guralp broadband CMG-40T and 1-Hz velocity transducers	30-min @ 100 Hz	1000 x 1000 m	20	Y
2009	West Vancouver	Pinocchio 1-Hz velocity sensors	10-20 min @ 100 Hz	500-750 x 600 m	40	Y
2009	North Vancouver	Pinocchio 1-Hz velocity sensors	10-20 min @ 100 Hz	500-750 x 600 m	66	Y
2009	Downtown & Stanley Park	Pinocchio 1-Hz velocity sensors	10-20 min @ 100 Hz	Sporadic	21	Y
2010-2011	Richmond	Pinocchio 1-Hz velocity sensors	30-min	~ 800 m	116	Y
2012	Vancouver Airport (YVR) Island	Tromino 1-Hz velocity sensors	30-min @ 128 Hz	Sporadic	17	N
2012	UBC	Tromino 1-Hz velocity sensors	16-min @ 128 Hz	100 x 400 m	100	Y
2012	Central Vancouver	Tromino 1-Hz velocity sensors	16-min @ 128 Hz	500 x 700 m	515	Y
2012	Burnaby	Tromino 1-Hz velocity sensors	16-min @ 128 Hz	500 x 700 m	150	Y
2018	Metro Vancouver	Tromino 1-Hz velocity sensors Guralp CMG-40T	15-60 min @ 100-200 Hz	Roughly 600 x 600 m	727	Y
2019	Metro Vancouver	Tromino 1-Hz velocity sensors Guralp 6T Medium Motion Seismometer Nanometrics Trillium Compact Posthole 20-s Seismometer	15-60 min @ 100-128 Hz	Roughly 600 x 600 m Sporadic	731	Y
2020	Surrey	Tromino 1-Hz velocity sensors	15-60 min @ 128 Hz	-	353	Y
2021	Metro Vancouver	Tromino 1-Hz velocity sensors	15-60 min @ 128 Hz	-	225	Y
2018-2021	Metro Vancouver (passive AVA array sites)	Tromino 1-Hz velocity sensors	15-60 min @ 128 Hz	-	3464	Y

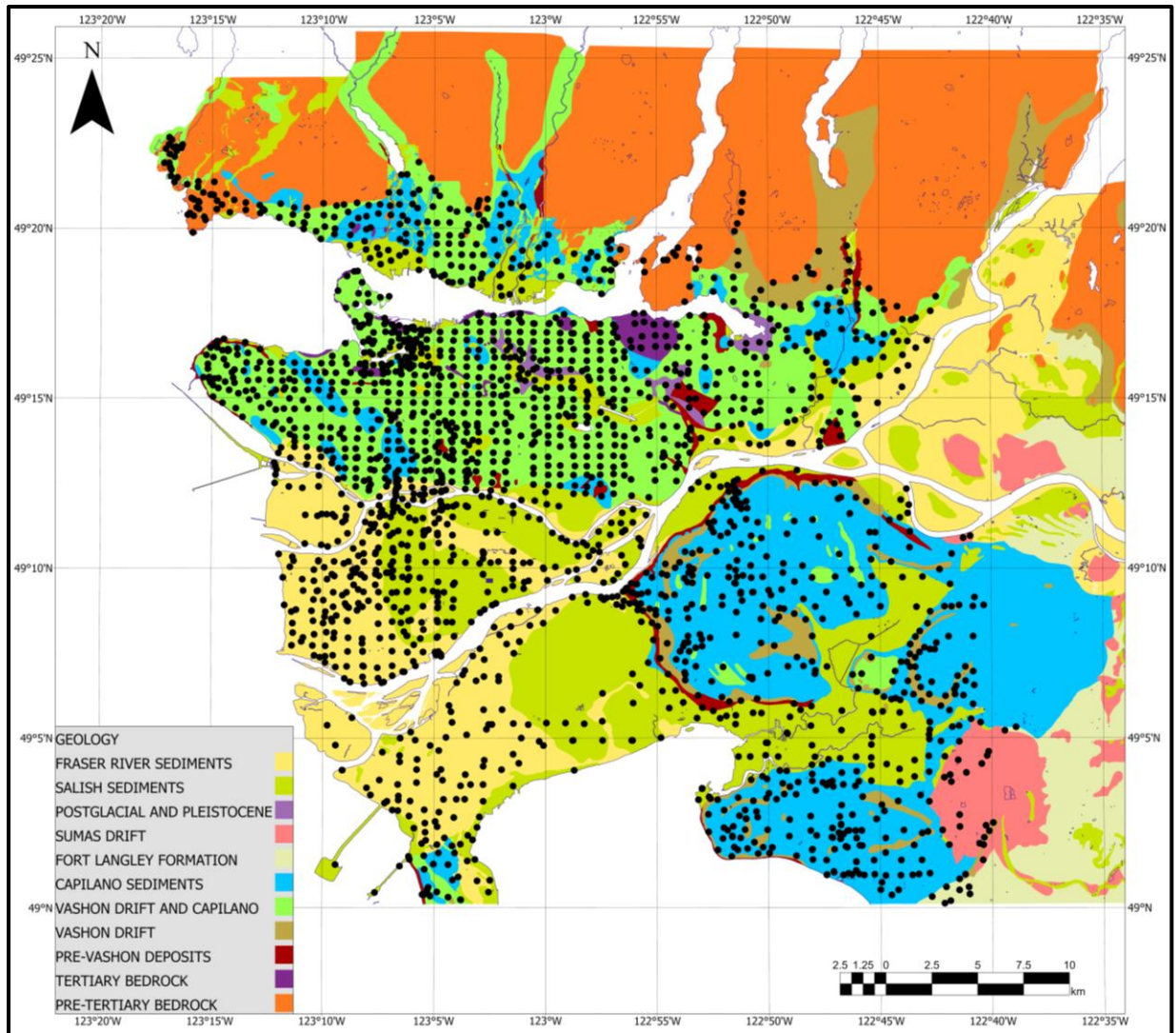


Figure 3-1. Locations of mHVSr measurements (black circles) acquired throughout the Metro Vancouver region. Background GSC surficial geology mapping (Armstrong 1979, 1980) is shown coloured according to geologic unit listed in the Legend.

Many of the investigations presented in the following section were not planned *a priori*, however, given the variability of the acquisition parameters and conditions under which the data were acquired by different personnel over time, it was possible to carry out parameter sensitivity tests and observe the impacts to the computed mHVSr result. The progression of investigations will begin with experimental setup (section 3.3) and end with data processing (section 3.4). Ensuring proper experimental setup is arguably the most

important aspect; if performed incorrectly, the recording is useless (mHVSR is not interpretable) and acquisition must be repeated. Decisions regarding processing parameters also affect the absolute values of the final computed mHVSR, so for example, can have an impact on the amplitude of $f_{\#HV}$.

3.3 Impact of Experimental Factors on mHVSR

There have been several investigations into the sensitivity of acquisition and processing parameters on the computed mHVSR, the most comprehensive of which resulted in the SESAME guidelines (Bard *et al.* 2008). The main conclusion of the SESAME project was that despite variations in tested parameters, f_{0HV} is a robust estimate of f_0 at a site. However, the rest of the curve, including the amplitude of peaks, is quite sensitive to some of the tested parameters (Chatelain *et al.* 2008, Strollo *et al.* 2008a).

3.3.1 Instrument Type

Many mHVSR studies suffer from not fully appreciating the many issues associated with instrumental seismology (Strollo, 2010). Seismometers are ‘tuned’ for their purpose, i.e., operational frequency bandwidths vary by sensor type. Figure 3-2 shows the operational frequency bandwidth (flat instrument response) of various sensor types. Therefore, the issue of the reliability of the averaged mHVSR amplification spectrum and its dependence on the acquisition equipment must be addressed to avoid mHVSR misinterpretation (Strollo, 2010).

The type of sensor used affects the computed mHVSR (Guillier *et al.* 2008, Strollo *et al.* 2008a, Castellaro and Mulargia 2009, Foti *et al.* 2011). Broadly speaking, there are three types of seismic sensors: accelerometers, short-period seismometers (< 5 s) and broadband seismometers (> 5 s). Due to limited sensitivity at lower frequencies, the use of accelerometers has typically been discouraged. It has been demonstrated that short-period seismometers can detect peaks below their corner frequency (e.g., Figure 3-2), but only if the signal-to-noise ratio (SNR) is high (e.g., Mucciarelli and Gallipoli, 2004; Strollo *et al.* 2008a). Broadband seismometers have a flat response over a wide bandwidth (Figure 3-2) and are therefore an attractive option when the frequency (wavelength, depth) of interest is unknown, i.e., assured correct measurement with a broadband seismometer compared to a

low gain short-period seismometer. Broadband seismometers are typically designed for permanent seismic network installation and their setup and initialization procedures are therefore not designed for the rapidity of the mHVSr method, i.e., more challenging to use than short-period seismometers.

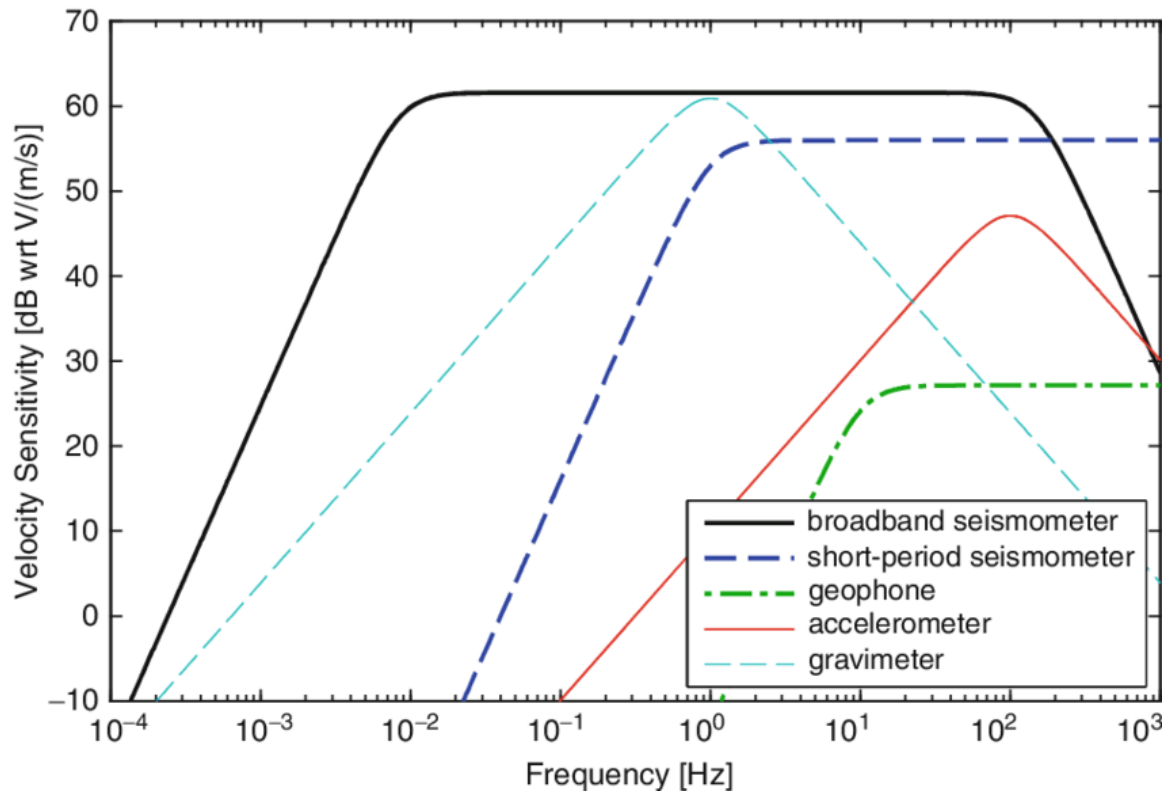


Figure 3-2. Response to velocity for inertial sensors. Adapted from Ackerly *et al.* (2014).

Several studies have been performed to examine the effect of short-period sensors on the detection of microtremor at frequencies lower than 1 Hz e.g., (Riedesel *et al.*, 1990; Rodgers, 1992; Rodgers *et al.*, 1995) or to test the performance of different kinds of seismic sensors by directly comparing the mHVSr obtained from the ground motion records of each sensor (Mucciarelli, 1998; Parolai *et al.*, 2001; Strollo, 2010). A comparison of mHVSrs obtained from different kinds of acquisition systems and sensor types was carried out by Guillier *et al.* (2008), with an experimental design optimized for investigating the effects in the higher frequency range (> 1 Hz). Strollo *et al.* (2008a) studied the effect of the acquisition system and sensor type on f_{0HV} , when it is expected to occur at frequencies

< 1 Hz. Their approach was to consider three different short-period electromagnetic sensors with resonance frequencies of 1, 2 and 4.5 Hz. Their results indicate that: a 1 Hz short period sensor can be used to detect microtremor vibration down to 0.2 to 1 Hz, but generally require a large gain; 2 Hz sensors always bias f_{0HV} toward higher frequencies for frequencies lower than 0.3 Hz; and 4.5 Hz sensors cannot detect microtremors for frequencies lower than 0.6 Hz. In another study by Strollo *et al.* (2008b), it was found that when using a calibrated short-period sensor, one can obtain the same results that would be obtained using a broadband seismometer over the frequency range of engineering interest (0.2 to 20 Hz). Parolai *et al.* (2020) used 15 weak-motion instruments (Guralp CMG-3ESP broadband sensors) and additional short-period (1 Hz) sensors to acquire around 220 microtremor measurements. When comparing mHVSRs obtained with the broadband vs short-period seismometer, they found that the results were nearly the same down to 0.1 Hz, depending on the existing microtremor amplitude.

Most of the microtremor measurements included in the Metro Vancouver database, specifically those acquired from 2012 to present, were acquired using a 3-component Tromino® seismometer. The Tromino® is an all-in-one compact 3-directional 24-bit digital seismometer developed by MoHo s.r.l. Two generations of this instrument were used: 9 older TEP-generation Trominos and 7 newer TE3-generation Trominos. Both versions have both low and high gain velocity channels, but the newer TE3 generation has greater sensitivity at lower frequencies.

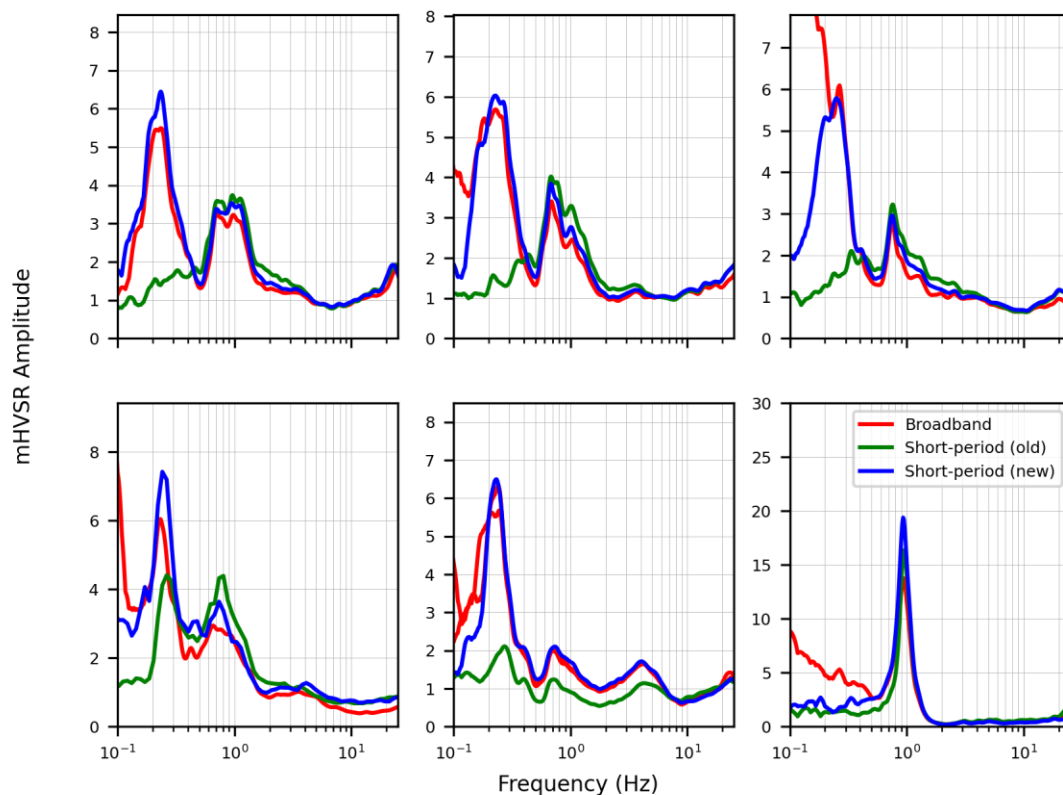


Figure 3-3. Comparison of mHVSRs at six Metro Vancouver sites from co-located microtremor recordings using a broadband seismometer and older (TEP generation) and newer (TE3) generation short period seismometers. The middle panel of the bottom row has the results from two different broadband seismometers displayed.

Broadband seismometers were used to validate low frequency peaks obtained in Metro Vancouver using the Tromino short-period seismometers. Similarities and differences in the resulting mHVSRs (Figure 3-3) are consistent with those reported previously (Guillier *et al.* 2008; Strollo *et al.* 2008a,b; Parolai *et al.* 2020). The newer short-period seismometer (used with full-scale gain option) could detect the low frequency (~ 0.2 Hz) peak, and due to decreased sensitivity at lower frequencies compared with the broadband seismometer (< 0.1 Hz), disturbances in this frequency range did not obscure the peak for the newer generation short-period seismometer, as was the case with the broadband seismometer at one of the test sites (top right panel of Figure 3-3). Figure 3-3 demonstrates that use of a short period seismometer with greater sensitivity is adequate for reliable mHVSR

measurement, consistent with mHVSRs obtained from broadband recordings, even for very low f_{0HV} sites in Metro Vancouver (e.g., the Fraser River delta). It should also be noted at this stage that at sites where the peak is expected at frequencies < 1 Hz, more careful attention is required to the experimental setup because it is in this frequency range (0.1 to 1 Hz) that many factors (e.g., wind, sensor coupling) affect the data. Sensitivity of the broadband to these external factors is observed at low frequencies (amplitude increases below f_{0HV} in 50% of the cases), whereas the short-period seismometer is not as sensitive (amplitude always decreases below f_{0HV}). The poorest performing seismometer is the older generation short-period seismometer (used with high-gain setting). In most cases, it fails to detect the very low (~ 0.2 Hz) f_{0HV} , and in the cases that it does, the f_{0HV} is biased to higher frequency and its corresponding amplitude lower when compared to that of the more sensitive short-period and broadband seismometers (bottom left panel of Figure 3-3). Additional benefits of the short period seismometers used were the size of the instruments and the removal of external hardware components such as cables, GPS antenna, batteries etc.; the instrument is entirely self-contained or designed for the mHVSR method.

Although the older generation of the short-period seismometer did not perform adequately in the presence of deep impedance contrasts with corresponding low frequency peaks, in the case of shallower impedance contrasts, a seismometer with less sensitivity at lower frequencies may perform better (Figure 3-4). This is because at lower frequencies there is increased noise due to wind and other disturbances. The reduced sensitivity of a seismometer in this frequency range (~ 0.1 to 1 Hz) means that if a low frequency (i.e., < 1 Hz) peak is not expected, the use of a less sensitive seismometer may provide more stable results, or equally, a seismometer with greater overall sensitivity, but using a lower gain.

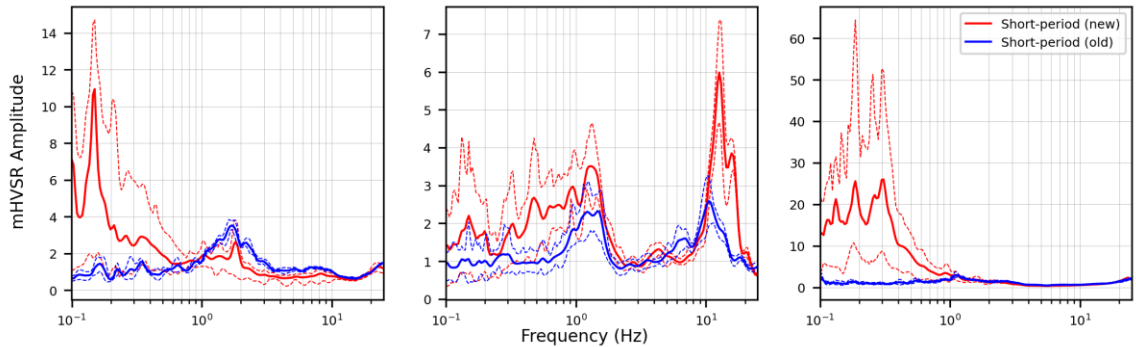


Figure 3-4. Comparison of co-located measurements obtained using both the newer and older generation short-period Tromino® seismometer.

The newer generation short period seismometer used for data acquisition has variable gain options, namely: full-scale, high gain and low gain. The low gain option produced results like those of the older generation short-period seismometer, when the older generation of short-period seismometer was used with high gain setting. A test was conducted to discern differences between the full-scale and high gain options of the newer short-period seismometer and involved installing two newer generation Tromino® sensors to record ambient vibrations at the same site (within m's). The results from six sites are provided in Figure 3-5. All six sites were located in the FR delta, and as such had very low f_{0HV} (~0.2 Hz). In all cases, the 'full-scale' gain setting produces a first peak that is at a slightly lower frequency and higher amplitude than that obtained using the 'high gain' setting. The full-scale gain setting is the recommended setting for use with this instrument if one is interested in $f_{\#HV}$ retrieval within 0.1 – 0.5 Hz. Although switching between high gain and low gain settings depending on the anticipated geology in a region may provide optimal results, the increased sensitivity at lower frequencies can amplify disturbances and extra care to minimize these disturbances during acquisition is needed. Ultimately, due to the presence of low frequency (< 1 Hz) peaks in the mHVSr for many sites in the Metro Vancouver region, the sensitivity of the selected seismometer used for data acquisition in this lower frequency range (0.2 – 1 Hz), must be verified prior to commencement of data acquisition.

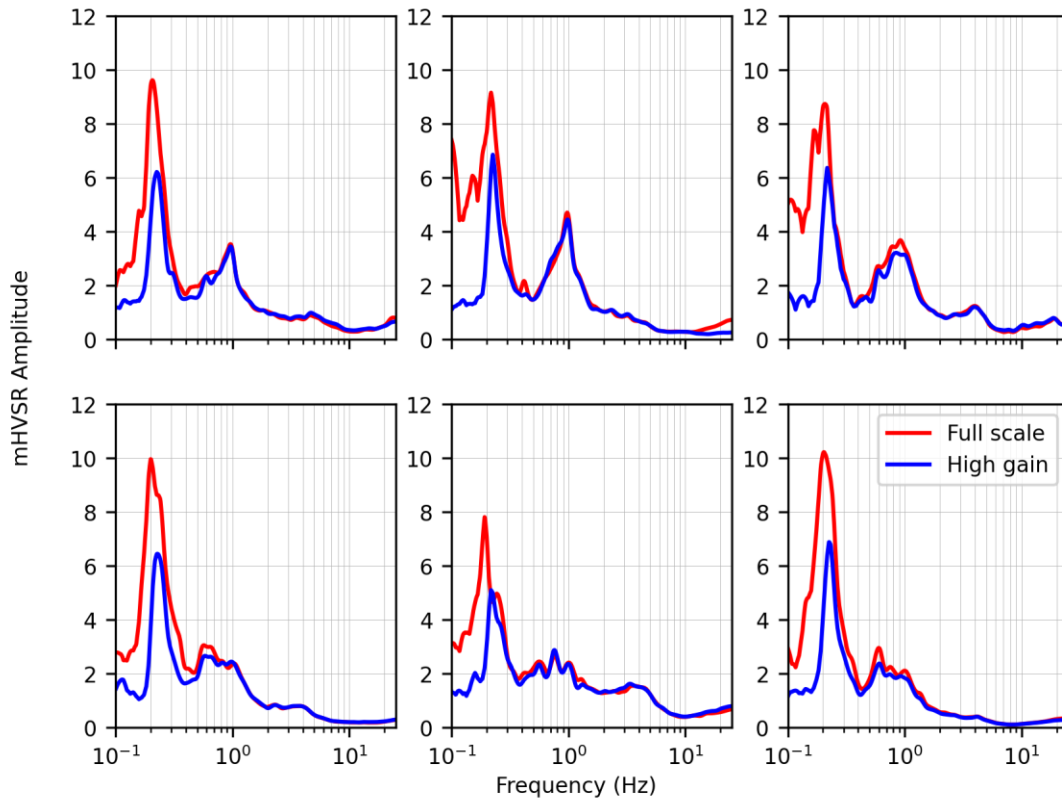


Figure 3-5. Comparison of mHVSR computed using co-located, contemporaneous measurements with different gain settings using the newer generation Tromino® seismometer.

The measurements acquired during 2010 in Richmond using the Pinnocchio velocity transducers did not provide measurements which adequately capture the microtremor amplification characteristics (Figure 3-6). As a result, these measurements are omitted from subsequent analyses in the present study, however, they are retained in the database.

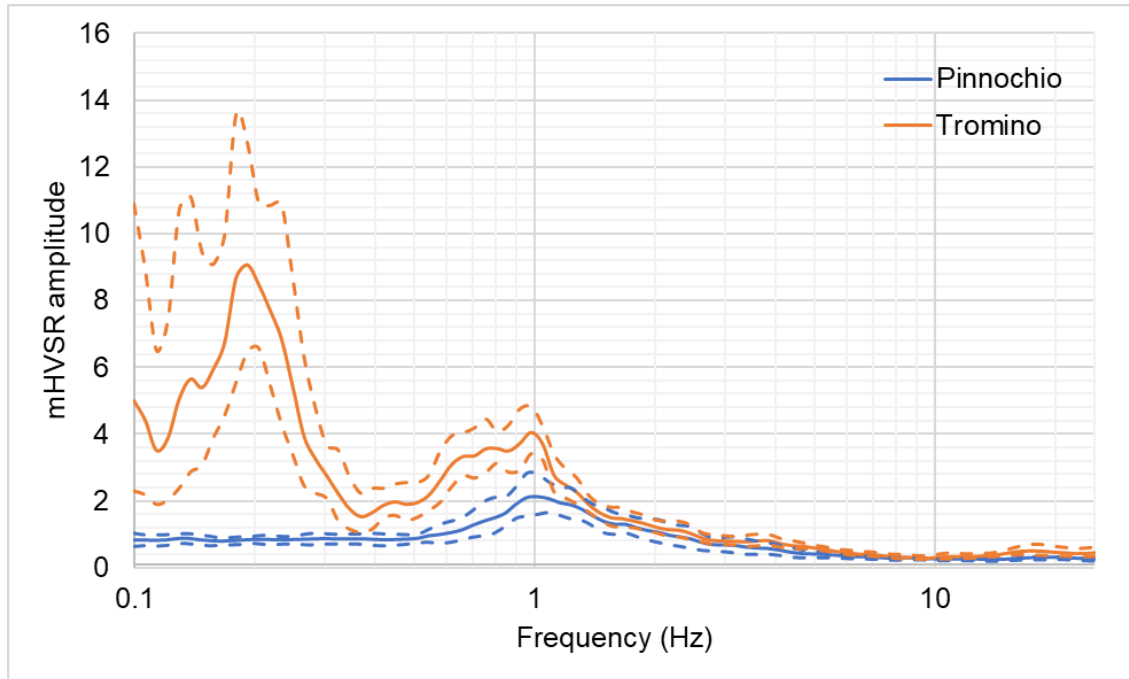


Figure 3-6. Comparison of mHVSr calculated from single-station microtremor measurements using a Tromino® short-period seismometer (RMD16) and a Pinnocchio velocity transducer (RI54). Measurements were obtained in the Fraser River delta. Dashed lines show upper and lower bound.

3.3.2 Sensor-Ground Coupling and Measurement Surface

Measurement of ambient vibrations should be made at a site with representative 'free-field' conditions. Measurements on stiff artificial surfaces encounter near-surface velocity inversions that may result in an mHVSr below one (deamplified) for a wide range of frequencies above f_{0HV} (Gallipoli *et al.* 2004, Castellaro and Mulargia 2009, Piña-Flores *et al.* 2020). More critical than the measurement surface is proper coupling of the sensor to the measurement surface (Foti *et al.* 2018). Meteorological disturbances such as wind and rain also impact the measurement. It has been observed that the effect of wind on mHVSr measurements is best correlated with low frequency disturbances (Withers *et al.* 1996, Cara *et al.* 2003, Mucciarelli *et al.* 2005). A weak negative, correlation exists between the peak frequency and amplitude of the mHVSr with rainfall (Mucciarelli *et al.* 2003).

While a theoretical argument can be made in support of placing the seismometer on a natural surface (i.e., soil or dirt), practically, it is often challenging to find a suitable area, prepare the soil/dirt surface (i.e., brush away gravel, remove grass) and properly couple and/or level the sensor in soil. In addition, burial or partial burial of the sensor will minimize against 'external' factors (wind, heat) but due to rapidity of the mHVSR method, burial depth more than half the sensor's height is not accomplished. Conversely, sensor deployment on a near-level hard surface (e.g., concrete or asphalt) is easier and faster but are more susceptible to 'exposure' (wind, heat) as well as the previously mentioned deamplification impact to the mHVSR caused by a velocity reversal if softer ground is below the hard surface. Improper coupling of the seismometer to the ground surface can yield the data useless for further analysis. Improper coupling results in a departure of the mHVSR at lower frequencies, which is similar to the effect that wind has on the mHVSR.

At many sites included in our mHVSR dataset, contemporaneous measurements were made, ideally with co-located Trominos on two different surfaces. In this way, mHVSR interpretation is made easier by the data redundancy. A comparison of co-located measurements made on natural and various types of artificial surfaces is provided in Figure 3-7. From an engineering perspective, further refinement of the types of artificial surfaces and knowledge of the thickness of artificial fill material is required and is a limitation that should be considered when interpreting the presented results. The results of comparison of 93 co-located microtremor measurements on the natural ground surface (soil), versus an artificial hard surface (asphalt, concrete, or gravel) indicate that when considering the average difference, calculated on a point-by-point basis (for each frequency at which the mHVSR curves were sampled) for each pair of mHVSR spectra, the spectra measured on soil was on average 0.3 ± 0.3 units greater than the curve measured on an artificial surface. This amplification difference is primarily caused at low frequencies, where external factors are more likely to impact measurements made on soil than artificial surfaces. Overall, no measurement surface consistently provided superior results. Hence the recommendation to obtain side-by-side microtremor measurements on a minimum of two different surfaces, one of which is representative of the natural ground conditions at the site.

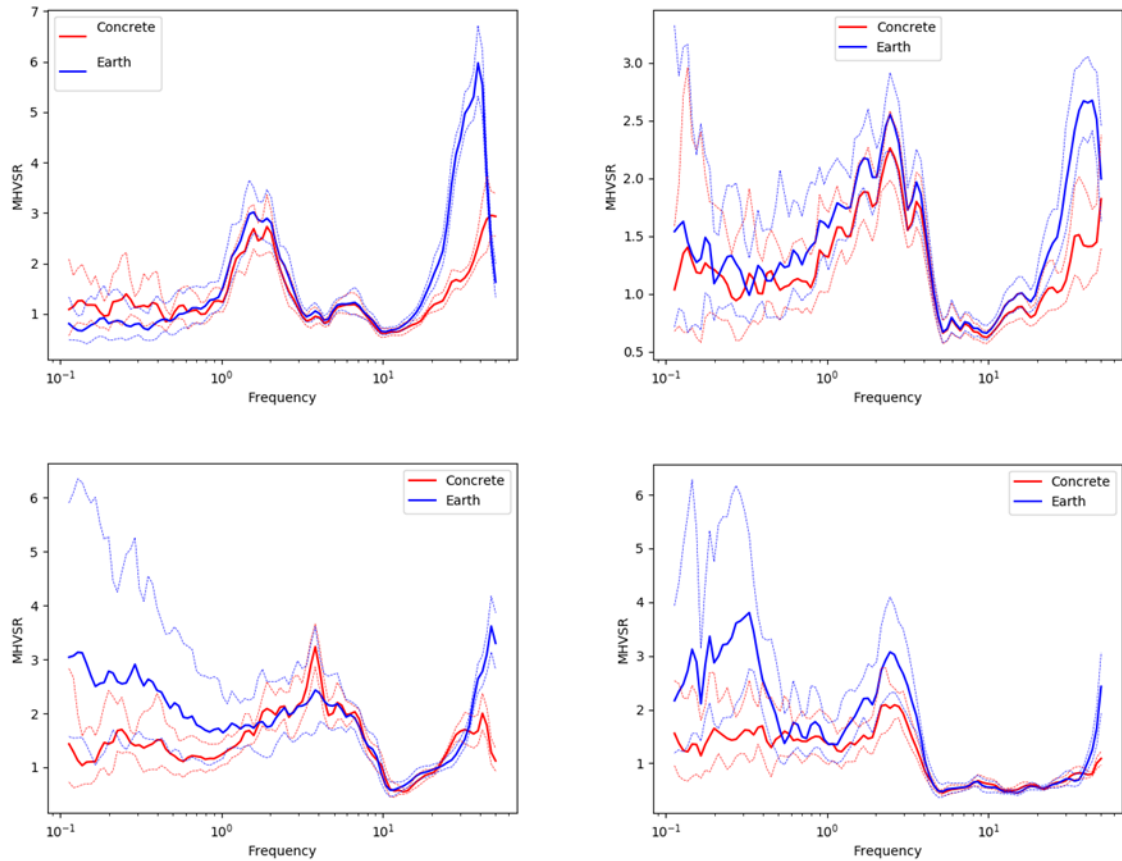


Figure 3-7. Comparison of co-located measurements made on both natural (i.e., soil/dirt and man-made (artificial) surfaces.

3.4 Impact of mHVSr Processing Parameters

Although the most crucial aspect of the mHVSr experiment is ensuring good experimental setup, the use of appropriate processing parameters is important to the clarity and reliability of $f_{\#HV}$ and therefore mHVSr interpretation. Understanding the effect of processing decisions on the computed mHVSr amplification spectrum aids the practitioner in selecting the optimal set of processing parameters for any given measurement.

Input mHVSr processing parameters include time series window length (s), window overlap (%), window selection procedure (i.e., manual vs. automatic), spectral smoothing operator, and method to define the representative horizontal spectrum. The essence of

mHVSR data processing involves: (1) windowing time series data, (2) using a particular selection of time windows to effectively remove ‘outliers’ from the ‘reliable’ mHVSR curve (discussed further in section 3.4.3) which may or may not require the following steps to be iterative, (3) tapering then converting the windowed time series data into the frequency domain, (4) filtering (smoothing) the frequency domain spectra, (5) combining the two horizontal component’s spectra, (6) computing the ratio between the merged horizontal component spectrum and the vertical component spectrum (steps 5 and 6 can be reversed, calculating the average for each of the component spectra considering all time windows and then combining the two time-averaged horizontal spectra), and (7) calculating the average of the ratios calculated from each window (or if 5 and 6 are reversed, calculating the ratio).

The chosen window length is a trade-off between spectral resolution and statistically meaningful results (Bard 1999, Picozzi *et al.* 2005). According to the SESAME guidelines (Bard *et al.*, 2008), the mHVSR peak frequency should be greater than 10 divided by the window duration in seconds (Gospe *et al.*, 2020). This means that for a 0.2 Hz peak, the recommended minimum window length is 50 s.

Selecting the optimal set of time windows from which to compute the mHVSR is arguably the most important aspect of processing. Manual selection through visual inspection of both time and frequency domain data often provides the best results but is time consuming and user dependent. Automatic window rejection through consideration of a short-term vs long-term average is implemented in much available software (Bignardi *et al.* 2018, Wathelet *et al.* 2020). However, the effect of inclusion of transients on the mHVSR is still debated (Horike *et al.* 2001, Mucciarelli and Gallipoli 2004, Parolai and Galiana-Merino 2006, Bard *et al.* 2008). In addition, often windows that appears anomalous in the frequency domain do not contain transients or any obvious spurious feature in the time domain. (Cox *et al.* 2020) introduced an automated window rejection algorithm that operates in the frequency domain through iterative rejection of time windows corresponding to mHVSR curves that deviate significantly from a statistically defined representative curve. D’Alessandro *et al.* (2016) and Martorana *et al.* (2018) use cluster analysis to group time windows that yield similar mHVSRs and identify an optimal set of

analysis windows. Mihaylov *et al.* (2016) observe that the low frequency branch of the mHVSr has increased uncertainty in the presence of high noise level. They observe that seismic waves from sources closer to measurement site may only propagate in shallow layers, thus obscuring lower frequency peaks due to deeper structure. They suggest an approach to separate low- and high-level noise windows from the single-station recording and calculate the mHVSr from all time windows, the low-level noise windows and the high level noise windows. The results obtained using this method at a site are illustrated in Figure 3-8 and show the difference in considering windows with variable signal level separately.

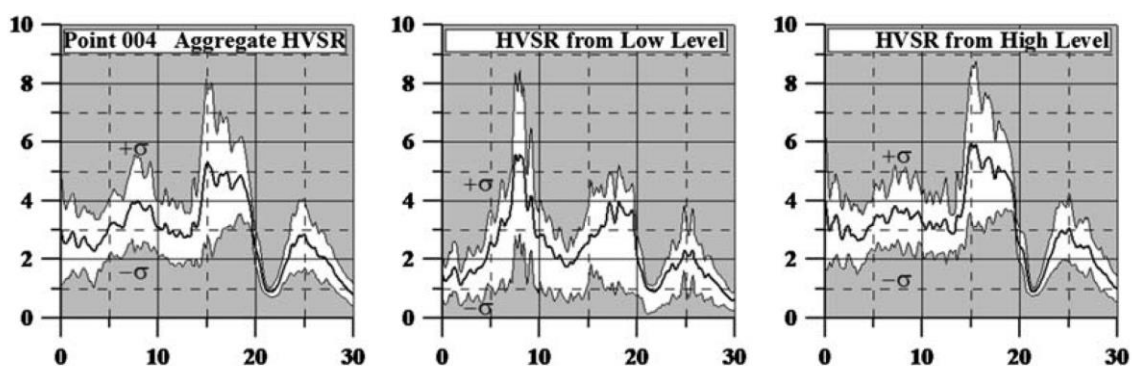


Figure 3-8. Example of mHVSr calculated from all time windows, time windows identified as having low level signal and time windows identified as having high level signal. Adapted from Mihaylov *et al.* (2016).

Generally, the velocity time-series data are converted into the frequency domain using Fourier techniques. After the data are converted to the frequency domain, spectral smoothing is typically applied. The Konno and Ohmachi (1998) smoothing filter (KO), which accounts for variable numbers of points at low frequency, is typically used and applied to the horizontal and vertical components (Wang *et al.*, 2021). Chatelain *et al.* (2008) use a KO filter bandwidth parameter of 40. Noisy data requires a lower bandwidth parameter (which produces a greater degree of smoothing). Constant bandwidth smoothing, such as the Parzen window, show a difference in height whenever their peak periods are different, even for ground motion models with identical velocity contrasts (Konno and Ohmachi, 1998). Mihaylov *et al.* (2019) observed that the Konno and Ohmachi

window function has side lobes present around the center peak, meaning that it introduces a wider range of frequencies with higher weights into calculation of the smoothed spectra. The side lobes can be decreased by increasing the steepness of the function (increasing the filter coefficient), but this will reduce its effective width and result in a rougher output spectrum. To avoid this problem and based on SDOF modelling by Malischewsky & Scherbaum (2004) they propose a band-pass filter that has a constant quality factor, independent of center frequency.

The decision to combine both horizontal components to define a single 'horizontal' spectrum is often made arbitrarily without proper consideration of its appropriateness. Albarello & Lunedei (2013) tested several approaches including no combination, arithmetic mean, geometric mean, vector summation, quadratic mean, and maximum horizontal value for calculating a representative horizontal spectrum from the two independent components and found that all of the considered estimators introduced some sort of bias into the results.

A statistical approach that considers azimuthal variability when extracting parameters from the mHVSR was proposed by Cheng *et al.* (2020). A useful output of this algorithm is a directivity plot that illustrates how much the ratio varies as a function of azimuth, allowing assessment of whether it is indeed appropriate to combine the two horizontal components. In practice, the geometric mean or squared average (e.g., square root of the sum of the two squared components) are used most. Some practitioners use RotD50 (Boore 2010), which is the 50th percentile of the spectra of the combined, as-recorded horizontal components after rotation. RodD50 has the benefit of being insensitive to the orientation of the sensor.

The mHVSR is finally calculated as a function of frequency by dividing the smoothed, merged horizontal component spectral amplitudes by the vertical amplitudes (Wang *et al.* 2021). Generally, this computation is performed for each window, and then results are averaged across windows to produce a mean curve. Commonly, the mHVSR curve is presented as the average curve bounded by a standard deviation (e.g., arithmetic/natural log standard deviation, percentiles).

The degree to which each of these parameters affect the computed mHVSR varies. Understanding the sensitivity of each parameter assists practitioners in making decisions at the acquisition and processing stage.

3.4.1 Existing mHVSR Processing Software

Several software suites are available for processing three-component microtremor recordings to provide an mHVSR. Three software packages were utilized and evaluated to determine the optimal processing strategy for a large database (100's to 1000's) of mHVSR measurements typical of seismic microzonation studies. The features of each software package are described, and analysed within the context of processing the Metro Vancouver mHVSR database.

3.4.1.1 Geopsy

Geopsy is an application dedicated to seismic signal processing (Wathelet *et al.*, 2010, 2020). High-level GUIs are developed on top of Qt libraries, however, the tools can also be run directly from the command line. Up until recently, calculating mHVSRS could only be done inside the GUI, however, in a recent release the ability to execute the computation using command line tools, has increased the utility of Geopsy for batch processing large datasets. The single station H/V module of Geopsy was the first Geopsy tool developed during the SESAME project (Bard *et al.*, 2008). FORTRAN codes developed by Bard (1999) served as inspiration for the core structure of the H/V module. Time window size, optional anti-trigger (short-term average/long-term average), and various parameters (see Wathelet *et al.*, 2010) are set up manually or can be loaded from a previous processing session. The time windows retained for computation of the mHVSR can be selected manually or automatically using an anti-triggering based window rejection algorithm. The horizontal spectrum can be obtained considering both horizontal components, either with a squared average, the total power merging procedure, or the power along a given direction may be used (Wathelet *et al.*, 2010). Through averaging the mHVSR curves for the selected time windows, the average mHVSR curve is obtained. The Konno-Ohmachi (1998) smoothing operator is implemented by the software, and is a common choice when processing mHVSR data, however, other spectral smoothing methods are also available.

Individual mHVSr plots display the average mHVSr curve, its standard deviation, the peak frequency with the highest amplitude, and its corresponding standard deviation. The peak frequency and its standard deviation are obtained by averaging the frequency of the maximum found on the mHVSr curve of each time window in a 10% interval around the peak of the average mHVSr curve. For this reason it may not always coincide exactly with the peak of the average mHVSr curve (Wathelet *et al.*, 2010). Several tools are available to further analyse a classical H/V measurement. ‘H/V rotate’ computes H/V in all directions of the horizontal plane. Performing a ‘damping’ analysis (calculates the viscous damping ratio) of $f_{\#HV}$ peaks helps to identify sustained peak frequencies (damping above 1 %) produced by anthropogenic sources (Dunand *et al.* 2002).

3.4.1.2 OpenHVSr

OpenHVSr was developed Bignardi (2018). The algorithm is organized into a main GUI, but it is Matlab-based, which restricts its use to those with licenses to the software. The processing options available through OpenHVSr do not differ significantly from those offered by Geopsy, however, OpenHVSr is better suited to handle batch processing of large datasets. It also places an emphasis on displaying the data in a manner that emphasizes spatial trends. OpenHVSr has several original features including providing a tiled view of the Fourier spectra from windows, and capability of window selection in this view. It displays the spectral ratio of windows not only for the HVSr, but also for the E/V and N/V, without requiring separate calculation of each. It facilitates direct comparison of mean HVSrs before and after data cleaning, visualization of all directional mHVSrs in one window, and automatic map creation for the peak frequency and amplitude among other quantities. An mHVSr profiler (Herak 2008, Herak *et al.* 2009) allows creation of multiple linear profiles and plots along defined lines for the mHVSr, E/V and N/V.

3.4.1.3 HVSRPy

Cox *et al.* (2020) emphasize the necessity to represent the mHVSr in a statistical manner. Their justification lies in the complex and site-dependent nature of noise wavefields that affect mHVSr measurements. HVSRPy is a python package for performing mHVSr processing developed by Joseph P. Vantassel with contributions from Dana M. Brannon

under the supervision of Dr. Brady Cox at the University of Texas at Austin (Vantassel, 2020). HVSRPy is run from the command line and is extremely effective for batch processing large datasets of microtremor data. Based on recommendations from Bard (2008), the default method to combine the horizontal component data is using the geometric mean, however the quadratic mean may also be used as well as specific orientations. An assumption of the HVSRPy processing routine is that for each window, at each frequency, the amplitude follows a lognormal distribution (LD) and the median amplitude at each frequency can be determined according to lognormal statistics. In the traditional deterministic approach, the peak frequency from the median HVSR curve ($f_{0HV,mc}$) is typically chosen as an estimate of the site resonance frequency, with no associated statistics. In the probabilistic method (implemented in HVSRPy), a sample set of f_{0HV} values result from collecting separate f_{0HV} values from each time window. Statistics such as the mean (μf_{0HV}) and standard deviation (σf_{0HV}) can then be computed. One of the major advancements in processing proffered by HVSRPy is an automated window rejection algorithm. To automate the rejection of non-representative time windows, Cox *et al.* (2020) propose a frequency domain window rejection algorithm based only on the statistics μf_{0HV} , σf_{0HV} and a parameter n , which represents the number of standard deviations in log space. Essentially, the algorithm functions by iteratively removing individual time windows for which the f_{0HV} value extracted deviate from μf_{0HV} until certain stopping criteria are met.

3.4.1.4 Evaluation of Existing mHVSR Processing Software

Many of the microtremor recordings from the Metro Vancouver mHVSR database were evaluated using all three described software packages. Consistency in the mHVSR processing choices (window length, type and degree of smoothing etc) was maintained between the three softwares. Figure 3-9 shows the computed mHVSR from Geopsy, OpenHVSR and HVSRPy are very similar. Both the Geopsy and OpenHVSR GUI allow quick assessment of the effect of changing processing parameters on the computed mHVSR, which is extremely useful when processing a single measurement at a time. However, since OpenHVSR requires Matlab, which requires a paid license as a prerequisite for its use, for the purpose of further analysis in this study, OpenHVSR was omitted as a processing option. There are many features that are unique to OpenHVSR,

and if practitioners have access to a licensed version of Matlab, they are encouraged to experiment with the batch processing capabilities as well as spatial data display options available in the software.

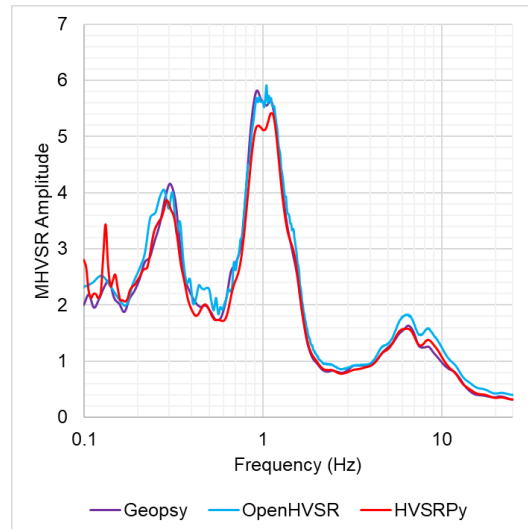


Figure 3-9. Comparison of mHVSr calculating using three different software, same parameters and same measurement.

3.4.2 Field Data Acquisition and Preliminary Data QC

HVSrPy was not released until 2020, as such, the Metro Vancouver mHVSr data were processed using Geopsy in 2018 and 2019. Since the start of the Metro Vancouver Microzonation Mapping project, the workflow for acquiring and processing mHVSr data involved: (1) pre-planning grid of microtremor locations, (2) field data acquisition using the MapsMe App to locate the pre-planned locations, (3) downloading data from each instrument each evening, (4) daily data quality control (e.g., updating any deviations in pre-planned measurement locations), and (5) preliminary mHVSr processing using Geopsy. Step 1 and 4 are accomplished by trained personnel from the Good Vibrations and Excitations Lab at the University of Western Ontario, steps two and three are accomplished by multiple and varying personnel, and step 5 was largely performed by me. During each summer field campaign, it was possible to acquire up to 82 measurements on a single day. To ensure instrument functionality for the next day of field work, each measurement was processed using Geopsy to check the time series data, ensure all components were

functioning, and check whether there was excessive industrial or natural noise in the data that could be obscuring geologic signal. At this stage, special attention was not paid to the processing parameters, nor window selection, and the resulting mHVSRs were considered preliminary and only for the purpose of data QC.

The importance of inspecting the Fourier amplitude spectra for each component prior to merging cannot be stressed enough. Not only does it provide insight into the quality of the measurement, but it is also straightforward at this stage to observe differences in the two horizontal components, prior to merging them and losing this information. It is also useful to check for the presence of monotonic industrial signals. Examples of the Fourier amplitude spectra for each component are provided for four different measurements to demonstrate their utility in terms of gauging the reliability of the data, and also further interpretation (Figure 3-10).

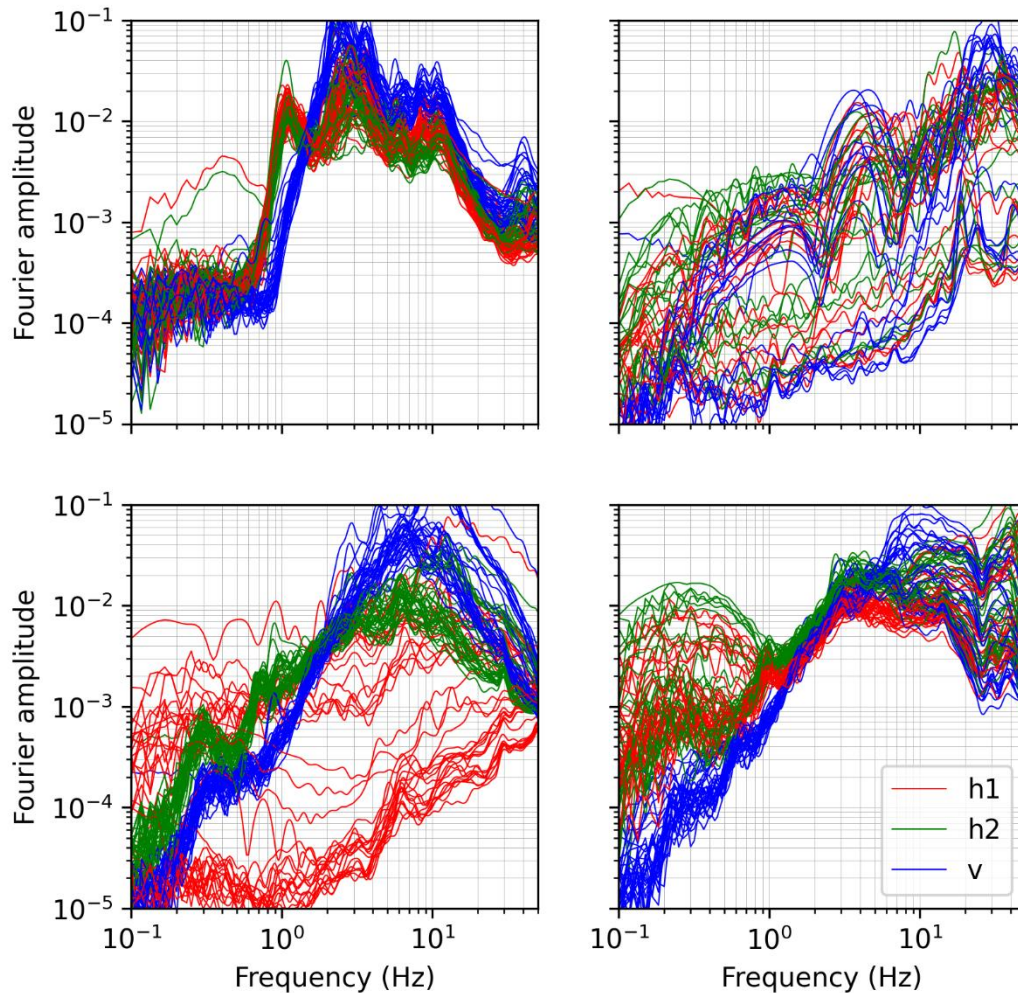


Figure 3-10. Four examples of the Fourier amplitude data for each component of recorded ground motion. Top left: example of good quality data with a geologic peak at ~1-2 Hz evident due to the ‘eye-shape’, top right: example where data is noisy on all three components, bottom right: example where data for two components, h2 and v, are good quality, and one component is not functioning properly, bottom right: example where data at low frequencies (<1Hz) is corrupted by noise.

Even prior to the start of the project, a database of mHVSR data already existed (measurements pre-2018). However, these data were acquired using different instruments, practitioners, processing methodologies, and as such, it was also re-processed with the rest of the data acquired during this project. The objectives of analysing this dataset are multi-

fold. First, understanding the effect of processing parameters on the final computed mHVSR needs to be established. To do this, each measurement was processed independently as part of exploratory data analysis. In the following section, a subset of the data is used to provide the results of a sensitivity analysis that tested various processing parameters to understand their impact on the computed mHVSR.

3.4.3 Processing Parameter Sensitivity Analysis

The choice of processing parameters impacts the final computed mHVSR. 50 sites were included in this analysis. mHVSRs were computed for window lengths of 15, 30, 45, 60 and 120 s (60 s considered reference), a Konno-Ohmachi smoothing coefficient of 20, 30, 40, 50 and 60 (40 considered reference), and the E/V and N/V ratio were computed, considering each horizontal component separately, as well as the HVSR by merging the two horizontal components and computing the geometric mean (geometric mean considered reference). HVSRPy was used for this analysis. The frequency-dependent impact of the parameters was quantified by computing the coefficient of variation (CoV) between the curves computed for each tested parameter; window length, degree of smoothing, decision to merge the two orthogonal horizontal spectra, or consider each independently. The CoV values may be artificially inflated under some circumstances because of the small number of samples considered in its calculation, for example, for the horizontal spectrum definition, only three data points were used to compute the CoV. The procedure of determining the CoV is explained in more detail considering the case of varying the horizontal spectrum definition; for each site, at each frequency which the mHVSR is sampled, there are only three data points, one corresponding to the HVSR, one to the E/V and one to the N/V, it is from these three values that the CoV would be computed for each site. However, these results reflect the experience of myself working with the data and are thus valid for identifying general trends in terms of the sensitivity of the output mHVSR curve on varying these input parameters. For the 50 sites included in the analysis, the CoV values were averaged across all sites as a function of frequency, and the 10th and 90th percentile defined (Figure 3-11).

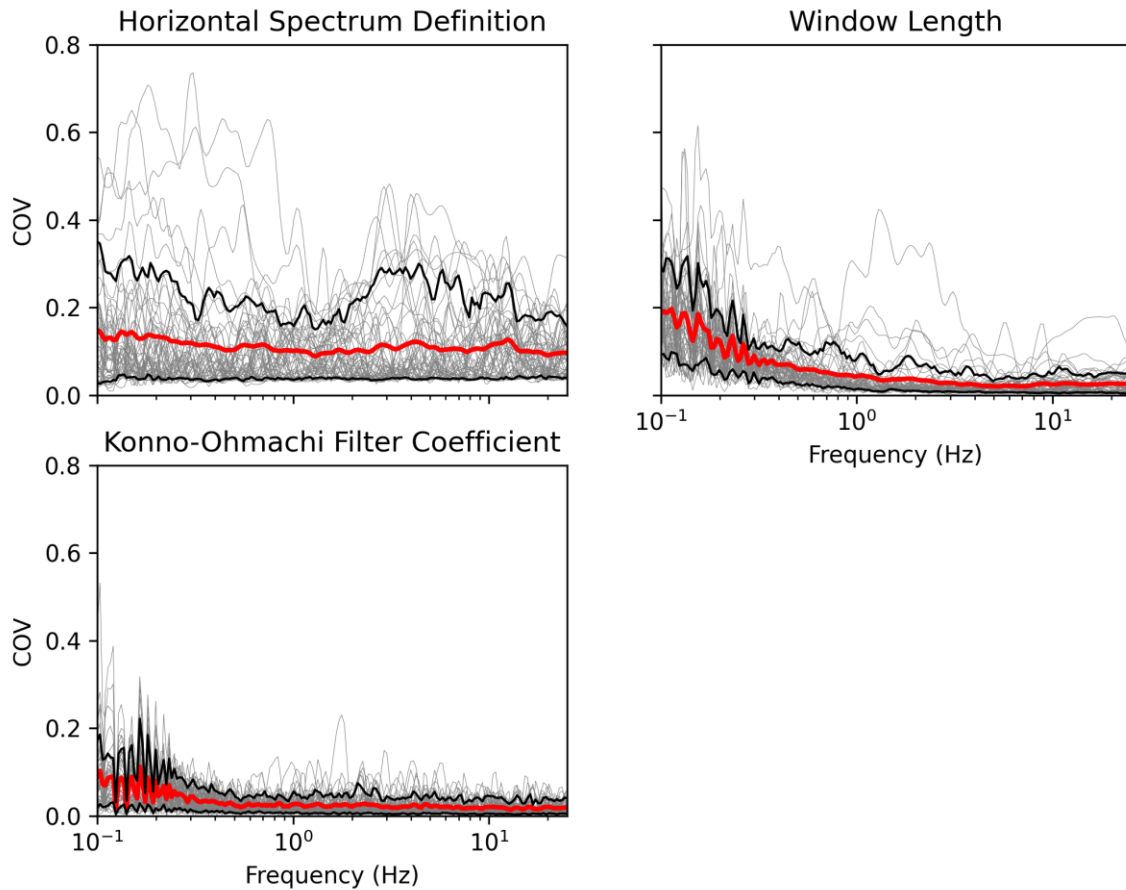


Figure 3-11. Coefficient of Variation (COV) computed for each frequency at which the mHVSr is sampled, for each site (gray line) included in the analysis.

3.4.4 Optimal Time Window Selection

Although the processing parameters already discussed are important to consider, particularly, checking the agreement between the two horizontal components to assess the appropriateness of merging them, the choice of the set of time windows used to compute the mHVSr is by far the most important processing decision, and the most time consuming. The optimal strategy is manual selection of time windows based on inspection of the frequency domain representation, because often it is not possible to identify bad windows in the time domain. However, manual selection of time windows for each measurement when working with such a large database is extremely time consuming.

Three automatic window selection/rejection algorithms were tested. The first two are implemented in existing software. One algorithm, implemented in Geopsy, involves use of an anti-triggering algorithm, which rejects windows based on consideration of a short-term vs. long-term average (Wathelet *et al.*, 2020). This algorithm requires the user to input four parameters: the width of the window to calculate the short-term average, the width of the window to calculate the long-term average, and a minimum and maximum STA/LTA ratio. This effectively removes windows in which the local signal is above or below an established threshold when compared to the average for the surrounding data. The algorithm using the Geopsy default parameters of 1.00 s, 30.00 s, 0.20 and 2.50 functions well, however, in some cases, when there are many transients and the values need to be adjusted, or when the issue in the frequency domain representation is not related to a transient feature in the time domain, the algorithm either requires the user to manually determine the most effective parameters, or simply fails in the case where the issue is not evident in the time domain. The other, implemented in HVSRPy, assesses the data in the frequency domain and rejects windows for which the automatically determined peaks deviate significantly from the peak of the median curve (Cox *et al.*, 2020). This technique works well (Figure 3-12), however, when measurements have multiple peaks of similar amplitude or there is significant noise at low frequencies, the method fails (Figure 3-13).

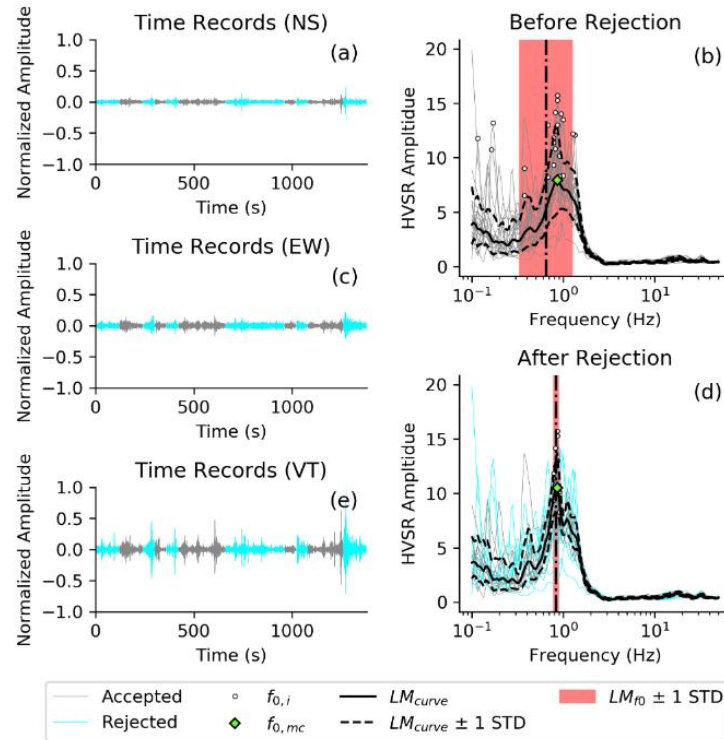


Figure 3-12. Results from HVSRPy in which frequency domain window rejection algorithm is successful in removing time windows which produce anomalous results in the frequency domain.

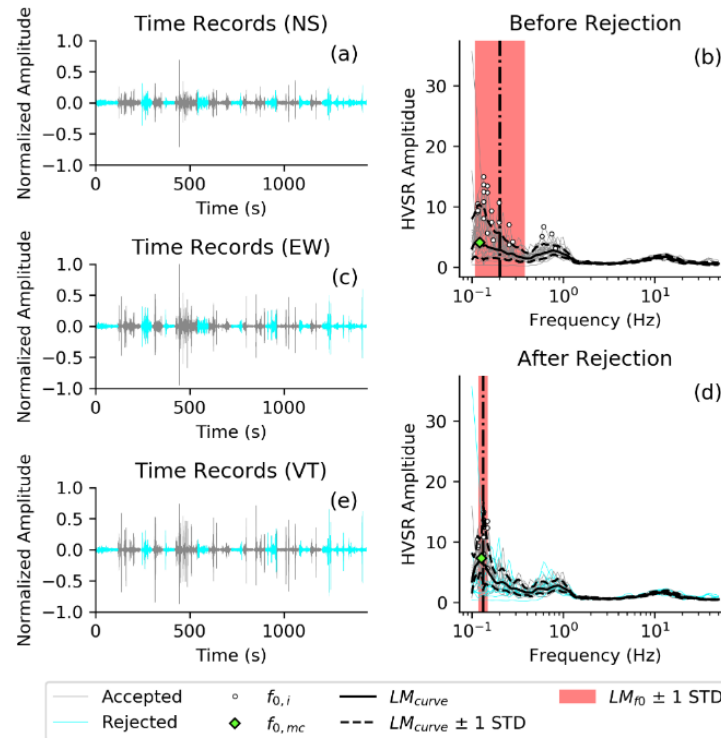


Figure 3-13. Results from HVSRPy for which frequency domain window rejection algorithm is not successful in terms of removing time windows that produce anomalous frequency response.

D'Alessandro *et al.* (2016) proposed using cluster analysis to select a set of time windows for optimal estimation of the average mHVSr. Their conclusions mirror those from the current study in that it is often very difficult to optimize the selection of time windows to be used for the calculation of the HVSR curve representative of a site. The use of subjective selection criteria produces results which depend on the practitioner and for which reliability cannot be assessed quantitatively (D'Alessandro *et al.*, 2016). Based on their work, we developed a similar agglomerative hierarchical clustering routine which we use to form clusters from the HVSR curves computed from individual windows. Several measures of proximity between two elements of the set were proposed in the literature to measure the similarity or dissimilarity of different kinds of objects (Gan *et al.* 2007, Everitt and Hothorn 2011). The type of proximity measure must respect specific criteria and should be optimized depending on the type of data and aim of clustering. We adopted the standard correlation.

The hierarchical/agglomerative clustering uses single-linkage clustering, which is based on grouping clusters in bottom-up fashion, at each step combining two clusters that contain the closest pair of elements not yet belonging to the same cluster as each other (Everitt *et al.*, 2011). When only one cluster remains, the algorithm stops, and this cluster becomes the root.

The clustering algorithm used in the present study used as input the HVSR curves for individual windows as computed by HVSRPy. The agglomerative hierarchical clustering routine was tested on the entire database. It performed equally or better than either the time domain anti-triggering algorithm implemented in Geopsy or the frequency domain window rejection proposed by Cox *et al.* (2020) and required little to no user input. The one downside of using such an approach is that the output is multiple clusters, and it is up to the user to decide which cluster provides the most representative curve. The clusters are indexed beginning from 1, and although clusters that contained fewer than 3 mHVSR curves were disregarded, they are still indexed. So for example, the output clusters may be 1, 5, 6, and then it is up to the practitioner to decide which cluster provides the most representative mHVSR curve for the site. The results of using the proposed cluster-based window selection routine are provided for 16 sites in Figure 3-14.

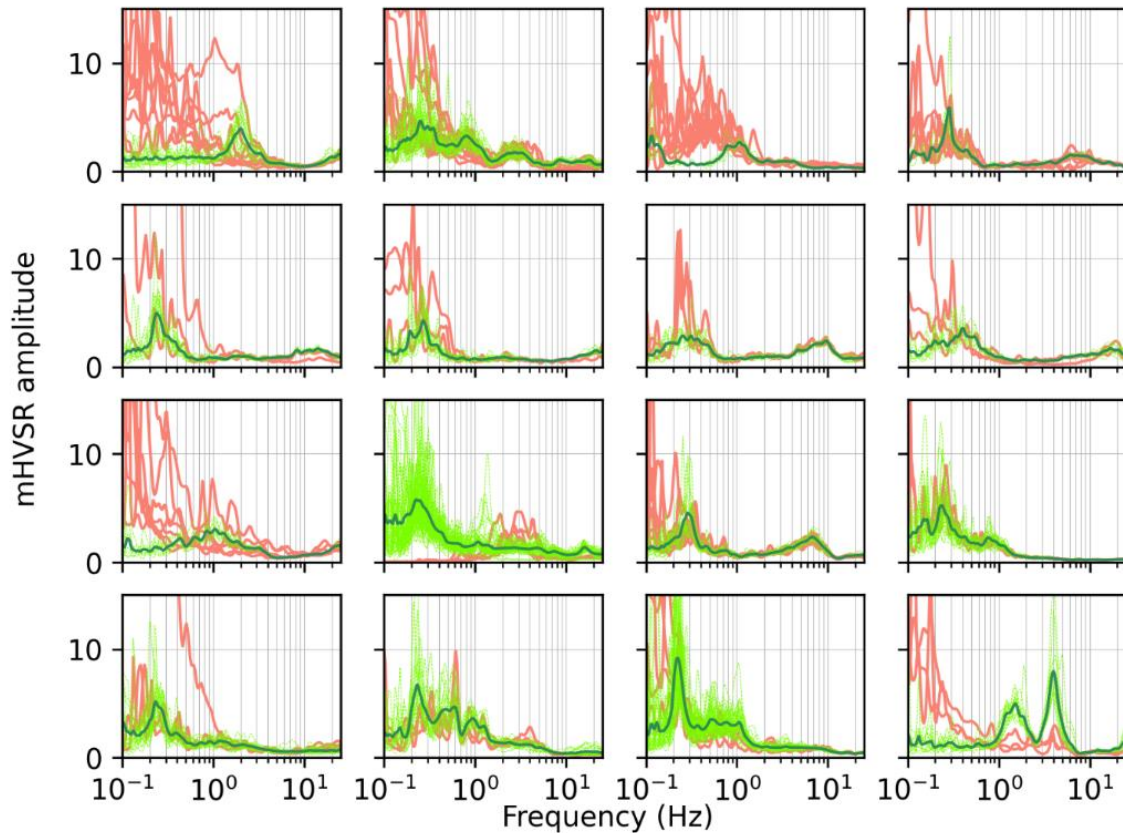


Figure 3-14. Results from proposed clustering-based window selection algorithm for 16 sites. Green windows are from the user-selected most self-consistent cluster, red traces are from other clusters identified.

3.4.5 Proposed mHVSr Batch Processing Methodology

Based on our investigations into the impact of processing parameter choices on the final computed mHVSr this is our proposal for a processing routine that is particularly well suited for batch proposal of large mHVSr datasets. We reconfigured the HVSRPy codes made available by Cox *et al.* (2020) to output the Fourier amplitude spectral for each component as well as the computed mHVSr curves for each time window as a comma-separated values (.csv) file. The HVSRPy parameters used to process the data are provided in Table 3-2. The code was also reconfigured to make a plot that included the Fourier amplitude spectra for each component. This processing output will aid with further interpretation of the measurement and deciding whether peaks are of natural or anthropogenic origin.

Table 3-2. Input parameters for HVSRPy.

Parameter	Value
Window length	60s
Filter_bool	FALSE
Width of cosine taper	0.1
Konno and Ohmachi smoothing constant	40
Resample_fmin	0.1
Resample_fmax	50
Method for combining horizontal components	Geometric mean
Rejection_bool	FALSE

An agglomerative hierarchical clustering routine was then used to group the time windows into groups with similar spectral shapes. The outputs of this stage of the processing are n clusters with an associated text file providing the average mHVSR, as well as a higher and lower bound calculated from the time windows included in that cluster, plots of the windows included in each individual cluster. Details of which time windows are included in each cluster are also provided.

3.5 Discussions

Given the inherent complexity regarding the theoretical basis of the mHVSR, ensuring standard and consistent practices regarding both the acquisition and processing of single-station microtremor data to derive the mHVSR is important. The microtremor wavefield is known to experience meteorological, diurnal and seasonal variations (Bour *et al.*, 1998, Mucciarelli & Monachesi, 1998; Volant *et al.*, 1998, Mucciarelli *et al.*, 2003, Guillier *et al.*, 2007). The wavefield composition is not something a practitioner is able to actively control, and thus effort must be taken to control for other variables.

The equipment used is one of the most critical parameters, as it is the quality of the raw time series data that is the limiting factor regarding the reliability of the computed mHVSR. While it is generally suggested to use a broadband seismometer, as they have the lowest sensor corner frequency, in our experience, ensuring proper setup of a broadband seismometer for short-duration data acquisition (30 min to 1 hour) is challenging and can often result in poor quality measurements – particularly at low frequencies. Based on results presented in this Chapter, a high sensitivity short-period seismometer with a

sufficiently low corner frequency can be reliably used to provide a more statistically stable mHVSR, particularly at low frequencies, than a broadband seismometer. It should be added that the type of seismometer should be carefully selected if the study area is known to have soft, thick sedimentary deposits. If the frequency range of interest is > 1 Hz (this is the frequency range in which f_{0HV} is expected to occur) then short-period seismometers with higher corner frequencies (> 1 Hz) and even accelerometers may provide reliable results.

Our recommendation is to first assess the geologic conditions in the study area and calculate the anticipated range of f_{0HV} values. If the range is > 1 Hz, a short-period seismometer should be used but the gain settings (sensitivity) should be adjusted such that it is at an appropriate level given the site's anthropogenic conditions (peak amplitudes > 1 Hz are not compromised) and to minimize environmental conditions (peak amplitudes < 1 Hz are not compromised). In contrast, if there are thick sediment deposits and mHVSR peaks below 1 Hz are expected, a short-period seismometer with a corner frequency of 1 Hz (or less) should be chosen, the gain level set as high as possible (highest sensitivity), and ideally, perform verification of one or more mHVSR results (lowest or suspected missing f_{0HV}) by a broadband seismometer. Once the results of the short-period seismometer have been validated against the broadband seismometer, it can be used for data acquisition and will result in a more efficient field campaign with typically lower variance in the microtremor recordings and thereby the mHVSR.

After the choice of equipment, the next most important parameter is the experimental conditions under which the microtremor recording is performed. The attractiveness of the mHVSR method comes from its ease of data acquisition, particularly in built up areas, requiring only a single three-component seismometer, thereby one person, for less than an hour. As a rule, free-field ground conditions should be sought. Measurements on stiff pavement over softer soils create velocity inversions in the subsurface which can lead to mHVSR deamplification (< 1) at frequencies above f_{0HV} (Castellaro and Mulargia 2009; Piña-Flores *et al.* 2020) but does not impact f_{0HV} or A_{0HV} (Chatelain *et al.* 2008). However, in this study, similar mHVSR results are calculated for simultaneous and co-located data recorded on dirt (free-field), asphalt, or gravel. Our recommendation is to perform two measurements per site visited, one on natural ground, and one on an artificial surface (e.g.,

concrete, asphalt). First, this provides data redundancy but also enables a reliability check of the two computed mHVSRs. Hence, in built up areas, the mHVSR method should be updated to one personnel deploying two three-component seismometers as close as possible but on different surficial materials for the same duration to ensure a reliable and robust mHVSR is obtained for interpretation. Many of the sites visited during the mHVSR field campaigns had low frequency (< 1 Hz) peaks, most likely necessitating a higher degree of care in deployment of the instrumentation to ensure proper coupling of the sensor, and mitigation of the impact of factors such as wind on the lower frequency branch of measurements. The presence of low frequency peaks (i.e., soft, deep sedimentary deposits) is also the reason why particular attention was required with regards to the choice of instrument to be used for data acquisition.

For proximity to structures that may be swaying during the microtremor recording (e.g., tall building, tree, flag/light pole, bridge), a general criterion is to offset the recording location by a distance equivalent to the height of the structure (Chatelain *et al.* 2008, Castellaro and Mulargia 2010); however, this is not always possible, in fact, rarely so if conducting an mHVSR survey in an urban environment. If this criterion must be violated, caution should be exercised when interpreting the results, as the resonant frequency of the structure may show up as a peak in the mHVSR. In these cases, testing the viscous damping ratio of the $f_{\#HV}$ is then mandatory and should be strongly less than 1.00 (as in the natural condition).

Poor decisions made during the data acquisition phase cannot easily be rectified without redoing the experiment. Processing parameter decisions are easily rectified for a single site, but when thousands of measurements are being considered and are required to be consistently processed, understanding the impact of the choices, and making the correct decisions so as not to process the significant amount of data multiple times is important for efficiency. The impact of processing choices of window length, degree of smoothing, and decision of how to treat/combine horizontal spectra is frequency dependent. Low frequencies are most affected by window length selection. For measurements with low frequency peaks, it is important to carefully consider the choice of window length.

Consistent with previous studies, longer time windows produce smaller dispersion of mHVSRs.

For spectral smoothing of the Fourier amplitude spectra, a smoothing function with a constant Q-factor should be used. The most commonly used filter is the smoothing function developed by Konno and Ohmachi (1998). As the results of this study indicate, the effects of altering the degree of smoothing using a constant bandwidth Konno-Ohmachi filter are minimal, but relatively more apparent for lower frequencies. The function has a constant width in logarithmic frequency, regardless of center frequency. However, the Konno and Ohmachi smoothing operator has side lobes present around the central peak. To diminish the effect of these side lobes, the 'b' value may be adjusted, however this has the undesired effect of a less smooth spectrum. An alternative to this smoothing function was proposed by Mihaylov *et al.* (2019), but it is not widely used.

There may be significant variation between the mHVSR computed from considering a single representative 'horizontal' spectrum vs. each component orthogonal spectrum separately. A processing parameter sensitivity analysis showed that the variations between considering a merged horizontal spectrum vs. each individual spectrum separately were present throughout the entire frequency band and greater than variations in window length or degree of smoothing. This further emphasizes the importance of properly establishing whether a single representative horizontal spectrum is appropriate – at least for further interpretation regarding the stratigraphy of the soil column. Some indication of the degree of similarity between the mHVSR calculated from each component separately may be useful to include as an output of mHVSR processing. Dietiker *et al.* (2018) propose calculation of a metric to quantify the difference between the two orthogonal components of horizontal motion. They propose that differences of more than 30% between the two components are indicative of strong subsurface changes, and these differences indicate an environment where 1-D subsurface assumptions are no longer valid and the mHVSR should not be used for depth calculations or velocity and depth inversions. Having access to plots of the Fourier amplitude spectra for each component is also useful during mHVSR processing to establish any directional differences.

One of the most important aspects of mHVSr processing is selecting an optimal set of time windows from which to calculate the average mHVSr. This involves selection of an optimal set of time windows, defined by window length and percent overlap. As previously discussed, the chosen window length does not have a significant impact on the computed mHVSr, except perhaps in the case of using very short time windows when interested in the low frequency range of the curve, however, the specific time windows retained to compute the representative mHVSr at a site are important. The best approach is manual de-selection of windows by checking the congruity of the mHVSr in the frequency domain and rejecting windows with anomalous mHVSr response. However, such an approach is not feasible when working with large databases of measurements, it is also somewhat subjective and difficult to replicate between different practitioners. The traditional anti-triggering approach which rejects windows based on a short-term vs. long-term average is successful in certain cases, however, unless the parameter values that define the short-term and long-term average and threshold are specified on a case-by-case basis, it is common that all or no windows will be rejected by this automated quantitative criteria. It is also often the case that windows rejected in the time domain are not anomalous in the frequency domain and vice versa. For this reason, a frequency domain window rejection algorithm is more attractive. Cox *et al.* (2020) implemented such a routine, and the approach produces promising results, however, it is unsuccessful in the presence of multiple peaks or low-frequency disturbances (e.g., wind, poor coupling). Given the non-stationary nature of the wavefield, developing/improving a clustering analysis of mHVSr results from individual time windows in this study to both reject and identify variability between time windows was quite successful. A clustered mHVSr approach to time window rejection is an attractive option because for certain sites it demonstrates the temporal instability of the mHVSr, shedding potential light on the impact that the composition or azimuthal dependence of the wavefield may have on the computed mHVSr. Future studies should investigate what causes the differences in the defined clusters.

3.6 References

Ackerley, N., Beer, M., Kougiumtzoglou, I. A., Patelli, E., & Au, S. K. (2014). Principles of broadband seismometry. *Encyclopedia of Earthquake Engineering*, (Springer, Berlin).

- Afak, E. (2001). Local site effects and dynamic soil behavior. *Soil Dynamics and Earthquake Engineering*, 21(5), 453–458. [https://doi.org/10.1016/S0267-7261\(01\)00021-5](https://doi.org/10.1016/S0267-7261(01)00021-5)
- Albarelo, D., & Lunedei, E. (2013). Combining horizontal ambient vibration components for H/V spectral ratio estimates. *Geophys J Int*, 194(2), 936–951. <https://doi.org/10.1093/gji/ggt130>
- Alfaro, A., Pujades, L. G., Goula, X., Susagna, T., Navarro, M., Sánchez, J., & Canas, J. A. (2002). Preliminary Map of Soil's Predominant Periods in Barcelona Using Microtremors. *Earthquake Microzoning*, 2499–2511. https://doi.org/10.1007/978-3-0348-8177-7_13
- Archuleta, R. J., Seale, S. H., Sangas, P. v., Baker, L. M., & Swain, S. T. (1992). Garner Valley downhole array of accelerometers: Instrumentation and preliminary data analysis. *Bulletin of the Seismological Society of America*, 82(4), 1592–1621. <https://doi.org/10.1785/BSSA0820041592>
- Armstrong J. E. (1990). *Vancouver Geology*. Geological Association of Canada.
- Bard, P.-Y. (1999). Microtremor measurements: A tool for site effect estimation? *The Effects of Surface Geology on Seismic Motion*, 3, 1251–1279.
- Bard, P.-Y., Acerra, C., Aguacil, G., Anastasiadis, A., Atakan, K., Azzara, R., Basili, R., Bertrand, E., Bettig, B., Blarel, F., Bonnefoy-Claudet, S., Paola, B., Borges, A., Sørensen, M., Bourjot, L., Cadet, H., Cara, F., Caserta, A., Chatelain, J.-L., & Zacharopoulos, S. (2008). Guidelines for the implementation of the H/V spectral ratio technique on ambient vibrations measurements, processing and interpretation. *Bulletin of Earthquake Engineering*, 6, 1–2.
- Bensalem, R., Chatelain, J.-L., Machane, D., Oubaiche, E. H., Hellel, M., Guillier, B., Djeddi, M., & Djadia, L. (2010). Ambient Vibration Techniques Applied to Explain Heavy Damages Caused in Corso (Algeria) by the 2003 Boumerdes Earthquake: Understanding Seismic Amplification Due to Gentle Slopes. *Seismological Research Letters*. <https://doi.org/10.1785/gssrl.81.6.928>
- Bignardi, S., Yezzi, A. J., Fiussello, S., & Comelli, A. (2018). OpenHVSR - Processing toolkit: Enhanced HVSR processing of distributed microtremor measurements and spatial variation of their informative content. *Computers & Geosciences*, 120, 10–20. <https://doi.org/10.1016/J.CAGEO.2018.07.006>
- Bonilla, L. F., Steidl, J. H., Gariel, J. C., & Archuleta, R. J. (2002). Borehole Response Studies at the Garner Valley Downhole Array, Southern California. *Bulletin of the Seismological Society of America*, 92(8), 3165–3179. <https://doi.org/10.1785/0120010235>
- Bonnefoy-Claudet, S., Köhler, A., Cornou, C., Wathelet, M., & Bard, P. Y. (2008). Effects of Love Waves on Microtremor H/V Ratio Effects of Love Waves on Microtremor H/V Ratio. *Bulletin of the Seismological Society of America*, 98(1), 288–300. <https://doi.org/10.1785/0120070063>

- Boore, D. M. (2010). Orientation-Independent, Nongeometric-Mean Measures of Seismic Intensity from Two Horizontal Components of Motion Short Note. *Bulletin of the Seismological Society of America*, 100(4), 1830–1835. <https://doi.org/10.1785/0120090400>
- Borcherdt, R. (1970). Effects of local geology on ground motion near San Francisco Bay. *Bulletin of the Seismological Society of America*, 60.
- Bour, M., Fouissac, D., Dominique, P., & Martin, C. (1998). On the use of microtremor recordings in seismic microzonation. *Soil Dynamics and Earthquake Engineering*, 17(7–8), 465–474. [https://doi.org/10.1016/S0267-7261\(98\)00014-1](https://doi.org/10.1016/S0267-7261(98)00014-1)
- Cara, F., di Giulio, G., & Rovelli, A. (2003). A Study on Seismic Noise Variations at Colfiorito, Central Italy: Implications for the Use of H/V Spectral Ratios. *Geophysical Research Letters*, 30(18). <https://doi.org/10.1029/2003GL017807>
- Cassidy, J. F., Brillon, C., Adams, J., & Rogers, G. C. Strong Motion Monitoring in Canada and Recent Datasets From Natural Resources Canada.
- Castellaro, S., & Mulargia, F. (2009). The effect of velocity inversions on H/V. *Pure and Applied Geophysics*, 166(4), 567–592. <https://doi.org/10.1007/S00024-009-0474-5>
- Castellaro, S., & Mulargia, F. (2010). How Far from a Building Does the Ground-Motion Free-Field Start? The Cases of Three Famous Towers and a Modern Building. *Bulletin of the Seismological Society of America*, 100(5A), 2080–2094. <https://doi.org/10.1785/0120090188>
- Chatelain, J. L., Guillier, B., & Parvez, I. A. (2008). False Site Effects: The Anjar Case, following the 2001 Bhuj (India) Earthquake. *Seismological Research Letters*, 79(6), 816–819. <https://doi.org/10.1785/GSSRL.79.6.816>
- Chávez-García, F. J., & Bard, P. Y. (1994). Site effects in Mexico City eight years after the September 1985 Michoacan earthquakes. *Soil Dynamics and Earthquake Engineering*, 13(4), 229–247. [https://doi.org/10.1016/0267-7261\(94\)90028-0](https://doi.org/10.1016/0267-7261(94)90028-0)
- Cheng, T., Cox, B. R., Vantassel, J. P., & Manuel, L. (2020). A statistical approach to account for azimuthal variability in single-station HVSR measurements. *Geophysical Journal International*, 223(2), 1040–1053. <https://doi.org/10.1093/GJI/GGAA342>
- Cox, B. R., Cheng, T., Vantassel, J. P., & Manuel, L. (2020). A statistical representation and frequency-domain window-rejection algorithm for single-station HVSR measurements. *Geophysical Journal International*, 221(3), 2170–2183. <https://doi.org/10.1093/GJI/GGAA119>
- D'Alessandro, A., Luzio, D., Martorana, R., & Capizzi, P. (2016). Selection of Time Windows in the Horizontal-to-Vertical Noise Spectral Ratio by Means of Cluster Analysis. *Bulletin of the Seismological Society of America*, 106(2), 560–574.

- Dietiker, B., Pugin, A. J. M., Crow, H. L., Mallozzi, S., Brewer, K. D., Cartwright, T. J., & Hunter, J. A. (2018). HVSR measurements in complex sedimentary environment and highly structured resonator topography - Comparisons with seismic reflection profiles and geophysical borehole logs. *Symposium on the Application of Geophysics to Engineering and Environmental Problems, 2018-March*.
<https://doi.org/10.4133/SAGEEP.31-025>
- Dunand, F., Bard, P.-Y., Chatelain, J.-L., Guéguen, P., Vassail, T., & Farsi, M. N. (2002, May). Damping and frequency from Randomdec method applied to in situ measurements of ambient vibrations. Evidence for effective soil structure interaction. In *12th European conference on earthquake engineering, London. Paper* (Vol. 869).
- Duval, A. M., Bard, P. Y., Lebrun, B., Lacave-Lache, C., Riepl, J., & Hatzip, D. (2001). n/v technique for site response analysis. Synthesis of data from various surveys. *Bollettino Di Geofisica Teorica Ed Applicata*, 42(3–4), 267–280.
- Edwards, W. N. (2015). *Analysis of measured wind turbine seismic noise generated from the Summerside Wind Farm, Prince Edward Island*. <https://doi.org/10.4095/296443>
- Everitt, B., & Hothorn, T. (2011). *An introduction to applied multivariate analysis with R*. Springer Science & Business Media.
- Fäh, D., Kind, F., & Giardini, D. (2001). A theoretical investigation of average HIV ratios. *Geophysical Journal International*, 145(2), 535–549. <https://doi.org/10.1046/J.0956-540X.2001.01406.X>
- Field, E. H., & Jacob, K. H. (1995). A comparison and test of various site-response estimation techniques, including three that are not reference-site dependent. *Bulletin of the Seismological Society of America*, 85(4), 1127–1143.
<https://doi.org/10.1785/BSSA0850041127>
- Foti, S., Hollender, F., Garofalo, F., Albarello, D., Asten, M., Bard, P. Y., Comina, C., Cornou, C., Cox, B., di Giulio, G., Forbriger, T., Hayashi, K., Lunedei, E., Martin, A., Mercerat, D., Ohrnberger, M., Poggi, V., Renalier, F., Sicilia, D., & Socco, V. (2018). Guidelines for the good practice of surface wave analysis: a product of the InterPACIFIC project. *Bulletin of Earthquake Engineering*, 16(6), 2367–2420.
<https://doi.org/10.1007/S10518-017-0206-7/FIGURES/34>
- Foti, S., Parolai, S., Albarello, D., & Picozzi, M. (2011). Application of Surface-Wave Methods for Seismic Site Characterization. *Surveys in Geophysics 2011* 32:6, 32(6), 777–825. <https://doi.org/10.1007/S10712-011-9134-2>
- Gallipoli, M. R., Mucciarelli, M., Castro, R. R., Monachesi, G., & Contri, P. (2004). Structure, soil–structure response and effects of damage based on observations of horizontal-to-vertical spectral ratios of microtremors. *Soil Dynamics and Earthquake Engineering*, 24(6), 487–495.

- Gan, G., Ma, C., & Wu, J. (2007). 1. Data Clustering. *Data Clustering: Theory, Algorithms, and Applications*, 3–17. <https://doi.org/10.1137/1.9780898718348.CH1>
- Gospe, T., Zimmaro, P., Wang, P., Buckreis, T., Ahdi, S., Yong, A., ... & Stewart, J. (2021). Supplementing shear wave velocity profile database with microtremor-based H/V spectral ratios.
- Guéguen, P., Chatelain, J. L., Guillier, B., & Yepes, H. (2000). An indication of the soil topmost layer response in Quito (Ecuador) using noise H/V spectral ratio. *Soil Dynamics and Earthquake Engineering*, 19(2), 127–133. [https://doi.org/10.1016/S0267-7261\(99\)00035-4](https://doi.org/10.1016/S0267-7261(99)00035-4)
- Guillier, B., Atakan, K., Chatelain, J.-L., Havskov, J., Ohrnberger, M., Cara, F., Duval, A.-M., Zacharopoulos, S., & Teves-Costa, P. (2008). Influence of instruments on the H/V spectral ratios of ambient vibrations. *Bulletin of Earthquake Engineering*, 6(1), 3–31.
- Guillier, B., Chatelain, J.-L., Bonnefoy-Claudet, S., & Haghshenas, E. (2007). Use of Ambient Noise: From Spectral Amplitude Variability to H/V Stability. *Journal of Earthquake Engineering*, 11, 925–942. <https://doi.org/10.1080/13632460701457249>
- Guillier, B., Machane, D., Oubaiche, E. H., Chatelain, J.-L., Meziane, Y., Bensalem, R., Dunand, F., Gueguen, P., Hadid, M., Hellel, M., Kibboua, A., Laouami, N., Nourredine, M., Nour, A., & Remas, A. (2004). Résultats préliminaires sur les fréquences fondamentales et les amplifications de sols, obtenus par l'étude du bruit de fond, sur la ville de Boumerdes - Algérie. *Mémoires Du Service Géologique de l'Algérie*, 103–114.
- Hellel, M., Chatelain, J.-L., Guillier, B., Machane, D., ben Salem, R., Oubaiche, E. H., & Haddoum, H. (2010). Heavier damages without site effects and site effects with lighter damages: Boumerdes City (Algeria) after the May 2003 earthquake. *Seismological Research Letters*, 81(1), 37.
- Herak, M. (2008). ModelHVSR—A Matlab® tool to model horizontal-to-vertical spectral ratio of ambient noise. *Computers & Geosciences*, 34(11), 1514–1526. <https://doi.org/10.1016/J.CAGEO.2007.07.009>
- Herak, M., Allegretti, I., Herak, D., Kuk, K., Kuk, V., Marić, K., Markušić, S., & Stipčević, J. (2009). HVSR of ambient noise in Ston (Croatia): comparison with theoretical spectra and with the damage distribution after the 1996 Ston-Slano earthquake. *Bulletin of Earthquake Engineering* 2009 8:3, 8(3), 483–499. <https://doi.org/10.1007/S10518-009-9121-X>
- Horike, M., Zhao, B., & Kawase, H. (2001). Comparison of Site Response Characteristics Inferred from Microtremors and Earthquake Shear Waves. *Bulletin of the Seismological Society of America*, 91(6), 1526–1536. <https://doi.org/10.1785/0120000065>
- Kanai, K., & Tanaka, T. (1961). On microtremor VIII. *Bulletin, Earthquake Institute*, 39, 97–114.

- Kaya, Y., Ventura, C., Huffman, S., & Turek, M. (2017). British Columbia smart infrastructure monitoring system. *Canadian Journal of Civil Engineering*, 44(8), 579-588.
- Kitagawa, Y., Ohkawa, I., & Kashima, T. (1988). Dense strong motion earthquake seismometer array at site with different topographic and geologic conditions in Sendai. *Proc. 9th WCEE*, 2, 215–220.
- Lachet, C. D., & Bard, P.-Y. (1994). Numerical and Theoretical Investigations on the Possibilities and Limitations of Nakamura's Technique. *Journal of Physics of the Earth*, 42, 377–397. <https://doi.org/10.4294/jpe1952.42.377>
- Langston, C. A. (1977). Corvallis, Oregon, crustal and upper mantle receiver structure from teleseismic P and S waves. *Bulletin of the Seismological Society of America*, 67(3), 713–724. <https://doi.org/10.1785/BSSA0670030713>
- Langston, C. A. (1979). Structure under Mount Rainier, Washington, inferred from teleseismic body waves. *Journal of Geophysical Research: Solid Earth*, 84(B9), 4749–4762. <https://doi.org/10.1029/JB084IB09P04749>
- Laouami, N. (2019). Vertical ground motion prediction equations and vertical-to-horizontal (V/H) ratios of PGA and PSA for Algeria and surrounding region. *Bulletin of Earthquake Engineering 2019 17:7*, 17(7), 3637–3660. <https://doi.org/10.1007/S10518-019-00635-Y>
- Laouami, N., Hadid, M., & Mezouar, N. (2018a). Proposal of an empirical site classification method based on target simulated horizontal over vertical spectral ratio. *Bulletin of Earthquake Engineering*, 16(12), 5843–5874.
- Laouami, N., Slimani, A., & Larbes, S. (2018b). Ground motion prediction equations for Algeria and surrounding region using site classification based H/V spectral ratio. *Bulletin of Earthquake Engineering 2018 16:7*, 16(7), 2653–2684. <https://doi.org/10.1007/S10518-018-0310-3>
- Lecocq, T., Hicks, S. P., van Noten, K., van Wijk, K., Koelemeijer, P., de Plaen, R. S. M., Massin, F., Hillers, G., Anthony, R. E., Apoloner, M.-T., & others. (2020). Global quieting of high-frequency seismic noise due to COVID-19 pandemic lockdown measures. *Science*, 369(6509), 1338–1343.
- Lermo, J., & Chávez-García, F. J. (1994). Are microtremors useful in site response evaluation?. *Bulletin of the seismological society of America*, 84(5), 1350-1364.
- Malischewsky, P. G., & Scherbaum, F. (2004). Love's formula and H/V-ratio (ellipticity) of Rayleigh waves. *Wave Motion*, 40(1), 57–67. <https://doi.org/10.1016/J.WAVEMOTI.2003.12.015>
- Marcillo, O. E., & Carmichael, J. (2018). The Detection of Wind-Turbine Noise in Seismic Records. *Seismological Research Letters*, 89(5), 1826–1837. <https://doi.org/10.1785/0220170271>

- Martorana, R., Capizzi, P., D'Alessandro, A., Luzio, D., di Stefano, P., Renda, P., & Zarcone, G. (2018). Contribution of HVSR measures for seismic microzonation studies. *Annals of Geophysics*.
- Mihaylov, A., el Naggar, H., Mihaylov, D., & Dineva, S. (2019). Approximate analytical HVSR curve using multiple band-pass filters and potential applications. *Soil Dynamics and Earthquake Engineering*, *127*, 105840. <https://doi.org/10.1016/J.SOILDYN.2019.105840>
- Mihaylov, D., el Naggar, M. H., & Dineva, S. (2016). Separation of High- and Low-Level Ambient Noise for HVSR: Application in City Conditions for Greater Toronto Area. *Bulletin of the Seismological Society of America*, *106*(5), 2177–2184. <https://doi.org/10.1785/0120150389>
- Mucciarelli, M. (1998). Reliability and applicability of Nakamura's technique using microtremors: An experimental approach. *Journal of Earthquake Engineering*, *2*(4), 625–638. <https://doi.org/10.1080/13632469809350337>
- Mucciarelli, M., & Gallipoli, M. R. (2004). The HVSR technique from microtremor to strong motion: empirical and statistical considerations. *Proc. of 13th World Conference of Earthquake Engineering, Vancouver, BC, Canada, Paper, 45*.
- Mucciarelli, M., Gallipoli, M. R., & Arcieri, M. (2003). The Stability of the Horizontal-to-Vertical Spectral Ratio of Triggered Noise and Earthquake Recordings. *Bulletin of the Seismological Society of America*, *93*(3), 1407–1412. <https://doi.org/10.1785/0120020213>
- Mucciarelli, M., Gallipoli, M. R., di Giacomo, D., di Nota, F., & Nino, E. (2005). The influence of wind on measurements of seismic noise. *Geophysical Journal International*, *161*(2), 303–308.
- Mucciarelli, M., & Monachesi, G. (1998). A quick survey of local amplifications and their correlation with damage observed during the Umbro-Marchesan (Italy) earthquake of September 26, 1997. *Journal of Earthquake Engineering*, *2*(2), 325–337.
- Nakamura, Y. (1989). A method for dynamic characteristics estimation of subsurface using microtremor on the ground surfac. *Quarterly Report of RTRI (Railway Technical Research Institute) (Japan)*, *30*.
- Natural Resources Canada (NRCAN Canada). (1975). Canadian National Seismograph Network [Data set]. International Federation of Digital Seismograph Networks. <https://doi.org/10.7914/SN/CN>
- Panou, A. A., Theodulidis, N., Hatzidimitriou, P., Stylianidis, K., & Papazachos, C. B. (2005). Ambient noise horizontal-to-vertical spectral ratio in site effects estimation and correlation with seismic damage distribution in urban environment: the case of the city of Thessaloniki (Northern Greece). *Soil Dynamics and Earthquake Engineering*, *25*(4), 261–274. <https://doi.org/10.1016/J.SOILDYN.2005.02.004>

- Parolai, S., Bormann, P., & Milkereit, C. (2001). Noise measurements in the Cologne area: Comparison of two different methods and assessment of the natural frequency of the sedimentary cover. *IAGA-IASPEI Joint Scientific Assembly, IASPEI Symposium (Hanoi, Vietnam 2001)*.
- Parolai, S., & Galiana-Merino, J. J. (2006). Effect of Transient Seismic Noise on Estimates of h/v Spectral Ratios. *Bulletin of the Seismological Society of America*, 96(1), 228–236. <https://doi.org/10.1785/0120050084>
- Picozzi, M., Parolai, S., & Albarello, D. (2005). Statistical Analysis of Noise Horizontal-to-Vertical Spectral Ratios (hvsr). *Bulletin of the Seismological Society of America*, 95(5), 1779–1786. <https://doi.org/10.1785/0120040152>
- Piña-Flores, J., Cárdenas-Soto, M., García-Jerez, A., Seivane, H., Luzón, F., & Sánchez-Sesma, F. J. (2020). Use of peaks and troughs in the horizontal-to-vertical spectral ratio of ambient noise for Rayleigh-wave dispersion curve picking. *Journal of Applied Geophysics*, 177, 104024. <https://doi.org/10.1016/J.JAPPGEO.2020.104024>
- Riedesel, M. A., Moore, R. D., & Orcutt, J. A. (1990). Limits of sensitivity of inertial seismometers with velocity transducers and electronic amplifiers. *Bulletin of the Seismological Society of America*, 80(6A), 1725–1752. <https://doi.org/10.1785/BSSA08006A1725>
- Rodgers, P. W. (1992). Frequency limits for seismometers as determined from signal-to-noise ratios. Part 1. The electromagnetic seismometer. *Bulletin of the Seismological Society of America*, 82(2), 1071–1098. <https://doi.org/10.1785/BSSA0820021071>
- Rodgers, P. W., Martin, A. J., Robertson, M. C., Hsu, M. M., & Harris, D. B. (1995). Signal-coil calibration of electromagnetic seismometers. *Bulletin of the Seismological Society of America*, 85(3), 845–850. <https://doi.org/10.1785/BSSA0850030845>
- Sánchez-Sesma, F. J., Rodríguez, M., Iturrarán-Viveros, U., Luzón, F., Campillo, M., Margerin, L., García-Jerez, A., Suarez, M., Santoyo, M. A., & Rodríguez-Castellanos, A. (2011). A theory for microtremor H/V spectral ratio: application for a layered medium. *Geophysical Journal International*, 186(1), 221–225. <https://doi.org/10.1111/J.1365-246X.2011.05064.X>
- Satoh, T., Kawase, H., & Sato, T. (1995). Evaluation of Local Site Effects and Their Removal from Borehole Records Observed in the Sendai Region, Japan. *Bulletin - Seismological Society of America*, 85. <https://doi.org/10.1785/BSSA0850061770>
- Stafford, P. J., Rodriguez-Marek, A., Edwards, B., Kruiver, P. P., & Bommer, J. J. (2017). Scenario Dependence of Linear Site-Effect Factors for Short-Period Response Spectral Ordinates. *Bulletin of the Seismological Society of America*, 107(6), 2859–2872. <https://doi.org/10.1785/0120170084>

- Steidl, J. H., Tumarkin, A. G., & Archuleta, A. J. (1996). What is a reference site? *Bulletin of the Seismological Society of America*, 86(6), 1733–1748.
<https://doi.org/10.1785/BSSA0860061733>
- Strollo, A. (2010). *Development of techniques for earthquake microzonation studies in different urban environment* (Doctoral dissertation, Universität Potsdam).
- Strollo, A., Bindi, D., Parolai, S., & Jäckel, K. H. (2008a). On the suitability of 1s geophone for ambient noise measurements in the 0.1–20Hz frequency range: experimental outcomes. *Bulletin of Earthquake Engineering* 2008 6:1, 6(1), 141–147.
<https://doi.org/10.1007/S10518-008-9061-X>
- Strollo, A., Parolai, S., Jäckel, K. H., Marzorati, S., & Bindi, D. (2008b). Suitability of Short-Period Sensors for Retrieving Reliable H/V Peaks for Frequencies Less Than 1Hz. *Bulletin of the Seismological Society of America*, 98(2), 671–681.
<https://doi.org/10.1785/0120070055>
- Tao, Y., & Rathje, E. (2020). The Importance of Distinguishing Pseudoresonances and Outcrop Resonances in Downhole Array Data. *Bulletin of the Seismological Society of America*, 110(1), 288–294. <https://doi.org/10.1785/0120190097>
- Vantassel, J. P. (2020). *jpvantassel/hvsrpy*.
- Volant, P., Cotton, F., & Gariel, J. C. (1998). Estimation of site response using the H/V method. Applicability and limits of this technique on Garner Valley downhole array dataset (California). *Proceedings of the 11th European Conference on Earthquake Engineering*.
- Wang, P., Zimmaro, P., Gospe, T., Ahdi, S. K., Yong, A., & Stewart, J. P. (2021). *Horizontal-to-vertical spectral ratios from California sites: Open-source database and data interpretation to establish site parameters*. California Geological Survey.
- Wathelet, M., Bard, P. Y., Chatelain, J. L., Cornou, C., Di Giulio, G., Fah, D., ... & Ohrnberger, M. (2010). Geopsy on-line documentation.
- Wathelet, M., Chatelain, J. L., Cornou, C., Giulio, G. di, Guillier, B., Ohrnberger, M., & Savvaidis, A. (2020). Geopsy: A User-Friendly Open-Source Tool Set for Ambient Vibration Processing. *Seismological Research Letters*, 91(3), 1878–1889.
<https://doi.org/10.1785/0220190360>
- Withers, M. M., Aster, R. C., Young, C. J., & Chael, E. P. (1996). High-frequency analysis of seismic background noise as a function of wind speed and shallow depth. *Bulletin of the Seismological Society of America*, 86(5), 1507–1515.
<https://doi.org/10.1785/BSSA0860051507>
- Yamazaki, F., & Ansary, M. A. (1997). Horizontal-to-vertical spectrum ratio of earthquake ground motion for site characterization. *Earthquake Engineering & Structural Dynamics*, 26(7), 671–689.

- Zhao, J. X., Irikura, K., Zhang, J., Fukushima, Y., Somerville, P. G., Asano, A., Ohno, Y., Oouchi, T., Takahashi, T., & Ogawa, H. (2006). An Empirical Site-Classification Method for Strong-Motion Stations in Japan Using h/v Response Spectral Ratio. *Bulletin of the Seismological Society of America*, 96(3), 914–925. <https://doi.org/10.1785/0120050124>
- Zhu, C., Cotton, F., & Pilz, M. (2020). Detecting Site Resonant Frequency Using HVSR: Fourier versus Response Spectrum and the First versus the Highest Peak Frequency. *Bulletin of the Seismological Society of America*, 110(2), 427–440. <https://doi.org/10.1785/0120190186>

Chapter 4

From 2002 to present, more than 5000 single-station microtremor measurements have been acquired throughout the Metro Vancouver region. Most of these measurements were acquired during an ongoing 5-year seismic microzonation mapping project. Significant effort went into ensuring all data were processed consistently, and that the outputs could be reliably regenerated by third-party practitioners, as discussed in the previous chapter. After ensuring consistently processed data, the challenge shifted toward how to present the data in a user-friendly manner. This chapter will describe a peak picking methodology, developed to account for the case of multiple peaks as well as how the acquired data – including raw, intermediate, and interpreted results - will be presented to end-users.

4 Preliminary Interpretation and Development of mHVSr Database

At present, estimation of seismic site effects has become a major challenge for efficient mitigation of seismic risk. In the case of moderate earthquakes, or moderate motion experienced at some distance from large events, severe damage is often limited to zones of geological and geotechnical conditions that give rise to significant site effects (Haghshenas, 2005). The standard spectral ratio (SSR) (Borcherdt, 1970) approach, based on the comparison of earthquake recordings obtained simultaneously on soil sites and on a reference rock site, is thought to be one of the more reliable methods for site response estimation but is not always easy to apply (Haghshenas, 2005). Numerical estimation of site effects requires detailed knowledge of geotechnical and geophysical parameters, in some cases up to large depths, which result in either very expensive costs of unreliable results (Haghshenas *et al.* 2008).

Seismic site response is influenced by a plethora of factors, some of which include topography, resonance, amplification due to impedance contrasts, and amplification related to wave propagation in sedimentary basins (Wang *et al.*, 2021). GMMs typically predict site response from relatively simple site parameters such as the time averaged shear wave velocity (V_s) to 30 m depth (V_{s30}) (Gospe *et al.*, 2020). These models are not site specific and are thus referred to as ergodic. Should such a model be applied to a particular site, the

actual, observed site amplification at the site would be expected to depart from the ergodic estimate due to site-specific geologic conditions. Non-ergodic models account for the effects of these features on site amplification. One feature of non-ergodic site response is resonance at one or more frequencies, which produce peaks that are smoothed out in ergodic models (Bonilla *et al.*, 1997, 2002; di Alessandro *et al.*, 2012; Wang *et al.*, 2020). While V_{S30} provides a reasonable, first order estimate of site response over a wide frequency range (Abrahamson *et al.* 2014, Campbell and Bozorgnia 2014, Chiou and Youngs 2014), an estimate of f_0 , can be effective for describing site amplification for frequencies proximal to resonant frequencies. For a simple model involving a single elastic layer over a half-space, f_0 at a site is related to V_{s_ave} (average shear-wave velocity of overlying layer) and h (depth) according to (Haskell, 1960),

$$f_0 = \frac{V_{s_ave}}{4h} \quad \text{equation 4-1}$$

Over the past several decades, the single-station mHVSr method has grown in popularity as a tool for shallow subsurface characterization (e.g., Bard, 1998, Fäh *et al.*, 2003, Scherbaum *et al.*, 2016, Lontsi *et al.*, 2015, 2016, Piña-Flores *et al.*, 2016, Spica *et al.*, 2018, García-Jerez *et al.*, 2019). The interest in the method stems from its practicability, cost efficiency, and the minimum investment of effort during microtremor field campaigns (Lontsi, 2016). The generic engineering parameter directly estimated from the spectrum of the mHVSr, f_{0HV} , is considered a reliable estimate of f_0 , (Nakamura, 1989, Lachet & Bard, 1994).

The applicability of the mHVSr technique has been the subject of many experimental studies and most observations emphasize the reliability of the estimate of f_0 derived from mHVSr processing. There are examples of disagreement in the literature, for example, either mHVSr curves are flat and fail to exhibit the amplification observed using other techniques, or the frequency of the mHVSr peak is different from values indicated by other techniques (Volant *et al.* 1998, Moya *et al.* 2000, Haghshenas *et al.* 2003, Maresca *et al.* 2003). Satoh *et al.* (2001) also documents a case where the correlation of the mHVSr peak frequency and the site fundamental frequency exhibits some restrictions. Their observations indicated that the microtremor H/V peak frequencies roughly coincide with

those of eHVSR and SSR for S-waves only for frequencies lower than 1 Hz and peak amplitude larger than 3.

A wide variety of wave propagation phenomena are involved in the mHVSR including body waves, surface waves, and various other ways that energy can be trapped in 3D geometries of geological structures. These phenomena affect both the numerator (i.e., horizontal components) and denominator (i.e., vertical components), so peaks in the ratio can be caused by troughs in the denominator.

With regards to the H/V peak amplitude ($A_{\#HV}$), the values are much less consistent with the amplification values than what is observed for f_{0HV} and the site fundamental frequency (Haghshenas, 2005). In many cases, the amplitude of the microtremor H/V peak is smaller than the amplification value given by the SSR method. Bard (1999) proposed that the difference of SSR and H/V amplification amplitudes may be related to 2D/3D effects, in such a way that this difference gets larger as 2D and 3D effects get more pronounced in the SSR method. This suggestion was made based on several site investigations in France and Greece (Duval 1994, Duval *et al.* 1996, 2001, Lebrun 1997, Riepl *et al.* 1998, Beauval *et al.* 2003) and observations in Coachella Valley (Field 1996). In a study completed for sites from the KiK-net, K-net and Nobi plain networks in Japan, Sawada *et al.* (2004) introduced an “integral” spectral intensity parameter taking into account both the amplitude and the bandwidth of the spectral peaks. The observed differences between microtremor H/V ratio and the two other spectral curves (eHVSR and SSR) exhibited a site dependence: the higher the site fundamental frequency, the better the agreement between the spectral intensity parameters derived from each spectral curve.

Regardless of the uncertainty inherent to both f_{0HV} and A_{0HV} practitioners typically provide an estimate of both quantities as interpreted from the processed spectral ratio. Although most mHVSR research is catered toward measurements with single peaks, observing multiple peaks is not uncommon. Secondary peaks could materialize from the presence of more than one strong impedance contrast or possibly represent higher modes (Lontsi, 2016).

The presentation of mHVSr data to the end-user and what to include in a database requires renewed consideration as there are many stages to processing and interpretation, which if not correctly communicated may not provide necessary information to appreciate the measured response. In general, the outcome of each mHVSr field campaign is a spreadsheet document which, for each site, includes the meta-data associated with each measurement as well as the interpreted value of the site fundamental frequency (f_{0HV}) and its associated amplitude. However, there is additional information contained in the mHVSr spectrum that cannot be communicated through simple reporting of these two peak quantities, for example, width of the peak, presence of secondary peaks, quality of the microtremor data, etc. As such, creating a database structure, which allows end-users of mHVSr-related products to interact with the processed data and verify the interpreted results presented in a spreadsheet increases the utility of the acquired data.

4.1 Picking Peaks in mHVSr Measurements

Consistent with the terminology used by Cox *et al.* (2020), we have opted to use ‘peak frequency’ to refer to the lowest frequency peak in the HVSr curve (f_{0HV}) which is commonly used to estimate the site fundamental resonance frequency (f_0). It should be mentioned that to our knowledge, all currently existing mHVSr software functions by identifying the global maximum peak of the mHVSr and in the case where there are multiple peaks in the measurement, if the lower frequency peak has a lower amplitude than the higher frequency peak, it will not be identified as the ‘peak frequency’. In the following, when discussing the available methods implemented through various softwares for identifying peaks in mHVSr spectra, peak frequency will always be referred to generically as $f_{\#HV}$, however, in most cases only a single peak is picked and although it is the lowest peak frequency in the mHVSr (f_{0HV}) it may not necessarily correspond to the site’s fundamental frequency (f_0).

The mean curve of HVSr plots can generally be classified as containing no peaks, one peak, or multiple peaks (Kwak *et al.* 2017). A single peak may indicate the site has strong impedance contrast(s) near one or more modal frequencies, whereas multiple peaks may indicate multiple impedance contrasts at different depths. When there are no peaks present in an mHVSr, this suggests that the site may either be underlain with a sedimentary

package that lacks a significant impedance contrast, or it is a rock site with nearly depth-invariant near-surface velocities (Wang *et al.*, 2021).

The SESAME guidelines (Bard *et al.*, 2008) provide a procedure for identification of peaks that first considers three criteria that assess the reliability of the mHVSr curve and then considers six conditions intended to establish the presence of a clear mHVSr peak. The first two criteria for the reliability of mHVSr curves constrain the minimum required number of sub-windows and duration.

Wang (2020) applied the SESAME criteria to the data from single-station microtremor measurements acquired in California. This resulted in very few sites identified as having peaks. He concluded that this was not reliable, because simple visual inspection of the data indicated far more sites with peaks. To devise a more reliable approach to peak identification two analysts were asked to inspect each HVSr to identify sites with or without peaks. The two analysts developed their own criteria for these assessments and based on the results, Wang (2020) adjusted elements of the SESAME criteria (Table 4-1).

Table 4-1. Comparison of original SESAME criteria (Bard *et al.*, 2008) vs. modified criteria proposed by Wang (2020).

Criteria	SESAME	Wang (2020)
Reliability: $f_{\#HV} > 0.5$ Hz, $f \in [0.5f_{\#HV}, 2f_{\#HV}]$	$\sigma_A(f) < 2$	$\sigma_A(f) < 2$
Reliability: $f_{\#HV} < 0.5$ Hz, $f \in [0.5f_{\#HV}, 2f_{\#HV}]$	$\sigma_A(f) < 3$	$\sigma_A(f) < 3$
Clear 1: $f \in [0.25f_{\#HV}, f_{\#HV}]$	$A_{H/V}(f) < 0.5A_{\#HV}$	$A_{H/V}(f) < 0.6A_{\#HV}$
Clear 2: $f \in [f_{\#HV}, 4f_{\#HV}]$	$A_{H/V}(f) < 0.5A_{\#HV}$	$A_{H/V}(f) < 0.6A_{\#HV}$
Clear 3	$A_{\text{peak}} \geq 2$	$A_{\text{peak}} \geq 1.6$
Clear 4: peak of SD curve $f_{\#HV}[A_{H/V}(f) - \sigma_A(f)]$	within $[f_{\#HV}/1.05, 1.05f_{\text{peak}}]$	within $[f_{\#HV}/1.15, 1.15f_{\text{peak}}]$
Clear 4: peak of SD curve $f_{\#HV}[A_{H/V}(f) + \sigma_A(f)]$	within $[f_{\#HV}/1.05, 1.05f_{\text{peak}}]$	within $[f_{\#HV}/1.12, 1.12f_{\text{peak}}]$
Clear 5: $f_{\#HV} < 0.2$ Hz	$\sigma_f < 0.25f_{\#HV}$	-
Clear 5: $f_{\#HV} \in [0.2, 0.5)$ Hz	$\sigma_f < 0.20f_{\#HV}$	-
Clear 5: $f_{\#HV} \in [0.5, 1.0)$ Hz	$\sigma_f < 0.15f_{\#HV}$	-
Clear 5: $f_{\#HV} \in [1.0, 2.0)$ Hz	$\sigma_f < 0.10f_{\#HV}$	-
Clear 5: $f_{\#HV} > 2.0$ Hz	$\sigma_f < 0.05f_{\#HV}$	-
Clear 6: $f_{\#HV} < 0.2$ Hz	$\sigma_A < 3$	$\sigma_A < 3$
Clear 6: $f_{\#HV} \in [0.2, 0.5)$ Hz	$\sigma_A < 2.5$	$\sigma_A < 2.5$
Clear 6: $f_{\#HV} \in [0.5, 1.0)$ Hz	$\sigma_A < 2$	$\sigma_A < 2$
Clear 6: $f_{\#HV} \in [1.0, 2.0)$ Hz	$\sigma_A < 1.78$	$\sigma_A < 1.78$
Clear 6: $f_{\#HV} > 2.0$ Hz	$\sigma_A < 1.58$	$\sigma_A < 1.58$

Rows labeled Clear # represent the #-th condition for a clear peak. $f_{\#HV}$ is the variable of interest (there could be multiple $f_{\#HV}$ values in a single curve), $A_{\#HV}$ is the amplitude at $f_{\#HV}$; $A_{H/V}(f)$ is the

amplitude of HVSR mean curve at frequency f ; $\sigma(f)$ is standard deviation of $f_{\#HV}$, and $\sigma_A(f)$ is standard deviation of $A_{HVave}(f)$

In the traditional deterministic method, the peak frequency from the mean HVSR curve is typically chosen as an estimate of the site resonance frequency, without any associated statistics. In the probabilistic method, a sample set of $f_{\#HV}$ values result from collecting $f_{\#HV}$ values for each time window included in analysis; these estimates of $f_{\#HV}$ from individual windows can be denoted as $f_{\#HV,i}$. Statistics such as the mean and standard deviation of $f_{\#HV}$ can be computed from these samples (Cox *et al.*, 2020).

Bard and SESAME-Team (2008) use the mean and standard deviation of $f_{\#HV}$ to statistically represent $f_{\#HV}$ and its variability. These two parameters are commonly used to describe a normal distribution. Cox *et al.* (2020) propose that a lognormal distribution would be more appropriate to use as an uncertainty estimate of $f_{\#HV}$ because it allows interchangeability of the statistics for $f_{\#HV}$ and its reciprocal, the fundamental site period ($T_{\#HV}$). The site period is an important parameter in several existing and proposed seismic site classification schemes (Zhao *et al.* 2006, Pitilakis *et al.* 2013, 2018). If $f_{\#HV}$ is assumed to follow a normal distribution, $T_{\#HV}$ follows a reverse normal distribution for which the mean and variance do not exist. If $f_{\#HV}$ follows a lognormal distribution $\ln(f_{\#HV})$ follows a normal distribution, and $-\ln(f_{\#HV})$ which is equivalently $\ln(T_{\#HV})$ also follows a normal distribution. Although we recognize the validity of this argument, for the present work, a normal distribution is considered. Future development will provide the option to calculate both normal and log-normal statistics.

To date, most available mHVSR processing software has been developed to interpret measurements with a single peak. A peak picking algorithm, usually in conjunction with the SESAME criteria, is used to find the global maximum for each time window included in the analysis and also for the mean curve. Statistics of $f_{\#HV}$ can be calculated using $f_{\#HV,i}$ from the individual windows, and these statistics (standard deviation of $f_{\#HV}$, for e.g.) are required if one wishes to check fulfillment of the SESAME criteria. For measurements with more than one peak, this becomes somewhat challenging, because it's possible that the average curve has two peaks, but for an individual time window included in the analysis, there is only a single peak, or perhaps three peaks which are identified. The

method of mapping peaks from the individual time windows to those picked from the average curve requires consideration.

IRIS developed a toolbox to compute the HVSR (Bahavar *et al.*, 2020). The toolbox offers ways to compute the ratio by providing different averaging options; from the simple average of spectral ratios to the ratio of spectral averages. This software facilitates identification of more than one HVSR peak. The toolbox offers the capability to detect local maxima of HVSR curves and rank them based on a set of predefined rules. The peak ranking method is similar to that of SESAME (Bard *et al.*, 2008) and tests each peak for three clarity and stability conditions of amplitude and based on these tests, assigns a value between 0-6 to each HVSR peak. An example of the output provided by the toolbox is illustrated in Figure 4-1.

TABLE 2

Frequency-Dependent Threshold Values for Stability Conditions (Bard and SESAME team, 2004)

Frequency Range (Hz)	<0.2	0.2–0.5	0.5–1.0	1.0–2.0	>2.0
$\varepsilon(f_0)$ Hz	$0.25f_0$	$0.20f_0$	$0.15f_0$	$0.10f_0$	$0.05f_0$
$\log \theta(f_0)$	0.48	0.40	0.30	0.25	0.20

TABLE 3

Ranking Report Generated for the Horizontal-to-Vertical Spectral Ratio (HVSR) Computed for Station XF.MA35, February 2007 Using Method M4

f_0 (Hz)	$A_0 > 2$	f^-	f^+	f_0^- within $\pm 5\%$ of f_0	f_0^+ within $\pm 5\%$ of f_0	$of < \varepsilon f_0$	$\Sigma \text{LogHVSR} < \text{Log} \theta$	Score
1.234	6.71	0.800	—	1.234 within $\pm 5\%$ of 1.234	1.234 within $\pm 5\%$ of 1.234	$0.0563 < 0.10 \times 1.234$	$0.1020 < 0.25$	5/6
4.150	5.66	—	7.611	4.150 within $\pm 5\%$ of 4.150	4.150 within $\pm 5\%$ of 4.150	$0.3834 < 0.05 \times 4.150$	$0.0995 < 0.20$	4/6

Figure 4-1. Example output of IRIS HVSR toolbox. Adapted from Bahavar *et al.* (2020).

The toolbox checks the SESAME criteria for each identified peak. Unfortunately, the toolbox was developed to be compatible with seismic sensors which are part of the IRIS network, and so the scripts must be significantly modified to allow compatibility with data of different formats. However, their methodology of identification of multiple peaks and

calculating statistics for each was the inspiration behind the peak picking methodology presented in this current work.

In addition to simply providing the frequency at which a peak occurs and its amplitude, and perhaps some associated statistics, additional information pertaining to the peak width, or the curve morphology is useful. Wang *et al.* (2022) follow a procedure adopted from Ghofrani & Atkinson (2014) and for mean HVSR plots with a peak, fit a Gaussian pulse function of the form,

$$F_{\frac{H}{V},i} = c_{0,i} + c_{1,i} \exp \left[-\frac{1}{2} \left(\frac{\ln(f/f_{pi})}{2w_i} \right)^2 \right], \quad \text{equation 4-2}$$

in which i is the order of peak (only 1 or 2 can be selected), $c_{0,i}$ is a frequency-independent constant indicating the amplitude of the flat tails, $c_{1,i}$ is the peak amplitude relative to $c_{0,i}$, f is frequency in Hz, f_{pi} is the fitting peak frequency in Hz and w_i controls the peak width. The fit is performed using the *optimize* function in the Python *Scipy* package, which uses non-linear regression to minimize the sum of squared errors. Fitting can also be performed in R using *TreeReg.R* script which was developed by Wang *et al.* (2021). Yazdi *et al.* (2022) also propose a set of automated methodologies for estimating site fundamental frequency and its uncertainty using HVSR curves.

Parolai *et al.* (2019) introduced a method to highlight the peaks in the H/V that are expected to indicate the presence of impedance contrasts at depth. The procedure is like that introduced by Wüster (1993) and applied by Parolai *et al.* (2002) for identifying similar features in sonograms. In the proposed approach, the visibility of local peaks in the HVSR are improved by smoothing the spectral ordinates using a Konno and Ohmachi (1998) window with two different values for the parameter b (smoothing constant). Through experimentation, they set the parameter b for the low level of smoothing to 30 and for the high level of smoothing to 5. The difference between the logarithms of the low- and highly-smoothed estimates at each frequency in the average H/V ratios is calculated and then considered as an indication of a local peak (if positive). This is an interesting approach that should be further investigated and applied, but was not applied in the present study.

Owing to the random nature of the microtremor wavefield, issues related to experimental setup (i.e., sensor coupling), as well as environmental conditions, peaks are not always clear in mHVSr measurements. For this reason, it is important to specify certain thresholds if using an automated algorithm for picking peaks to ensure spurious peaks are generally not picked and only those with a likely geologic origin are. The present study aims to develop a methodology to pick multiple peaks from mHVSr curves, provide statistics for each peak, and extract additional quantitative information parameterizing each peak that can be contained in a database and are (or may be in future) useful for site condition interpretation. A proposed structure for a database of large-quantity mHVSr data is also presented.

4.1.1 Peak Picking and Ranking Algorithm

The processing methodology used to prepare the input mHVSr spectra is described in Chapter 3 of this thesis. The output of that methodology is several clusters of mHVSr curves derived from analysis of the curves from individual time windows that share similar morphology. The practitioner judges the cluster which provides the most representative mHVSr response for the site, and then the mHVSr curves computed from individual time windows grouped into that cluster are what are considered in the following procedure.

The peak picking and ranking algorithm proposed in this current work has its roots in that developed by IRIS (Bahavar *et al.* 2020). Processing of the single-station microtremor measurements is accomplished by using the mHVSr curves from individual time windows, output by HVSRPy (Cox *et al.* 2020). These time windows are then supplied as input to a curve clustering algorithm. The agglomerative hierarchical clustering defines n clusters which correspond to the variability in the shape of mHVSr response over the duration of the measurement. For each defined cluster the following peak picking algorithm is executed.

The Python package *Scipy* has a peak picking function (*find_peaks*). The function takes as input a 1-D array and locates all local maxima by comparison with neighbouring values. The function allows the user to specify conditions for a peak's properties such as:

1. Amplitude: required amplitude of peaks
2. Distance: required minimal horizontal distance in samples between neighboring peaks. Smaller peaks are removed first until the condition is fulfilled for all remaining peaks
3. Prominence: required prominence of peaks

First, for the mean mHVSR curve defined for each cluster, peaks are identified based on the *find_peaks* function made available through the Python *Scipy* package. The parameters presented in Table 4-2, were determined optimal for this study to ensure peaks of geologic origin were generally identified, while simultaneously suppressing the number of spurious peaks, mostly due to disturbances at low frequencies, that were identified. It should be noted that the distance variable is in units of samples, and thus will depend upon how the mHVSR curve has been discretized. Most often mHVSR curves are provided using logarithmically spaced samples, so effectively what this means is in that at lower frequencies you can have peaks closer together and at higher frequencies they will be further apart. Only mHVSR peaks greater than 0.15 Hz are considered.

Table 4-2. Parameters used as input to peak picking algorithm.

Property	Value
Amplitude	2
Distance	20
Prominence	1

Identifying peaks from the average curve is straightforward, however, establishing statistics about the peak and checking the SESAME criteria are more challenging, especially when measurements have more than one peak.

One of the SESAME criteria involves checking the location of peaks in the lower and upper bound mHVSR curve. The peaks of the upper and lower bound curves must be within $[f_{\#HV}/1.05, 1.05f_{\#HV}]$. The SESAME criteria specifically state that $A_{\#HVave}(f) \pm \sigma_A(f)$ should be used, but in the present work we opt to use the 10th and 90th percentile mHVSR curve

for this. This is the first instance at which the issue of having more than one peak needs to be considered. To ensure that at least as many peaks are found in the lower and upper bound curves, the properties to define what is considered a valid peak for the lower and upper bound peak are considered more liberally than those presented in Table 2 for the average curve. This now generally creates the issue of identifying more peaks in the bounding curves than in the average. This issue is overcome through implementation of an algorithm which considers the peaks determined from the average curve and searches through the peaks determined from the bounding curve to find the closest matches. Since we are using a clustering routine which ensures that only curves with similar morphology are considered together, this is a valid approach because it is expected that any significant peak would be present in the curves for all time windows and in the average and bounding curves.

Another criterion involves calculating the standard deviation of $f_{\#HV}$ which requires picked peaks from each individual time window. A similar approach to the one used to pick the peaks from the upper and lower bound curves is used when picking the peaks from individual time windows. Then the same algorithm as described previously - used to find the closest matching peaks - is used to match peaks from each individual window with peaks picked from the average curve. Then, for each peak picked from the average curve, statistics about the values of $f_{\#HV}$ and $A_{\#HV}$ are calculated based on the matched peaks from the individual windows. In this manner, two other SESAME criteria pertaining to the standard deviation of $f_{\#HV}$ and $A_{\#HV}$ can be verified. The remaining criteria are straightforward to implement.

A common concern among mHVSR practitioners has been how to pick peaks in the case where the peak is broad. Guillier *et al.* (2006) suggest that in the case of mHVSR curves that exhibit a 'plateau like' shape, the mHVSR peak frequency should be defined as the right-hand cut-off of the plateau. They also suggest that, from a practical use of mHVSR, mHVSR curves exhibiting broad peaks or plateau-like shapes of low amplitude should not be used for deriving any quantitative information of average shear-wave velocity or average sediment thickness by using the simple relation $f_0 = V_{s_{ave}}/4h$. We agree with this point.

To address the issue of the broadness of peaks, two additional metrics are provided by the proposed peak picking algorithm in this study to parameterize the peak; the half-width of the peak (width of the peak at half max amplitude), and the width of the peak at 0.25 times the maximum amplitude. These metrics are computed from analysis of the mean curve.

Working from the same concept as Ghofrani and Atkinson (2014) and Wang *et al.* (2022), a single (or multi-peak) Gaussian curve is also fit to the average mHVS curve. The initial guess to the optimization scheme to fit the non-linear Gaussian curve is provided based on the computed parameters for each peak of the experimental curve (i.e., frequency, amplitude, and width of peak as determined from the mean curve). The *curve_fit* function from the Python *Scipy.optimize* library is used. Below are several examples of the types of measurements acquired throughout the Metro Vancouver area and the application of the described peak picking algorithm (Figure 4-2, Figure 4-3). All of the example measurements provided demonstrate successful identification of all peaks of geologic origin, as corroborated by their signature in the plots of the Fourier amplitude spectra for all three components presently separately (Figure 4-3).

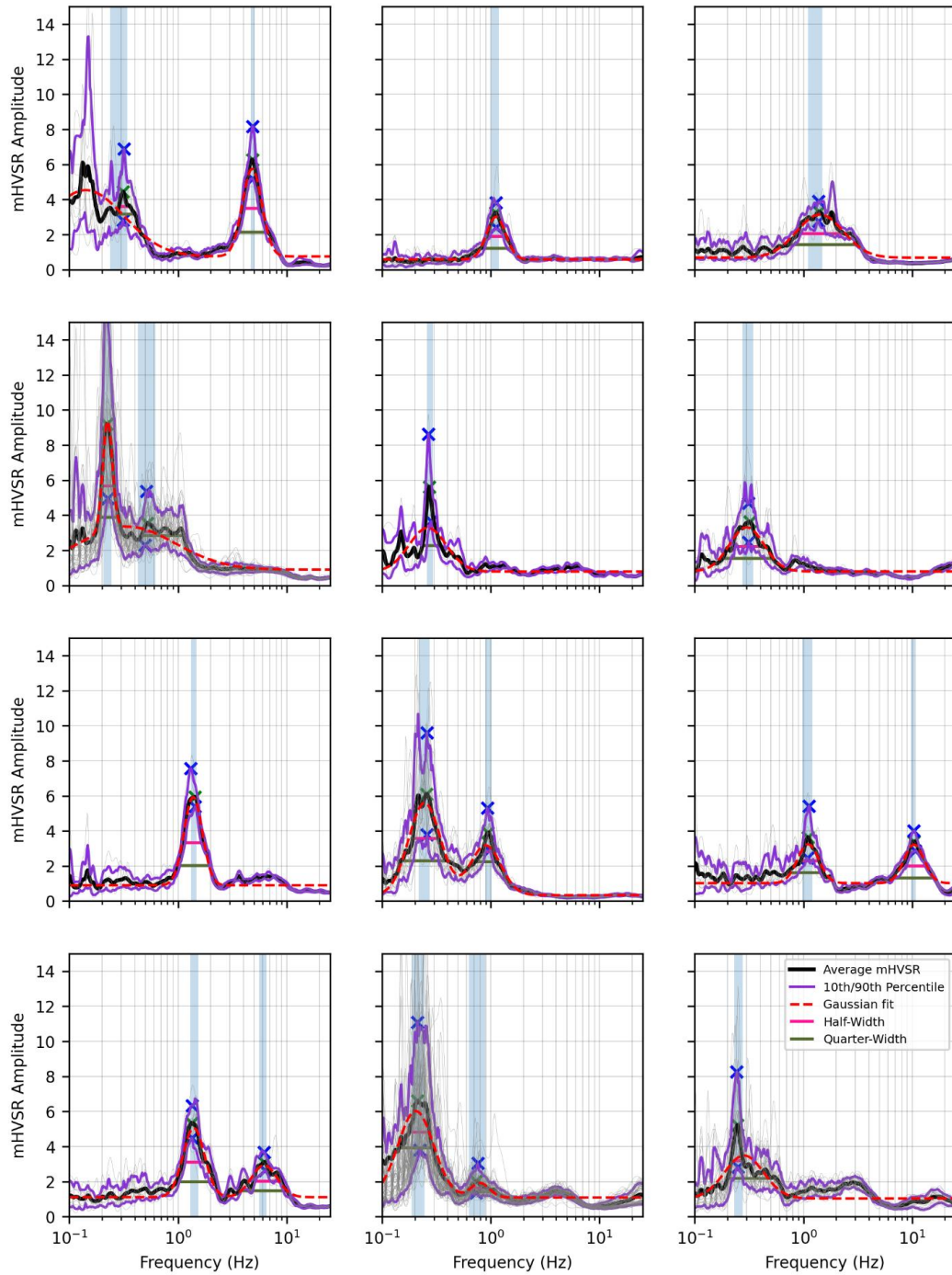


Figure 4-2. Examples of proposed peak picking algorithm applied to mHVSr curves at 12 sites. Only the mHVSr curves for the user-selected optimal cluster are considered. Blue crosses are peaks determined from the 90% and 10% quartile curves, green crosses are peaks determined from the average curve. Shaded blue region shows standard deviation of $f_{\#HV}$, and horizontal lines denote peak broadness

measures (half- and quarter-width). The optimal Gaussian curve fit to the average mHVSr is also displayed.

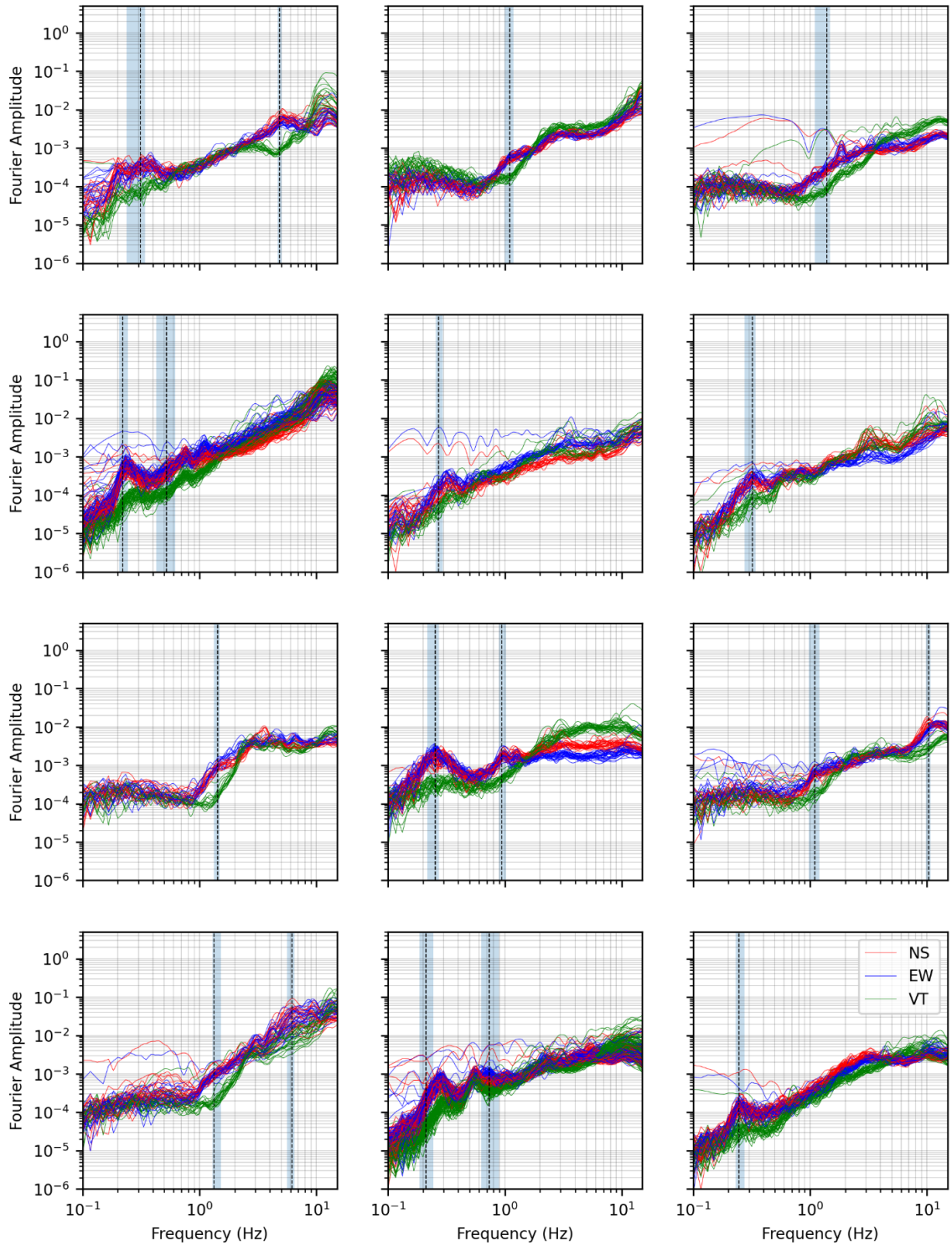


Figure 4-3. Fourier spectra shown for the same 12 sites in Figure 4-2 are shown with the location of $f_{\#HV}$ (vertical dashed line) and its shaded standard deviation. Fourier

spectra for each component are shown and for all time windows; not only windows included in the user-defined optimal cluster.

4.1.2 Development of f_{0HV} Map

The performance of the lowest frequency (first) peak (f_{0HV}) versus the highest amplitude peak (f_{peak}) in characterizing site response was studied by Zhu *et al.* (2020a). Their results demonstrate that using the frequency of the highest significant peak is a more stable parameter because it is less affected by the definition of the significant peak than the first peak and because f_{0HV} is more sensitive to the Konno-Ohmachi smoothing parameter than f_{peakHV} . Zhu *et al.* (2020b) concluded that the site's first significant peak (f_{0HV}) is a better proxy for estimating site effects than using $Z_{0.8}$, $Z_{1.0}$, V_{S20} and V_{S30} .

The lowest peak observable in an mHVSr curve (f_{0HV}) is assumed to represent the fundamental resonant frequency (f_0) of the soil column. f_0 is related to both the softness (expressed by shear-wave velocity, V_s) as well as the thickness of sediments. A map showing the spatial distribution of f_0 (i.e., a map of f_{0HV}) has utility in terms of understanding the variability of seismic site response in an area as well as assessing the depth to an impedance contrast, usually an unconformable geologic contact.

Di Stefano *et al.* (2014) completed a first level seismic microzonation of the urban area of Oliveri using mHVSr measurements. From 23 measurements, they were able to pick 42 peaks. Cluster analysis of the peaks revealed two distinct clusters; one spanning the frequency range from 0.7 to 1.6 Hz – likely due to a covering layer delimited at its base by the same discontinuity surface with variable depth – and the second characterized by higher frequencies – likely showing the resonance effect of the sedimentary cover down to a shallower impedance contrast. Through clustering peaks in this way, two different maps can be created, representing the trends of peak frequencies for each subsurface structure/interface.

Geologically Metro Vancouver is underlain by Tertiary sedimentary bedrock. Pleistocene glacial deposits cover this Tertiary bedrock, which is in turn overlain by Holocene deposits that consist of sands, silty clay and peat. The younger Holocene deposits consist of alluvial,

deltaic and bog deposits. The Fraser River delta, of Holocene age, consists of deltaic silt and sand with thickness of up to 300 m (Cassidy and Rogers, 2004). The Quaternary deposits of the Fraser lowlands are underlain by plant-bearing, fresh water, sediment rocks including sandstone, siltstone, mudstone, shales and conglomerates. The thickness of geological units is different based on the environment of deposition e.g., Salish sediments in marine shore environments are around 8 m, whereas in the fluvial deltaic environments, the same sediments can be up to 20 m thick. Pleistocene sediments mostly consist of over-consolidated glacial till that are present at the surface across Burnaby and Vancouver. Holocene post-glacial, and Pleistocene glacial sediments overlie Tertiary bedrock with a maximum thickness of 800-900 m under the Delta and pinch out to the north (Britton *et al.*, 1995); indicating quite variable geology. In downtown Vancouver, Tertiary sediments can be found within a few m's of the surface.

Due to the complex geology in the Metro Vancouver region, development of an f_{0HV} map where the values correspond to the same resonator (geologic interface) was challenging. In most cases, the lowest frequency peak can be interpreted as resulting from the Pleistocene-Tertiary interface. However, in the Fraser River delta, once the thickness of the Holocene post-glacial sediments exceeds a certain threshold, the lowest frequency peak should be interpreted as resulting from the interface between the Holocene post-glacial sediments and the Pleistocene glacial sediments with contributions from the deeper interface between Pleistocene sedimentary and Tertiary bedrock as well; this will be further elaborated upon in the next Chapter.

Another issue is related to data quality. For sites with peaks < 1 Hz, it is possible that environmental factors or the type of sensor used may obscure a low frequency peak. In fact, during the 2010 to 2011 field campaign in Richmond, all of the measurements were discarded from creation of the f_{0HV} map because the Pinnocchio velocity transducer was not capable of detecting low frequency peaks, and thus the measurements were considered unreliable. There are also cases where certain measurements do not fit into the general trend observed in an area, for e.g., a very high frequency estimate for f_{0HV} . To work around this, for all measurements in which at least one peak was identified, the lowest frequency peak was considered an estimate of f_{0HV} . To curate the database and remove spurious

values, cluster and outlier analysis (Anselin Local Moran's I test) was performed. Once outliers were removed, further inspection of the mHVSR data was manually completed to remove f_{0HV} measurements which appeared to be anomalous or as though they were missing the lowest frequency peak, mostly due to use of equipment with insufficient sensitivity or environmental/experimental. The remaining measurements were included to produce a map of f_{0HV} , which provides some indication of the variability in thickness of the sediment package overlying Tertiary bedrock throughout the Metro Vancouver region. The results are presented as a point layer, and also an interpolated raster produced through Kriging spatial estimation techniques (Figure 4-4, Figure 4-5). The low f_{0HV} in the FRD has been known since the 2000's (Onur et al. 2004), but the f_{0HV} values and trends outside of the FRD are new or a novel outcome of this thesis and thereby the Metro Vancouver microzonation project. Specifically, the f_{0HV} values in the Vancouver, Burnaby and Surrey uplands, underlain by relatively stiff glaciated (and interglacial) sediments, are generally low. This implies the thickness of the glacial and interglacial sediment package above the Tertiary bedrock is very thick (100's of meters). This outcome could be anticipated to a degree (e.g., available sporadic deep boreholes, previous geologic studies stating surface topography does not necessarily mimic depth to rock), but the significant thickness of glacial and interglacial sediments outside of the FRD is now shown for the first time here, by mapping f_{0HV} consistently and at a relatively high lateral resolution throughout the region. A graph demonstrating the statistics of f_{0HV} for various classes of surficial geology is presented in Figure 4-6. In general, there is an expected trend in increasing f_{0HV} (stiffer and/or thinner site conditions) for the older geologic units.

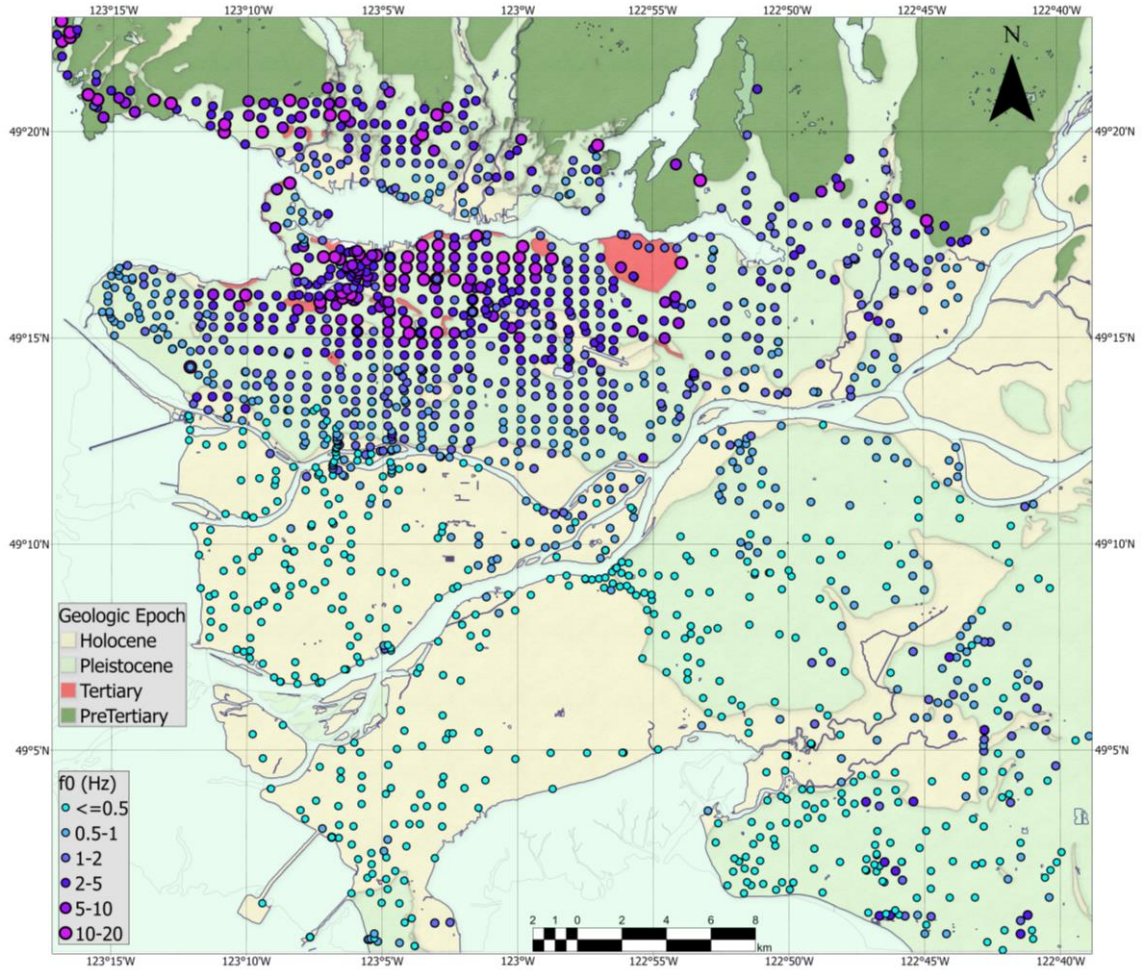


Figure 4-4. Map of sites for which an estimate of f_{0HV} was obtained from the mHVSR, symbology based on value of f_{0HV} .

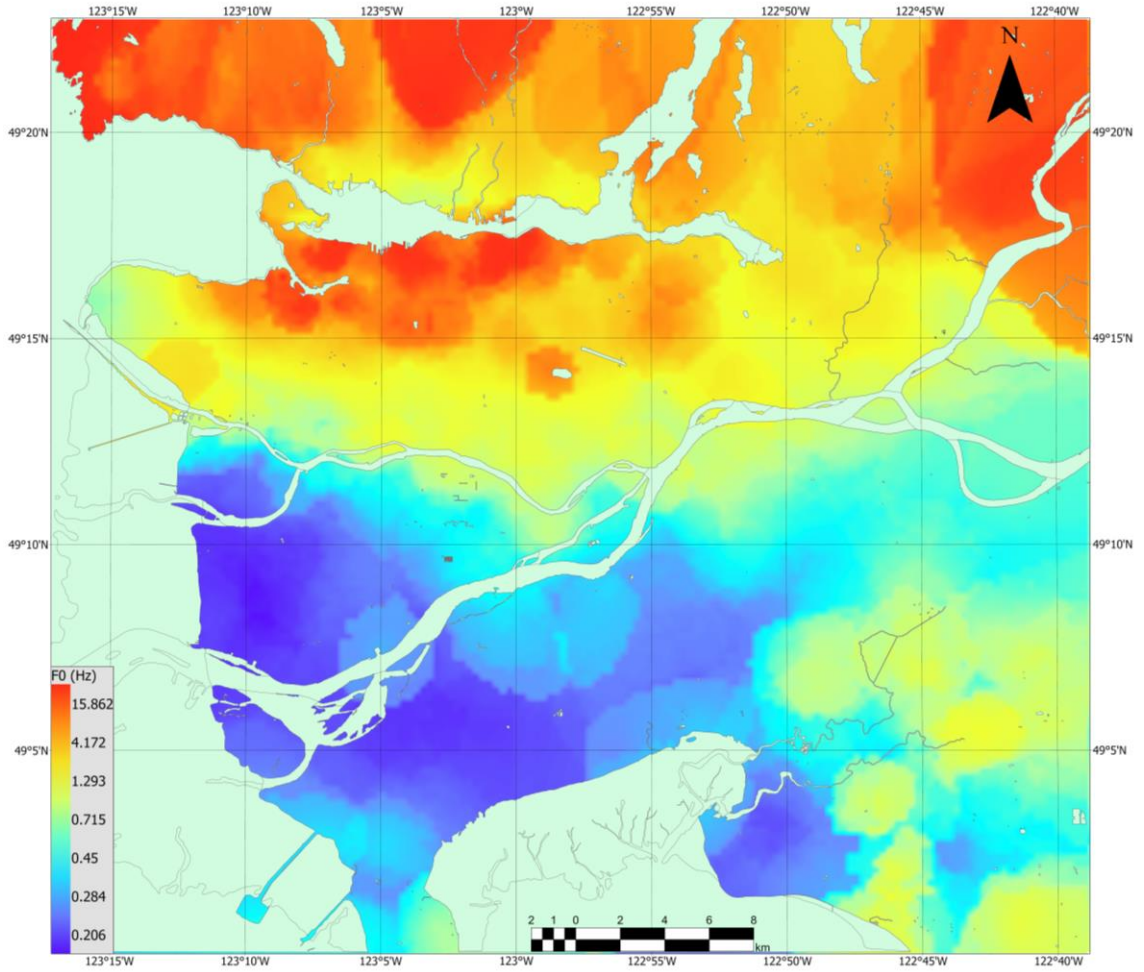


Figure 4-5. Interpolated f_{0HV} map, estimated from f_{0HV} values extracted from mHVSR measurements.

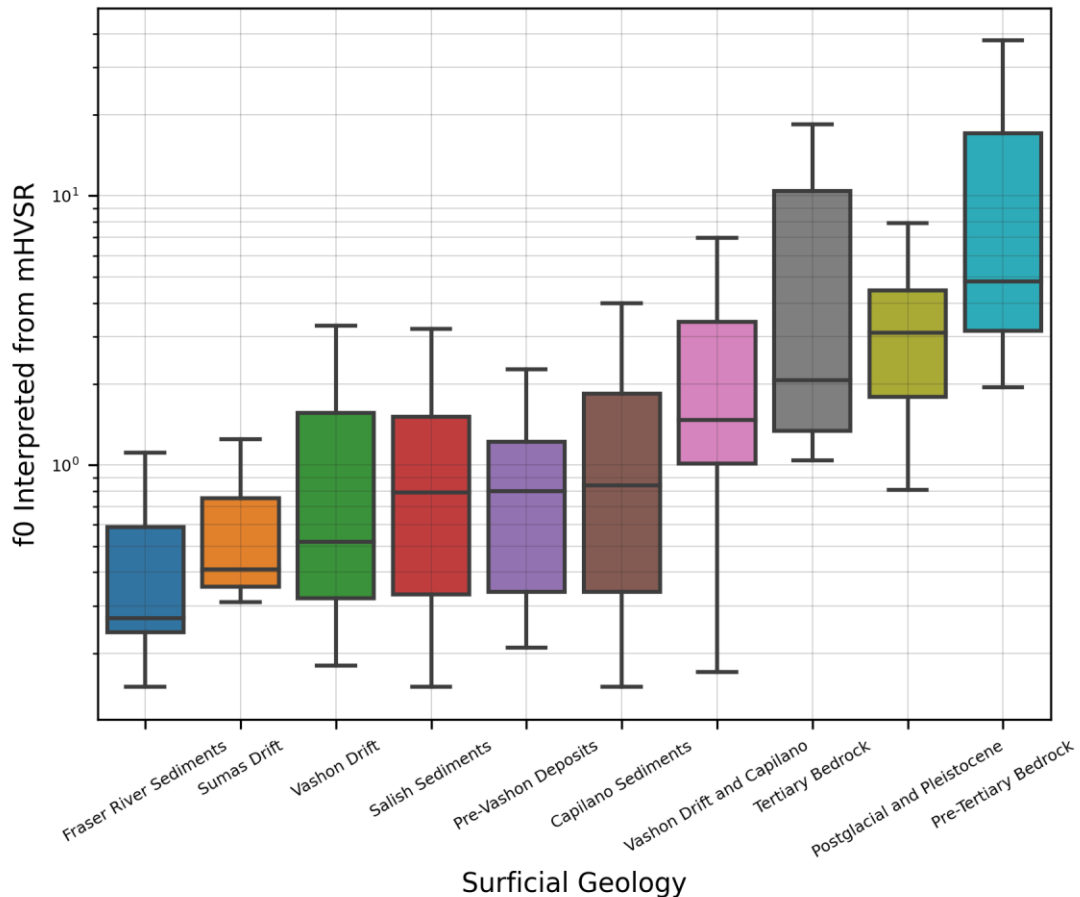


Figure 4-6. f_{0HV} values for different classes of surficial geology.

4.1.3 Interpretation of mHVSr Peaks

The mHVSr response throughout the Metro Vancouver region is quite diverse. In general, the thicker, softer sediments of the Fraser River Delta produce peaks at lower frequencies (< 1 Hz). It is also common to observe multiple peaks in these measurements, corresponding to multiple strong impedance contrasts, for example, the interface between post-glacial and glacial sediments, the interface between glacial sediments and sedimentary bedrock, etc.. Broad low frequency peaks are characteristic of the Surrey area. Low amplitude and broad peaks are common throughout the City of Vancouver and Burnaby area. Well-defined, relatively high amplitude peaks are common in Coquitlam, Port Coquitlam and along the North Shore, where there are Salish Sediments. Through this small subset of measurements presented in this chapter (Fig 4-2 & Fig 4-3) half have more

than one peak. Thus, the development of a procedure that statistically treats each peak was important.

A simple, first-level interpretation of an mHVSr curve generally utilizes the following formula to predict the depth to the resonator, making some approximation for the shear-wave velocity,

$$f_0 = \frac{V_s}{4h}, \quad \text{equation 4-3}$$

where the lowest frequency peak of the mHVSr is used as an approximation for f_0 , and h is the depth to the impedance contrast (Haskell 1960). However, as mentioned previously, in the presence of 2D/3D geology, as well as multiple impedance contrasts, this simple approximation fails to predict h accurately. Dobry *et al.* (1976) proposed simplified procedures for estimating the fundamental period of a layered soil profile with more than two layers. Most soil profiles can be modeled by n uniform layers. There are several methods to calculate the fundamental period of a layered profile (Idriss and Seed 1968, Hagmann 1969, Tsai and Housner 1970).

When assessing the resonant frequencies of a soil column, it is important to consider the soil profile down to seismological bedrock. Kawase *et al.* (2019) presented the following example where they predicted the SH-wave transfer function for a model with 14 layers and progressively removed two layers from the bottom. As the P- and S-wave velocities of the bottommost layer of the model decrease, the peak in the lower frequency range disappears, however, not only this, the peak and trough amplitudes in the higher frequency range also increase. This demonstrates that deeper sediments contribute to spectral ratios even in the high frequency range, and considering simple stratigraphic profiles (i.e., only considering 2 layers of a 3-layer model) can provide incorrect estimates of f_0 or its amplification.

As already discussed, f_0 is closely related to the depth of sediments overlying stiff rock. Several empirical relationships have been developed to relate mHVSr peaks to depth (Seht and Wohlenberg 1999, Delgado *et al.* 2000, D'Amico *et al.* 2008, Gosar and Lenart 2009, Motazedian *et al.* 2011, Smith *et al.* 2013, Scheib *et al.* 2016, Tün *et al.* 2016, Jakica 2018,

Pratt 2018, Moon *et al.* 2019). mHVSr measurements should be calibrated using detailed information about the local subsurface structure to provide reliable depth estimates. A power-law gradient model has been widely used for mapping depth to impedance contrast from microtremor data:

$$z = a f_{\#HV}^{-b} \quad \text{equation 4-4}$$

where a and b are unknown regression coefficients. The values of a and b determined for several sedimentary basins worldwide are provided in Table 4-3. Several of these relationships are plotted and displayed in Figure 4-7. The relationships share similar trends, the differences, for example in terms of their intercept, are related to differences in the shear-wave velocities of the geologic materials. Assaf *et al.* (2022) developed a relationship using mHVSr data from the Metro Vancouver region. Future work will aim to refine this relationship for Metro Vancouver. The b -parameter has a mean and standard deviation of 1.3 ± 0.3 , whereas it is 110 ± 40 for the a -parameter. The larger variability in the a -parameter is the result of differences in the velocity ranges of the sediments overlying the stiff bedrock. Regions with greater shear-wave velocities have greater a -parameter (intercept) values, because for an equivalent value of f_{0HV} the corresponding depth to the impedance contrast is less. Conceptually this can be related to the equation 4-3.

Table 4-3. Model coefficients a and b of f_{OHV} -depth relationships for various sedimentary basins across the world. Adapted from Rugar & Gosar (2020).

Author	Sedimentary Basin	a	b
Ibs-von Seht and Wohlenberg (1999)	Lower-Rhine West, Germany	96	1.388
Delgado <i>et al.</i> (2000)	Segura River valley, Spain	55	1.256
Parolai <i>et al.</i> (2002)	Cologne, Germany	108	1.551
Hinzen <i>et al.</i> (2004)	Lower-Rhine West, Germany	137	1.19
Garcia-Jerez <i>et al.</i> (2006)	Zafarraya Basin, Spain	194.6	1.14
Motamed <i>et al.</i> (2006)	Bam, Iran	135.19	1.979
Gosar and Lenart (2010)	Ljubljana Moor, Slovenia	105.53	1.25
Mascondolla <i>et al.</i> (2019)	Po Plain, Italy	98	1.17
Poggi <i>et al.</i> (2012)	Lucerne, Switzerland	158.54	2.45
D'Amico <i>et al.</i> (2008)	Florence, Italy	140	1.172
Birgoren <i>et al.</i> (2009)	Istanbul, Turkey	150.99	1.1531
Del'Monaco <i>et al.</i> (2013)	L'Aquila, Italy	53.461	1.01
Dinesh <i>et al.</i> (2010)	Bangalore, India	58.3	0.95
Maresca and Berrino (2016)	Vulturara Irpina, Italy	129	1.38
Ozalaybey <i>et al.</i> (2011)	Izmit Bay, Turkey	141	1.27
Paudyal <i>et al.</i> (2013)	Kathmandu Basin, Nepal	146.01	1.2079
Sukumaran <i>et al.</i> (2011)	Narmada Valley, India	102.1	1.47
Joshi <i>et al.</i> (2018)	Aravalli, India	56.8	1
Sant <i>et al.</i> (2017)	Banni Plains, India	110.18	1.97
Liang <i>et al.</i> (2018)	Pearl River Delta, China	55	1.02
Pugin <i>et al.</i> (2013)	Ottawa, Canada	64.98	1.198
Rugar and Gosar (2020)	Iska alluvial fan, Slovenia	202.97	1.139
Assaf <i>et al.</i> (2022)	Fraser River Delta, British Columbia	54.72	1.34
Moon <i>et al.</i> (2019)	Bukit Timah, Singapore	92.5	1.06
Tun <i>et al.</i> (2016)	Eskisehir Basin, Turkey	136	1.36

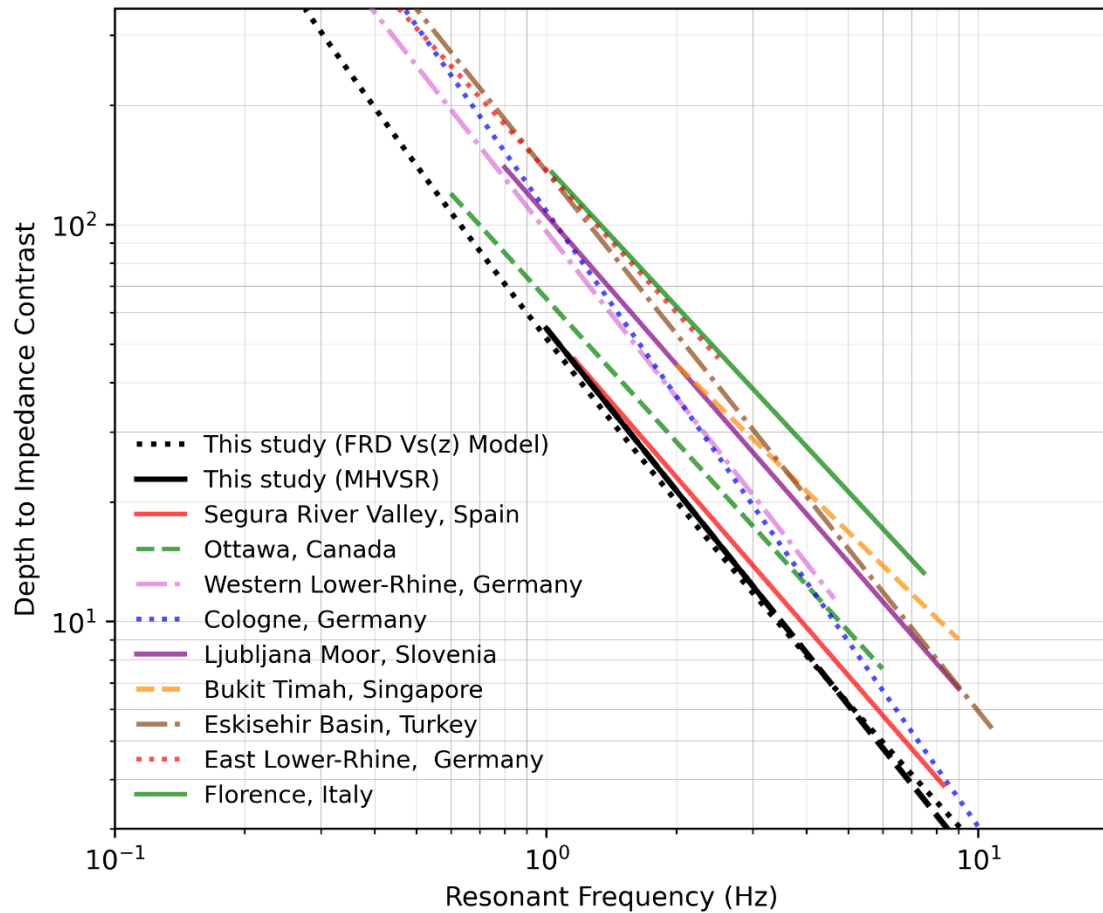


Figure 4-7. Examples of depth vs f_{0HV} relationships developed for seven regions. Adapted from Assaf *et al.* (2022), the two relations specific to the Fraser River delta using mHVSr data of this study are referred to as “This study” in the legend.

4.2 Proposed mHVSr Database Structure

Considering the complex physical basis of the mHVSr, in addition to the many factors that impact the microtremor measurement, the methodology of presenting the final mHVSr data must be given renewed consideration. It is somewhat common practice to present only the interpreted peaks as well as meta-data pertaining to experimental conditions, however, this is not sufficient information to allow an end user to develop an adequate understanding of the site’s mHVSr response. For example, without the ability to analyze the Fourier spectrum for each component separately, it is difficult to ascertain the quality of the chosen peaks or whether the site may have directional (2D or 3D) effects.

Without being able to see the mHVSr spectrum from which peaks were picked, and if only the amplitude and frequency of the peak are reported, it is not possible to know the shape of the mHVSr spectrum, the broadness of the peak, etc., and thus gauge the appropriateness of using a simple relationship to relate peak frequency(ies) with depth.

Recently, Wang *et al.* (2022) proposed a publicly accessible relational database to facilitate utilization of HVSr data. The structure is an adaptation of a similar repository for Vs data and provides HVSr data and supporting metadata, but not parameters derived from the data. Users can directly interact with the data through a web portal that contains a GUI or through external tools that perform cloud-based computations. Using external interactive tools, users can replot mHVSr. These tools can also derive parameters, often as a binary variable, indicating whether an mHVSr plot contains peaks as well as the fitted properties of those peaks. Metadata are also accessible which includes site location, details about the instruments used to make the measurements, and data processing information related to windowing, anti-trigger routines and filtering. This provides a standard which should be implemented when creating mHVSr databases. Our own database developed from the mHVSr data from Metro Vancouver follows a very similar approach.

The first step in creating our mHVSr database was reformatting the microtremor recording or time-series data. The time-series data were in multiple file formats and so all of the raw time-series data were converted to miniSEED (.mseed) format. The original data formats are also retained within the database structure. The use of “.mseed” file format facilitates compatibility with many available mHVSr processing platforms (e.g., Geopsy, HVSrPy), and is a format which can store metadata about the measurement (sampling rate, identification of each component; N, E, V, etc.) within the file itself.

The next step in creating our mHVSr database involved assigning a unique identifier (UID) that mapped each mHVSr time series measurement file to its meta-data. For each measurement, a UID was assigned, the first four digits of which correspond to the year in which the measurement was obtained, and the following characters are either a number that incremented from one for field campaigns that did not assign their sites a site name.

In addition to the raw time-series data, the metadata for each mHVSR measurement needed to be concatenated. Reporting for each field campaign differed slightly, but information such as measurement ID, location, measurement surface conditions, type of sensor used, and surficial geology were standard. For some sites, there is some additional information describing the conditions at the site during the measurement (traffic, etc). One challenge when dealing with location was with regards to unknown coordinate reference system information (this was often resolvable) as well as errors in transcription of coordinates (this led to removal of certain measurements from the database which could not be accurately located), or total neglect to note the coordinates at which the measurement was obtained for some sites. The initial database comprising the metadata of measurements was created as an Excel Spreadsheet, compiled from the Excel spreadsheets for each of the four summer field campaigns between 2018-2020. Coordinates are provided as latitude and longitude, utilizing the WGS-84 datum and projected northing and easting, utilizing the datum WGS-84 and projection UTM Zone 10N.

To retain as flat of a file structure as possible, there is a root directory, and within the root directory, there is a sub-folder corresponding to each uniquely identified measurement; co-located measurements were treated as two unique measurements. Within the subfolder is the raw time series data for all three components as a single “.mseed” file, three “.csv” files which contain the Fourier Amplitude Spectra for each time window (each row?) for the three components of recorded motion (three columns?), the saved “.png” image illustrating the Fourier Amplitude spectra for each time window and each component of motion, and a “.csv” file with the processed mHVSR curve for each time window (which is the input data provided to the mHVSR window clustering algorithm), calculated using the standard batch parameters described in the previous section. Through experience, having access to these raw and intermediary data products are extremely important for interpreting mHVSR results. It also provides the end user with the ability to easily reprocess the data (access to raw time-series data), and develop and test new processing and interpretation techniques (access to Fourier amplitude spectra for each time window and access to processed mHVSR curves for each time window).

Deviating from the approach of Wang *et al.* (2022), some interpreted results are also provided in the database. For each measurement, the results of clustering time windows to define clusters of time windows that demonstrate similar mHVSR response are included. We refrain from only presenting what we have decided as the optimal cluster in the database. Instead, for each cluster identified with more than two time windows, we present a text file with the average mHVSR curve, as well as the upper and lower bound curves, and a saved image illustrating the average and two bounding mHVSR curves, the interpreted peaks (both as determined from the average curve and from the individual windows), and the associated standard deviation of each peak. When possible, the Gaussian fit of the average mHVSR curve is also included in the image.

Within the subfolder for each mHVSR location, we also include a text file which repeats the meta-data included in the spreadsheet, and includes the parameters for the peaks identified ($f_{\#HV}$, $A_{\#HV}$, $f_{\#HV}$ std deviation, half-width, quarter-width) and the Gaussian fit (where possible). This text file of mHVSR peak picking is provided for each cluster identified. In the spreadsheet, for each measurement with an identified peak (or peaks) of geologic origin, the following parameters are included: the cluster from which the peaks were identified (only a single cluster is used), the frequency and amplitude at which the peak occurs in the average curve as well as the upper and lower bound curve, the standard deviation of the frequency of the peaks and its amplitude, as well as the half-width and quarter-width of the peak as determined from the average curve. For measurements where it was possible to model the curve using a multi/single-peak Gaussian curve, the parameters of the modelled Gaussian are also provided in the spreadsheet.

4.3 Discussions

The simplest interpreted result from an mHVSR is the frequencies at which peaks occur. In general, the lowest frequency peak corresponds to the deepest impedance contrast. Multiple peaks in mHVSRs are generally related to multiple impedance contrasts. The shape of a peak depends on the geometry of the subsurface; narrow peaks are mainly associated with strong impedance contrasts, while broad peaks are common in the presence of lateral variations (e.g., near valley edges, faulted areas) or stiffer stratigraphy with a weaker and/or deeper impedance contrast (Bonnfoy *et al.*, 2006). Most currently available

peak picking algorithms look for the global maximum peak of a mHVSr spectrum, based on the assumption of there only being a single peak in the measurement.

The current study developed and tested a peak picking algorithm which can identify and parameterize multiple peak frequencies ($f_{\#HV}$) from an mHVSr measurement. Extraction and quantification of additional parameters such as the broadness of peaks through the half-width and the quarter-width were also developed. Using the identified f_{0HV} values, an interpolated map was developed that can be used as a proxy to estimate the depth to bedrock throughout the Metro Vancouver region.

The combination of V_{S30} and f_0 has the ability to enhance estimation of site amplification. f_0 intrinsically contains information about depth to impedance contrasts, and the frequency(ies) at which resonant amplification is likely to occur. Thus, a map of the distribution of f_{0HV} has value in terms of ability to predict the distribution of site effects in a region and being able to delineate regions with thick, soft sediment deposits versus those with relatively shallow sediments underlain by engineering bedrock. Depiction or display of peak frequencies above f_{0HV} was not investigated here. Although present in previous literature (e.g., di Stefano et al., 2014), it is not common practice and thereby reinforces difficulties in communicating the full mHVSr spectrum to date.

Future work with the mHVSr data from the Metro Vancouver region will focus on using site period classification schemes (e.g., Zhao *et al.*, 2006; di Alessandro *et al.*, 2012; Pitilakis *et al.*, 2018) to create mapped products based on assigning a classification to each site based on its estimated f_0 value (from f_{0HV}). In addition, the geology of Metro Vancouver is known to have multiple strong impedance contrasts, and as such the presence of multiple peaks in the mHVSr have been shown via site response modelling to relate to these multiple impedance contrasts (Onur et al. 2004, see section 5.2.1). By categorizing the peaks according to which impedance contrast they are likely related to, point maps or interpolated maps can be created to act as a proxy of the depth to the impedance contrast under consideration.

The database structure developed for this large database of microtremor measurements was designed with the intention of providing the most transparency to the end-user in terms of

the progression of the data. However, end-users may only be interested in the retrieved peak frequencies of a site and likely confused by being provided with more than one reported peak frequency. Further work will focus on developing tools that ease the ability of a user to interface with the data (reprocessing, displaying) and generally improve the intractability of the database. The fundamental site frequency (f_0) or natural site period ($T_0=1/f_0$) is growing in popularity and use in GMMs worldwide (di Alessandro *et al.* 2012, Ghofrani and Atkinson 2014, Hassani and Atkinson 2016, Hashash *et al.* 2019). Therefore, a mHVSr database that includes $f_{\#HV}$ values has application as input to GMMs in the immediate future; the database and its content has been developed to impact regional seismic hazard analyses into the future.

4.4 References

- Abrahamson, N. A., Silva, W. J., & Kamai, R. (2014). Summary of the ASK14 Ground Motion Relation for Active Crustal Regions. *Earthquake Spectra*, 30(3), 1025–1055. <https://doi.org/10.1193/070913EQS198M>
- Assaf, J., Molnar, S., El Naggar, M. H., & Sirohey, A. (2022). Seismic site characterization in Fraser River Delta in Metropolitan Vancouver. *Soil Dynamics and Earthquake Engineering*, 161, 107384.
- Bahavar, M., Spica, Z. J., Sánchez-Sesma, F. J., Trabant, C., Zandieh, A., & Toro, G. (2020). Horizontal-to-Vertical Spectral Ratio (HVSr) IRIS Station Toolbox. *Seismological Research Letters*, 91(6), 3539–3549. <https://doi.org/10.1785/0220200047>
- Bard, P.-Y. (1998). Microtremor measurements: A tool for site effect estimation? *The Effects of Surface Geology on Seismic Motion*, 3, 1251–1279
- Birgören, G., Özel, O., & Siyahi, B. (2009). Bedrock depth mapping of the coast south of Istanbul: comparison of analytical and experimental analyses. *Turkish Journal of Earth Sciences*, 18(2), 315–329.
- Beauval, C., Bard, P. Y., Moczo, P., & Kristek, J. (2003). Quantification of Frequency-Dependent Lengthening of Seismic Ground-Motion Duration due to Local Geology: Applications to the Volvi Area (Greece). *Bulletin of the Seismological Society of America*, 93(1), 371–385. <https://doi.org/10.1785/0120010255>
- Bonilla, L. F., Steidl, J. H., Gariel, J. C., & Archuleta, R. J. (2002). Borehole Response Studies at the Garner Valley Downhole Array, Southern California. *Bulletin of the Seismological Society of America*, 92(8), 3165–3179. <https://doi.org/10.1785/0120010235>

- Bonilla, L. F., Steidl, J. H., Lindley, G. T., Tumarkin, A. G., & Archuleta, R. J. (1997). Site amplification in the San Fernando Valley, California: Variability of site-effect estimation using the S-wave, coda, and H/V methods. *Bulletin of the Seismological Society of America*, 87(3), 710–730. <https://doi.org/10.1785/BSSA0870030710>
- Campbell, K. W., & Bozorgnia, Y. (2014). NGA-West2 Ground Motion Model for the Average Horizontal Components of PGA, PGV, and 5% Damped Linear Acceleration Response Spectra. *Earthquake Spectra*, 30(3), 1087–1115. <https://doi.org/10.1193/062913EQS175M>
- Chiou, B., & Youngs, R. (2014). Update of the Chiou and Youngs NGA Model for the Average Horizontal Component of Peak Ground Motion and Response Spectra. *Earthquake Spectra*, 30, 1117–1153. <https://doi.org/10.1193/072813EQS219M>
- Cox, B. R., Cheng, T., Vantassel, J. P., & Manuel, L. (2020). A statistical representation and frequency-domain window-rejection algorithm for single-station HVSR measurements. *Geophysical Journal International*, 221(3), 2170–2183. <https://doi.org/10.1093/GJI/GGAA119>
- D'Amico, V., Picozzi, M., Baliva, F., & Albarello, D. (2008). Ambient Noise Measurements for Preliminary Site-Effects Characterization in the Urban Area of Florence, Italy. *Bulletin of the Seismological Society of America*, 98(3), 1373–1388. <https://doi.org/10.1785/0120070231>
- de Risi, R., Penna, A., & Simonelli, A. L. (2019). Seismic risk at urban scale: the role of site response analysis. *Soil Dynamics and Earthquake Engineering*, 123, 320–336. <https://doi.org/10.1016/J.SOILDYN.2019.04.011>
- Del Monaco, F., Tallini, M., De Rose, C., & Durante, F. (2013). HVNSR survey in historical downtown L'Aquila (central Italy): site resonance properties vs. subsoil model. *Engineering Geology*, 158, 34–47.
- Delgado, J., Lopez Casado, C., Giner, J., Estevez, A., Cuenca, A., & Molina, S. (2000). Microtremors as a Geophysical Exploration Tool: Applications and Limitations. *Pure and Applied Geophysics* 2000 157:9, 157(9), 1445–1462. <https://doi.org/10.1007/PL00001128>
- di Alessandro, C., Bonilla, L. F., Boore, D. M., Rovelli, A., & Scotti, O. (2012). Predominant-Period Site Classification for Response Spectra Prediction Equations in Italy. *Bulletin of the Seismological Society of America*, 102(2), 680–695. <https://doi.org/10.1785/0120110084>
- Di Stefano, P., Luzio, D., Renda, P., Martorana, R., Capizzi, P., D'Alessandro, A., ... & Zarcone, G. (2014). Integration of HVSR measures and stratigraphic constraints for seismic microzonation studies: the case of Oliveri (ME). *Natural Hazards and Earth System Sciences Discussions*, 2(4), 2597–2637.

- Dinesh, B. V., Nair, G. J., Prasad, A. G. V., Nakkeeran, P. V., & Radhakrishna, M. C. (2010). Estimation of sedimentary layer shear wave velocity using micro-tremor H/V ratio measurements for Bangalore city. *Soil Dynamics and Earthquake Engineering*, *30*(11), 1377-1382
- Dobry, R., Oweis, I., & Urzua, A. (1976). Simplified procedures for estimating the fundamental period of a soil profile. *Bull. Seism. Soc. Am.*, *66*.
- Duval, A. M., Bard, P. Y., Lebrun, B., Lacave-Lache, C., Riepl, J., & Hatzip, D. (2001). H/V technique for site response analysis. Synthesis of data from various surveys. *Bollettino Di Geofisica Teorica Ed Applicata*, *42*(3-4), 267-280.
- Duval, A.-M. (1994). *Détermination de la réponse d'un site aux séismes à l'aide du bruit de fond : évaluation expérimentale*.
- Duval, A.-M., Bard, P.-Y., Méneroud, J.-P., & Vidal, S. (1996). Mapping site effect with microtremors. *International Conference on Seismic Zonation*, 1522-1529.
- Fäh, D., Kind, F., & Giardini, D. (2003). Inversion of local S-wave velocity structures from average H/V ratios, and their use for the estimation of site-effects. *Journal of Seismology*, *7*(4), 449-467. <https://doi.org/10.1023/B:JOSE.0000005712.86058.42>
- Field, E. H. (1996). Spectral amplification in a sediment-filled Valley exhibiting clear basin-edge-induced waves. *Bulletin of the Seismological Society of America*, *86*(4), 991-1005. <https://doi.org/10.1785/BSSA0860040991>
- García-Jerez, A., Luzón, F., Navarro, M., & Pérez-Ruiz, J. A. (2006). Characterization of the sedimentary cover of the Zafarraya basin, southern Spain, by means of ambient noise. *Bulletin of the Seismological Society of America*, *96*(3), 957-967
- García-Jerez, A., Seivane, H., Navarro, M., Martínez-Segura, M., & Piña-Flores, J. (2019). Joint analysis of Rayleigh-wave dispersion curves and diffuse-field HVSR for site characterization: The case of El Ejido town (SE Spain). *Soil Dynamics and Earthquake Engineering*, *121*, 102-120. <https://doi.org/10.1016/J.SOILDYN.2019.02.023>
- Ghofrani, H., & Atkinson, G. M. (2014). Site condition evaluation using horizontal-to-vertical response spectral ratios of earthquakes in the NGA-West 2 and Japanese databases. *Soil Dynamics and Earthquake Engineering*, *67*, 30-43. <https://doi.org/10.1016/J.SOILDYN.2014.08.015>
- Gosar, A., & Lenart, A. (2010). Mapping the thickness of sediments in the Ljubljana Moor basin (Slovenia) using microtremors. *Bulletin of Earthquake Engineering 2009 8:3*, *8*(3), 501-518. <https://doi.org/10.1007/S10518-009-9115-8>
- Guillier, B., Cornou, C., Kristek, J., S, B.-C., Bard, P.-Y., Fäh, D., & Moczo, P. (2006, May). Simulation of seismic ambient vibrations: does the H/V provide quantitative information in 2D-3D structure. *Proceedings of the Third International Symposium on the Effects of Surface Geology on Seismic Motion*.

- Haghshenas, E. (2005). Conditions Geotechnique et Alea Sismique Local a Teheran (Doctoral dissertation, Université Joseph-Fourier-Grenoble I).
- Haghshenas, E., Bard, P.-Y., Jafari, M. K., & Hatzfeld, D. (2003, May). Effets de site et risque sismique à Téhéran: Premiers résultats d'une étude expérimentale. *Paris France*.
- Haghshenas, E., Bard, P.-Y., Theodulidis, N., & Team, S. W. (2008). Empirical evaluation of microtremor H/V spectral ratio. *Bulletin of Earthquake Engineering*, 6(1), 75–108. <https://doi.org/10.1007/s10518-007-9058-x>
- Hagmann, A. J. (1969). *RV Whitman Compar i son of methods for analyzing so il de posits during earth-quakes Research Report No. R69-29*. MIT.
- Hashash, Y., Ilhan, O., Harmon, J., Parker, G., Stewart, J., Rathje, E., Campbell, K., & Silva, W. (2019). Nonlinear Site Amplification Model for Ergodic Seismic Hazard Analysis in Central and Eastern North America. *Earthquake Spectra*, 36. <https://doi.org/10.1177/8755293019878193>
- Haskell, N. A. (1960). Crustal reflection of plane SH waves. *Journal of Geophysical Research*, 65(12), 4147–4150. <https://doi.org/10.1029/JZ065i012p04147>
- Hassani, B., & Atkinson, G. M. (2016). Applicability of the NGA-West2 Site-Effects Model for Central and Eastern North America. *Bulletin of the Seismological Society of America*, 106(3), 1331–1341. <https://doi.org/10.1785/0120150321>
- Hinzen, K. G., Weber, B., & Scherbaum, F. (2004). On the resolution of H/V measurements to determine sediment thickness, a case study across a normal fault in the Lower Rhine Embayment, Germany. *Journal of Earthquake Engineering*, 8(06), 909-926.
- Ibs-von Seht, M., & Wohlenberg, J. (1999). Microtremor measurements used to map thickness of soft sediments. *Bulletin of the Seismological Society of America*, 89(1), 250-259.
- Idriss, I. M., & Seed, H. B. (1968). Seismic Response of Horizontal Soil Layers. *Journal of the Soil Mechanics and Foundations Division*, 94(4), 1003–1031. <https://doi.org/10.1061/JSFEAQ.0001163>
- Joshi, A. U., Sant, D. A., Parvez, I. A., Rangarajan, G., Limaye, M. A., Mukherjee, S., ... & Mistry, S. P. (2018). Subsurface profiling of granite pluton using microtremor method: southern Aravalli, Gujarat, India. *International Journal of Earth Sciences*, 107(1), 191-201.
- Jakica, S. (2018, May). *Using Passive Seismic to Estimate the Thickness of the Leonora Breakaways, Western Australia*.
- Kwak, D. Y., Stewart, J. P., Mandokhail, S. U. J., & Park, D. (2017). Supplementing VS30 with H/V Spectral Ratios for Predicting Site Effects. *Bulletin of the Seismological Society of America*, 107(5), 2028–2042. <https://doi.org/10.1785/0120160353>

- Lebrun, B. (1997). *Les effet de site: etude experimentale et simulation de trios configurations*. l'université Joseph Fourier-Grenoble I.
- Liang, D., Gan, F., Zhang, W., & Jia, L. (2018). The application of HVSR method in detecting sediment thickness in karst collapse area of Pearl River Delta, China. *Environmental earth sciences*, 77(6), 1-9.
- Lonsi, A. M., Ohrnberger, M., Krüger, F., & Sánchez-Sesma, F. J. (2016). Combining surface-wave phase-velocity dispersion curves and full microtremor horizontal-to-vertical spectral ratio for subsurface sedimentary site characterization. *Interpretation*, 4(4), SQ41–SQ49. <https://doi.org/10.1190/INT-2016-0021.1>
- Lonsi, A. M., Sánchez-Sesma, F. J., Molina-Villegas, J. C., Ohrnberger, M., & Krüger, F. (2015). Full microtremor H/V(z, f) inversion for shallow subsurface characterization. *Geophysical Journal International*, 202(1), 298–312. <https://doi.org/10.1093/GJI/GGV132>
- Maresca, R., Castellano, M., de Matteis, R., Saccorotti, G., & Vaccariello, P. (2003). Local Site Effects in the Town of Benevento (Italy) from Noise Measurements. *Pure and Applied Geophysics* 2003 160:9, 160(9), 1745–1764. <https://doi.org/10.1007/S00024-003-2376-2>
- Maresca, R., & Berrino, G. (2016). Investigation of the buried structure of the Volturara Irpina Basin (southern Italy) by microtremor and gravimetric data. *Journal of applied geophysics*, 128, 96-109.
- Mascandola, C., Massa, M., Barani, S., Albarello, D., Lovati, S., Martelli, L., & Poggi, V. (2019). Mapping the Seismic Bedrock of the Po Plain (Italy) through Ambient-Vibration Monitoring. *Bulletin of the Seismological Society of America*, 109(1), 164-177.
- Moon, S. W., Subramaniam, P., Zhang, Y., Vinoth, G., & Ku, T. (2019). Bedrock depth evaluation using microtremor measurement: empirical guidelines at weathered granite formation in Singapore. *Journal of Applied Geophysics*, 171, 103866. <https://doi.org/10.1016/J.JAPPGEO.2019.103866>
- Mori, F., Gaudiosi, I., Tarquini, E., Brammerini, F., Castenetto, S., Naso, G., & Spina, D. (2020a). HSM: a synthetic damage-constrained seismic hazard parameter. *Bulletin of Earthquake Engineering*, 18(12), 5631–5654. <https://doi.org/10.1007/S10518-019-00677-2/FIGURES/14>
- Mori, F., Gena, A., Mendicelli, A., Naso, G., & Spina, D. (2020b). Seismic emergency system evaluation: The role of seismic hazard and local effects. *Engineering Geology*, 270, 105587. <https://doi.org/10.1016/J.ENGEO.2020.105587>
- Motamed, R., Ghalandarzadeh, A., Tawhata, I., & Tabatabaei, S. H. (2007). Seismic microzonation and damage assessment of Bam city, southeastern Iran. *Journal of Earthquake Engineering*, 11(1), 110-132.

- Motazedian, D., Hunter, J. A., Pugin, A., & Crow, H. (2011). Development of a Vs30 (NEHRP) map for the city of Ottawa, Ontario, Canada. *Canadian Geotechnical Journal*, 48(3), 458–472. <https://doi.org/10.1139/T10-081>
- Moya, A., Schmidt, V., Segura, C., Boschini, I., & Atakan, K. (2000). Empirical evaluation of site effects in the metropolitan area of San José, Costa Rica. *Soil Dynamics and Earthquake Engineering*, 20(1–4), 177–185. [https://doi.org/10.1016/S0267-7261\(00\)00049-X](https://doi.org/10.1016/S0267-7261(00)00049-X)
- Parolai, S., Maesano, F. E., Basili, R., Silacheva, N., Boxberger, T., & Pilz, M. (2019). Fingerprint Identification Using Noise in the Horizontal-to-Vertical Spectral Ratio: Retrieving the Impedance Contrast Structure for the Almaty Basin (Kazakhstan). *Frontiers in Earth Science*, 7, 336. <https://doi.org/10.3389/FEART.2019.00336/BIBTEX>
- Parolai, S., Bormann, P., & Milkereit, C. (2002a). New relationships between Vs, thickness of sediments, and resonance frequency calculated by the H/V ratio of seismic noise for the Cologne area (Germany). *Bulletin of the seismological society of America*, 92(6), 2521–2527.
- Parolai, S., Trojani, L., Frapiccini, M., & Monachesi, G. (2002b). Seismic Source Classification by Means of a Sonogram- Correlation Approach: Application to Data of the RSM Seismic Network (Central Italy). *Pure and Applied Geophysics* 2002 159:11, 159(11), 2763–2788. <https://doi.org/10.1007/S00024-002-8758-Z>
- Paudyal, Y. R., Yatabe, R., Bhandary, N. P., & Dahal, R. K. (2013). Basement topography of the Kathmandu Basin using microtremor observation. *Journal of Asian Earth Sciences*, 62, 627–637.
- Piña-Flores, J., Perton, M., García-Jerez, A., Carmona, E., Luzón, F., Molina Villegas, J., & J Sánchez-Sesma, F. (2016). The inversion of spectral ratio H/V in a layered system using the Diffuse Field Assumption (DFA). *Geophysical Journal International*, 208. <https://doi.org/10.1093/gji/ggw416>
- Pitilakis, K., Riga, E., Anastasiadis, A., Fotopoulou, S., & Karafagka, S. (2018). Towards the revision of EC8: Proposal for an alternative site classification scheme and associated intensity dependent spectral amplification factors. *Soil Dynamics and Earthquake Engineering*, 126. <https://doi.org/10.1016/j.soildyn.2018.03.030>
- Pitilakis, K., Roumelioti, Z., Raptakis, D., Manakou, M., Liakakis, K., Anastasiadis, A., & Pitilakis, D. (2013). The EUROSEISTEST Strong-Motion Database and Web Portal. *Seismological Research Letters*, 84(5), 796–804. <https://doi.org/10.1785/0220130030>
- Poggi, V., Fäh, D., Burjanek, J., & Giardini, D. (2012). The use of Rayleigh-wave ellipticity for site-specific hazard assessment and microzonation: application to the city of Lucerne, Switzerland. *Geophysical Journal International*, 188(3), 1154–1172.
- Pratt, T. L. (2018). Characterizing and Imaging Sedimentary Strata Using Depth-Converted Spectral Ratios: An Example from the Atlantic Coastal Plain of the Eastern United States.

Bulletin of the Seismological Society of America, 108(5A), 2801–2815.
<https://doi.org/10.1785/0120180046>

- Pugin, A. M., Brewer, K., Cartwright, T., Pullan, S. E., Perret, D., Crow, H., & Hunter, J. A. (2013). Near surface S-wave seismic reflection profiling—new approaches and insights. *First Break*, 31(2).
- Riepl, J., Bard, P.-Y., Hatzfeld, D., Papaioannou, C., & Nechtschein, S. (1998). Detailed evaluation of site-response estimation methods across and along the sedimentary valley of volvi (EURO-SEISTEST). *Bulletin of the Seismological Society of America*, 88(2), 488–502. <https://doi.org/10.1785/BSSA0880020488>
- Rupar, L., & Gosar, A. (2020). Mapping the thickness of Quaternary sediments in the Iska alluvial fan (central Slovenia) using microtremor method. *Acta Geodynamica et Geomaterialia*, 177–190.
- Sant, D. A., Parvez, I. A., Rangarajan, G., Patel, S. J., Bhatt, M. N., & Salam, T. S. (2017). Subsurface profiling along Banni Plains and bounding faults, Kachchh, Western India using microtremors method. *Journal of Asian Earth Sciences*, 146, 326–336.
- Sawada, Y., Taga, M., Watanabe, M., Nakamoto, T., Nagumo, H., Kudo, K., Horike, M., Sakajiri, N., & Sasatani, M. (2004). Applicability of microtremor H/V method for KiK-net strong motion observation sites and Nobi plain. *Proceedings of 13th WCEE, Paper*, 855.
- Scheib, A., Morris, P., Murdie, R., & Delle Piane, C. (2016). A passive seismic approach to estimating the thickness of sedimentary cover on the Nullarbor Plain, Western Australia. <Http://Dx.Doi.Org/10.1080/08120099.2016.1233455>, 63(5), 583–598.
<https://doi.org/10.1080/08120099.2016.1233455>
- Scherbaum, F., Hinzen, K. G., & Ohrnberger, M. (2003). Determination of shallow shear wave velocity profiles in the cologne, Germany area using ambient vibrations. *Geophysical Journal International*, 152(3), 597–612.
- Seht, M. I. von, & Wohlenberg, J. (1999). Microtremor measurements used to map thickness of soft sediments. *Bulletin of the Seismological Society of America*, 89(1), 250–259.
<https://doi.org/10.1785/BSSA0890010250>
- Smith, N. R. A., Reading, A. M., Asten, M. W., & Funk, C. W. (2013). Constraining depth to basement for mineral exploration using microtremor: A demonstration study from remote inland Australia Using microtremor for mineral exploration. *Geophysics*, 78(5), B227–B242. <https://doi.org/10.1190/GEO2012-0449.1>
- Spica, Z., Pertou, M., Nakata, N., Liu, X., & Beroza, G. C. (2018). Shallow VS Imaging of the Groningen Area from Joint Inversion of Multimode Surface Waves and H/V Spectral Ratios. *Seismological Research Letters*, 89(5), 1720–1729.
<https://doi.org/10.1785/0220180060>

- Sukumaran, P., Parvez, I. A., Sant, D. A., Rangarajan, G., & Krishnan, K. (2011). Profiling of late Tertiary–early Quaternary surface in the lower reaches of Narmada valley using microtremors. *Journal of Asian Earth Sciences*, *41*(3), 325–334.
- Tsai, N. C., & Housner, G. W. (1970). Calculation of surface motions of a layered half-space. *Bulletin of the Seismological Society of America*, *60*(5), 1625–1651. <https://doi.org/10.1785/BSSA0600051625>
- Tün, M., Pekkan, E., Özel, O., & Guney, Y. (2016). An investigation into the bedrock depth in the Eskisehir Quaternary Basin (Turkey) using the microtremor method. *Geophysical Journal International*, *207*(1), 589–607. <https://doi.org/10.1093/GJI/GGW294>
- Volant, P., Cotton, F., & Gariel, J. C. (1998). Estimation of site response using the H/V method. Applicability and limits of this technique on Garner Valley downhole array dataset (California). *Proceedings of the 11th European Conference on Earthquake Engineering*.
- Volti, T., Burbidge, D., Collins, C., Asten, M., Odum, J., Stephenson, W., Pascal, C. H., & Holzschuh, J. (2016). Comparisons between VS 30 and spectral response for 30 sites in Newcastle, Australia, from collocated seismic cone penetrometer, active-and passive-source VS data. *Bulletin of the Seismological Society of America*, *106*(4), 1690–1709.
- Wang, P. (2020). *Predictability and repeatability of non-ergodic site response for diverse geological conditions*. University of California, Los Angeles.
- Wüster, J. (1993). Discrimination of chemical explosions and earthquakes in central Europe—a case study. *Bulletin of the Seismological Society of America*, *83*(4), 1184–1212. <https://doi.org/10.1785/BSSA0830041184>
- Yazdi, M., Motamed, R., & Anderson, J. G. (2022). A New Set of Automated Methodologies for Estimating Site Fundamental Frequency and Its Uncertainty Using Horizontal-to-Vertical Spectral Ratio Curves. *Seismological Research Letters*, *93*(3), 1721–1736. <https://doi.org/10.1785/0220210078>
- Zhao, J. X., Irikura, K., Zhang, J., Fukushima, Y., Somerville, P. G., Asano, A., Ohno, Y., Oouchi, T., Takahashi, T., & Ogawa, H. (2006). An Empirical Site-Classification Method for Strong-Motion Stations in Japan Using h/v Response Spectral Ratio. *Bulletin of the Seismological Society of America*, *96*(3), 914–925. <https://doi.org/10.1785/0120050124>
- Zhu, C., Cotton, F., & Pilz, M. (2020). Detecting site resonant frequency using HVSR: Fourier versus response spectrum and the first versus the highest peak frequency. *Bulletin of the Seismological Society of America*, *110*(2), 427–440.
- Zhu, C., Pilz, M., & Cotton, F. (2020). Which is a better proxy, site period or depth to bedrock, in modelling linear site response in addition to the average shear-wave velocity?. *Bulletin of Earthquake Engineering*, *18*(3), 797–820.

Chapter 5

5 Representative mHVSR Curves for Metro Vancouver Region

Methods for estimating site response, in the form of a site amplification function, can be divided into two major groups: empirical and theoretical. Since empirical methods are based on actual recorded ground motion, they are often found to be more effective. One of the most widely used reference site technique is the standard spectral ratio (SSR), introduced by Borchardt (1970). It is assumed that the records from the reference site (in general, a station installed on a hard outcrop) contain the same source and propagation effects as records from other sites. Hence, the ratio of the ground motion spectra measured on a soil site versus the reference site expresses only the effect of the local soil conditions at the specific site. However, in many cases, it becomes difficult to choose a reference site. Outcrops of bedrock are usually weathered, and the resulting surficial velocity gradient can create site effects, which impact the ‘reference’ ground motion (Tucker et al., 1984; Steidl et al., 1996; Boore & Joyner, 1997).

Another empirical site response estimation technique is the surface-to-borehole spectral ratio (SBSR) method. This method involves installation of two sensors at the same location; one at the surface and one at the sediment-bedrock interface. If the receiver at the bottom of the borehole is installed in the bedrock unit, and the surface receiver is on soft sediment where amplification is expected, the ratio between the recorded ground motion spectra of the two can be treated as a measure of site amplification. Because the hard reference site is at the same location, the assumption that the incident wavefield is the same is valid (i.e., no issues with selecting an appropriate reference site as with SSR). However, a drawback of this technique is that because of the free surface involved, the surface-to-borehole spectral ratio requires correction of the destructive interference involved in the down-going wavefield (Bonilla *et al.*, 2002). Another limitation of this method is that if the bedrock receiver is installed above the sediment-bedrock interface, then only amplification between the two sensors will be considered and not the total amplification resulting from the local soil column. Another method for determining site effects is to

perform regression on a ground motion database to determine the source, path and site terms.

When the local soil column is known, the site amplification function is routinely evaluated in the frequency domain by computing the 1D transfer function. However, in the case of 2D or 3D structure, additional factors must be considered such as the trapping of surface waves which develop off heterogeneities and are then trapped within the structure. Consideration of a simple 1D model in the case of complex 2D/3D geology fails to properly quantify the multi-dimensional site effects experienced. This failure is spectacular in small-size and deep sedimentary alpine valleys (Faccioli *et al.*, 2002, Lebrun *et al.*, 2004).

Availability of ground motion records, suitability of reference sites, and the cost involved with installing a receiver at the bedrock interface all limit the utility of the empirical site response evaluation procedures described so far. Imperfect knowledge of the soil column and its physical properties, and assumptions and generalizations inherent to modelling, limit the utility of theoretical methods. Considering this, alternative methods have been proposed to relate the amplification spectrum anticipated at a site to simple metrics such as the time-averaged shear-wave velocity of the upper 30 m of the soil column (V_{S30}) as well as the fundamental resonant frequency of the soil column (f_0). Based on these simple metrics an elastic response spectrum is assigned to a site.

The single-station microtremor horizontal-to-vertical spectral ratio (mHVSR) method has rapidly risen in popularity as a cost-effective alternative for seismic microzonation and site effects characterization. When a sufficiently strong impedance contrast exists at depth, mHVSRs can be used to approximate the shear-wave resonant frequency (Field and Jacob, 1993, Lachet and Bard, 1994) and/or the fundamental-mode Rayleigh wave ellipticity (f_{Ellip}) (Poggi and Fäh 2010). Empirical evidence from sites with measured V_s profiles down to bedrock and from small-strain earthquake recordings have shown that the lowest frequency mHVSR peak, f_{0HV} , occurs at f_0 (see references in Molnar *et al.*, 2022). mHVSRs have been used to map the depth to bedrock or stiff sediments using empirical knowledge of the V_s variation with depth (e.g., Seht and Wohlenberg, 1999; Delgado *et al.*, 2000; Parolai *et al.*, 2002; Hinzen *et al.*, 2004; D'Amico *et al.*, 2008; Gosar and Lenart, 2010,

Tun *et al.*, 2016; Molnar *et al.*, 2018; Moon *et al.*, 2019). Many studies have pointed out that this correlation between secondary peaks in mHVSR and depths to shallow interfaces with strong impedance contrasts is in fact of geologic origin (Guéguen *et al.*, 2000, García-Fernández & Jiménez, 2012, Macau *et al.*, 2014, Castellaro, 2016, Oubaiche *et al.*, 2016, Teague *et al.*, 2018, Wotherspoon *et al.*, 2018, Rohmer *et al.*, 2020, Rahimi *et al.*, 2021). Fewer studies found good agreement between secondary peaks in mHVSR and higher modes of f_0 (e.g., Bodin *et al.*, 2001; Goetz, 2009).

Site predictor variables (e.g., V_{S30} , f_0) are useful for understanding the overall amplification characteristics at a site, or in the case of f_0 getting a sense of the thickness of sediments overlying stiffer rock, however, they do not capture the full site-specific, frequency-dependent amplification at a site. The use of the mHVSR amplification spectrum is generally not accepted as a valid proxy for the site amplification function, as the mHVSR has not been shown to accurately replicate the local amplification characteristics at a site determined empirically (e.g., through SSR or SBSR). The mHVSR amplification spectrum does contain more information than is communicated through the extracted $f_{\#HV}$ values and much of this information is contained in the shape of the spectrum. Regardless of its lack of correspondence with the site amplification function from earthquake ground motions, through understanding of the distribution of a certain shape/morphology of mHVSR response in a region, this allows for another type of SM, or each style of mHVSR response may be linked to a generic soil profile, among other things.

Using a compiled mHVSR database from the Metro Vancouver region, first, a brief investigation is completed to form a preliminary understanding of double-peak responses commonly observed in the FR Delta and relate this to the multi-layered geology expected in the region. Then the processed mHVSR amplification spectra are used as input to a clustering algorithm to determine a set of representative mHVSR spectra to be used for site classification.

5.1 Metro Vancouver Geology

The FR delta, south of Vancouver, British Columbia is the largest and most important delta on the west coast of Canada. Recent concerns about the stability of the FR delta in the event

of a moderate to large earthquake have highlighted the need for subsurface geologic and geotechnical information in this area (Luternauer & Finn, 1983, Luternauer *et al.*, 1986, Luternauer *et al.*, 1988).

In the FR delta, Tertiary bedrock is observed between 200 – 1000 m depth, with the average depth of 500 m (Britton *et al.*, 1995). Bedrock is overlain by (inter)glacial Pleistocene sediments. The Pleistocene surface is irregular in shape, with some localized topographic highs (Hunter *et al.*, 1998). Holocene sediments pinch out rapidly to the north, from a thickness of ~300 m in the basin center, to only a few meters on the north shore of the FR.

The near surface Vs at Tertiary bedrock sites is 1500 m/s (Hunter *et al.*, 1998). The Vs of Pleistocene sediments is on average 500 m/s but is variable and no velocity-depth relation has been formulated. The Vs of Pleistocene deposits increases linearly from 400-1000 m/s regardless of depth to Pleistocene (Luternauer & Hunter, 1996, Hunter *et al.*, 1998). The Vs of Holocene deposits increases with depth, with average values of about 200 m/s, but about 100 m/s at the surface in many places (Hunter 1995).

Monahan and Levson (2001) proposed to divide the near-surface deposits of the Metro Vancouver region into four principal units: bedrock, older Pleistocene sediments, including Vashon Till, Capilano sediments, and Salish sediments. Older Pleistocene deposits comprise the Vashon Till of the Late Wisconsinian Fraser Glaciation as well as earlier glacial and non-glacial deposits (Armstrong 1984, Clague 1994). These deposits have been overridden by thick glaciers and consequently are overconsolidated. These deposits commonly form rolling uplands up to 200 m above sea level in the Fraser Lowlands. The average shear-wave velocity of these sediments ranges between 400-600 m/s.

Capilano sediments were deposited at the close of the Fraser Glaciation (Armstrong 1981, 1984, Clague 1994). These include raised coarse-grained deltas, raised beaches and glaciomarine silts and clays. These deposits have not been overridden by glaciers. Capilano glaciomarine silt and clay are widespread in the western part of the Fraser Lowland (Armstrong 1981, Nasmith *et al.* 1998).

Salish sediments have been deposited since post glacial sea level became established close to its current position, approximately 11,000 ^{14}C year B.P. The most significant of these sediments volumetrically are the Holocene fluvial and deltaic deposits of the Fraser River. The Salish sediments also include alluvial fans, organic deposits, lacustrine deposits, coarse-grained alluvial and deltaic deposits of smaller rivers, shoreline sands and marine sands. Deposits of the Fraser River delta reach a maximum known thickness of 305 m (Clague *et al.* 1998). Hunter *et al.* (1999) have shown that the Vs of these deposits varies from 90 m/s to 500 m/s, generally increasing with depth. A map showing the interpreted depth to bedrock in the FR delta is illustrated in Figure 5-1

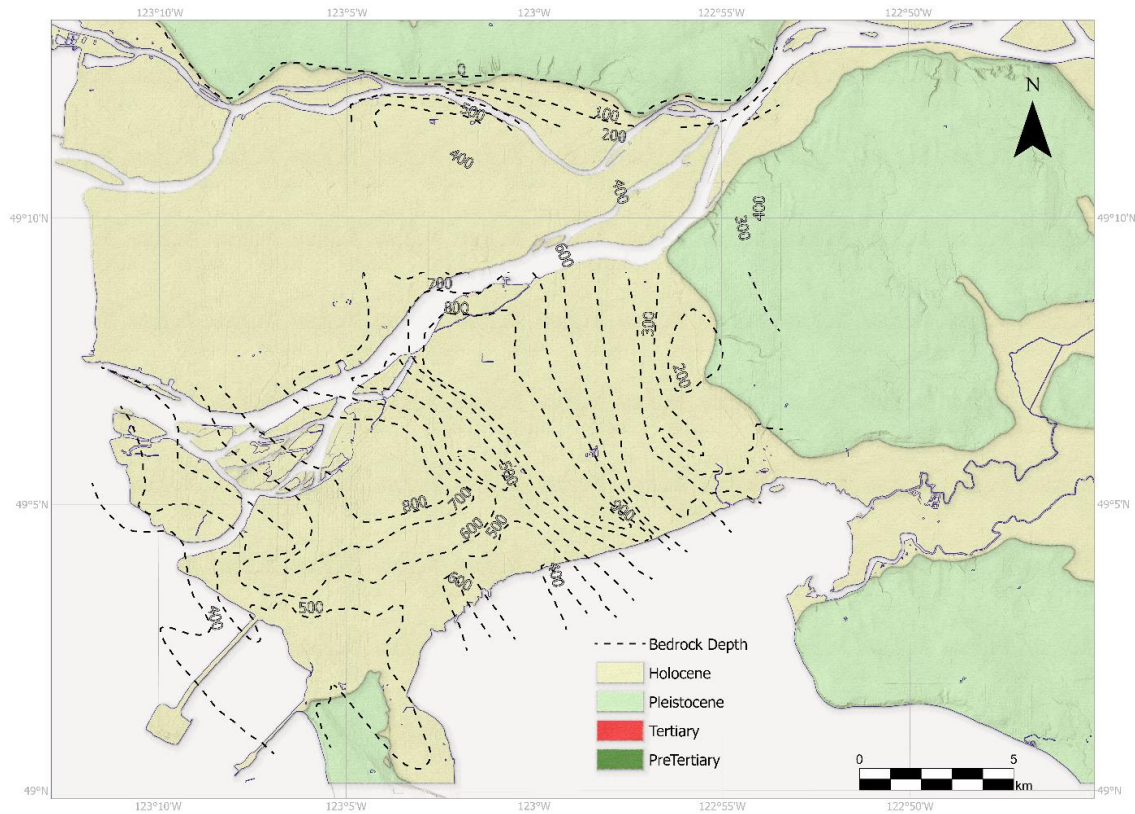


Figure 5-1. Contours of interpreted depth to Tertiary sedimentary bedrock in the Fraser River Delta. Contours from Britton *et al.* (1995).

5.2 Theoretical Basis of mHVSR

Ambiguity regarding the composition of the microtremor wavefield has made it challenging to theoretically model the mHVSR in terms of shear-wave velocity profiles, which from a site response assessment perspective would be attractive as this velocity profile could be used as input to theoretical site effect modelling routines. The wavefield itself is subject to meteorological, diurnal, and seasonal variations. Over the years, different authors have attempted to explain the mHVSR in terms of SH waves (Nakamura, 1989, Herak, 2008) Rayleigh waves (Lermo and Chavez-Garcia 1994, Fäh *et al.* 2001, Arai and Tokimatsu 2004, Malischewsky and Scherbaum 2004, Tran *et al.* 2011) and by adding the effects of Love waves (van der Baan 2009). Recent studies consider the role of all waves, the so-called total field approach (Lunedei and Albarello 2010, Sánchez-Sesma *et al.* 2011).

Nakamura (1989), in his pioneering interpretation of the mHVSR, assumed that the microtremor wavefield was primarily comprised of S- and Rayleigh waves. He postulated that the effects of Rayleigh waves are effectively eliminated by considering the spectral ratio. By assuming that the H/V ratio at the sediment-bedrock interface is unity, and the vertical component motions do not undergo amplification, the mHVSR at the surface can be treated as a ‘quasi transfer function’. This interpretation has since proven to be false, however, the attractiveness of being able to use the mHVSR as a proxy for the site transfer function remains.

Cassidy & Molnar (2009) showed that mHVSRs at earthquake recording sites on firm-to-soft sediments across British Columbia agree with eHVSRs and earthquake standard spectral ratio (SSR; reference rock site) up to and including the first peak (f_0). mHVSRs do not typically replicate eHVSR amplification at high frequencies (i.e., higher modes). Generally, if there is a sufficiently strong impedance contrast, mHVSRs across Canada are able to provide a reliable measure of f_0 and its amplification (Cassidy and Molnar 2009, Braganza *et al.* 2016, Farrugia *et al.* 2018) but does not replicate the entire earthquake site amplification spectrum.

5.2.1 Short investigation into Theoretical Site Response in the Fraser River Delta

The site response in the Fraser River delta is controlled by the thickness of the glacial and post-glacial sediments, overlying Tertiary bedrock. Broadly speaking, there are three different scenarios which are possible in terms of the overall composition of the soil column. The first is no post-glacial sediments, with only glacial sediments overlying Tertiary bedrock. The second scenario is a layer of post-glacial sediments, nominally less than 100 m thick, overlying glacial sediments, all overlying Tertiary bedrock (Assaf et al., 2022 investigated this scenario in detail). The third scenario is a thick layer of post-glacial sediments (> 100 m) overlying glacial sediments and Tertiary bedrock.

In the FR delta the thickness of post-glacial sediments can reach up to 300 m, while the entire sediment package comprising post-glacial and glacial sediment can reach 1000 m. First, a simple test in the variation of the 1-D site transfer function within the FR delta, considering the effect of increasing the thickness of post-glacial sediments overlying glacial sediments and sedimentary bedrock, is performed. The Matlab script `rattle.m` was used to accomplish the 1-D modelling (written by C. Mueller, USGS, based on Bill Joyner's original code). Representative parameter values used for the 1-D modelling are adopted from the parameter ranges presented in Assaf *et al.* (2022) and are shown in Table 5-1.

Table 5-1. Model parameter ranges for rock types in Fraser River delta. Adapted from Assaf *et al.* (2022).

Geologic unit	Vs (m/s)	Vp (m/s)	Density (kg/m ³)
Post-glacial	50-500	1400-2000 ⁺ 80-1050 ^{&}	1884 ⁺ 1438 ^{&}
Glacial	400-1100	1400-2800 ⁺ 625-2300 ^{&}	2162 ⁺ 1750 ^{&}
Bedrock	1000-2500	1600-4700	2500

+dry/unsaturated, &wet/saturated

First, the results of considering the effect of increasing the thickness of post-glacial sediments overlying glacial sediments and sedimentary bedrock were tested. The results are included in Figure 5-2. The thickness of the post-glacial sediments was 25, 50, 75, 100,

150 and 250 m. Although realistically the average velocity of the sedimentary layer will increase as the thickness of these sediments increases, this does not have significant impact on what is hoped to be communicated by the results. The shear-wave velocity of the post-glacial sediments was considered fixed at 250 m/s with a density of 1.8g/cm^3 , the thickness of the glacial sediments was fixed at 250 m, the shear-wave velocity fixed at 500 m/s and density at 2.1 g/cm^3 . The bedrock half-space had a shear-wave velocity of 1500 m/s and a density of 2.5 g/cm^3 .

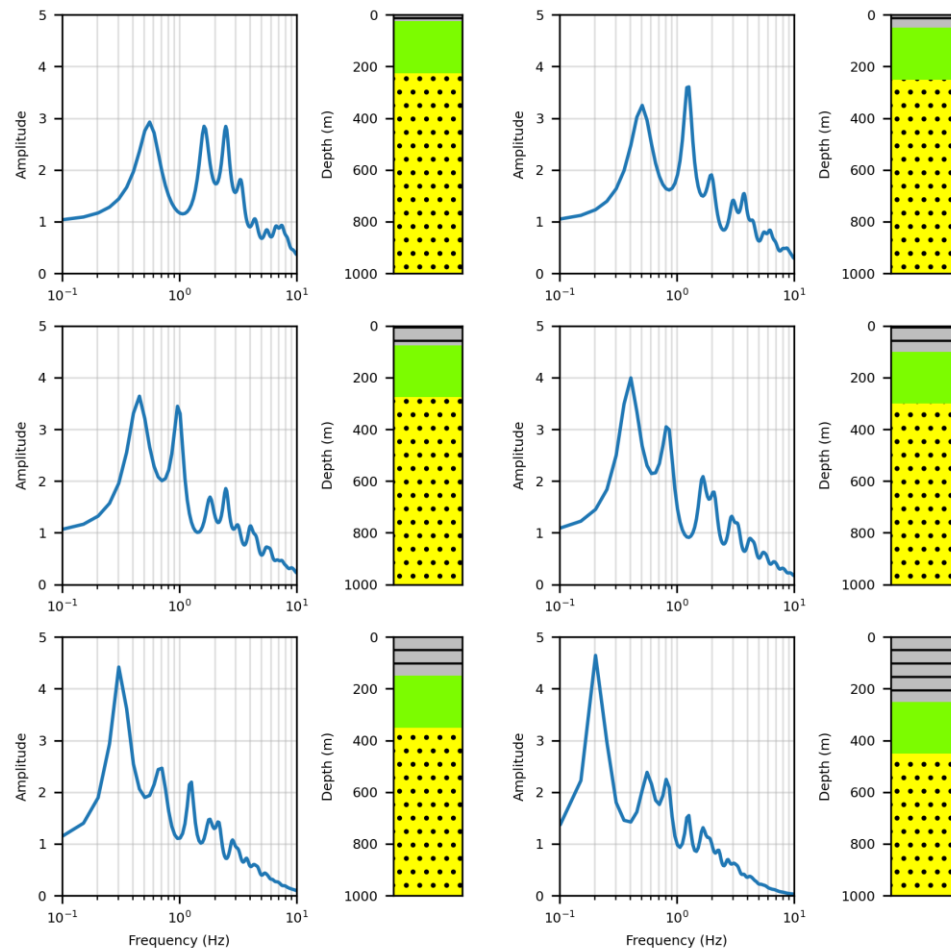


Figure 5-2. Results of forward modelling the 1-D SH transfer function for different thicknesses of post-glacial sediments considering material properties of the sediments in the FR delta.

The 1-D site amplification spectrum for the six considered cases of increasing post-glacial sediment thickness is shown in Figure 5-2. When the post-glacial sediments are relatively

thin, there are two defined separate peaks. This is generally consistent with clear double peak mHVSR response in a wide zone around the FR Delta edges. However, as the thickness of the post-glacial sediments increases, the resonance at the lowest frequency peak is a combination of the resonance related to both impedance contrasts, and the higher frequency peaks are higher modes of resonance of this two-layered system. In other words, as the post-glacial sediment thickness increases, the second peak shifts to lower frequencies until it merges with the lowest frequency peak. This is generally consistent with single peak mHVSR response in the central-west part of the FR Delta; however, the mHVSR A_0 is not as high as modelled here. In the examples shown, the lowest frequency peak shifts towards lower frequency as post-glacial thickness is increased since the glacial layer thickness is fixed. Hence f_{0HV} should be a reliable proxy of bedrock depth below the FR delta.

Microtremor recordings were performed at six sites in the FR delta, nearby (within 300 m) selected boreholes (Table 5-2), as part of the Metro Vancouver microzonation project. These boreholes either logged into glacial sediments or had an interpreted depth to glacial sediments and Tertiary bedrock (J. Hunter, GSC, pers. comm.). For these sites, agreement between the mHVSR and the forward modelled 1-D SH-wave site transfer function is evaluated here. Material properties, *in situ* or nearby, of the boreholes are extracted from the Vs database of Hunter *et al.* (1998) and the Metro Vancouver microzonation project (J. Assaf, pers. comm.). The parameters used as input to rattle.m are provided in Table 5-2. The underlying half-space was assumed to have a density of 2.5 g/cm^3 and a Vs of 1500 m/s.

Figure 5-3 shows the theoretical 1-D amplification spectrum compared to the empirical mHVSR for the six considered sites. Both the theoretical and empirical results confirm that the thickness of post-glacial sediments have a controlling effect on amplification spectrum. For relatively shallow post-glacial sediments, there are two peaks in the amplification spectrum, and the thinner the post-glacial sediments are, the greater the amplitude of the secondary peak in comparison to the first peak. Then, as the thickness of these post-glacial sediments increases, the shape of the amplification spectrum shifts to exhibiting only one significant peak, with contributions from both impedance contrasts, and even in the empirical mHVSR there is some evidence of higher modes of this two-layer system.

Although the results in Figure 5-3 are initial investigations to explain the empirical mHVSR response, it demonstrates some first-order correspondence between the mHVSR and forward modelled 1-D SH transfer functions in the FR delta, and provides motivation for future investigations. There is potential to exploit the full mHVSR spectrum further to elucidate deep FR Delta profiles or even to use the mHVSR as a quasi-transfer function, perhaps with some calibration.

Table 5-2. Parameters used as input to forward model SH-transfer function of two-layer model overlying half-space through rattle.m.

Layer	Thickne ss (m)	Density (g/cm ³)	Velocity (m/s)	Dampin g factor
Borehole 94-4				
1	236	1.8	350	25
2	290	2.1	700	25
Borehole 87-1				
1	185	1.8	250	10
2	354	2.1	600	10
Borehole 93-2				
1	235	1.8	210	25
2	287	2.1	600	25
Borehole 96-1				
1	305	1.8	350	25
2	231	2.1	700	25
Borehole 96-2				
1	45	1.8	206	25
2	317	2.1	600	25
Borehole 95-2				
1	52	1.8	220	25
2	364	2.1	600	25

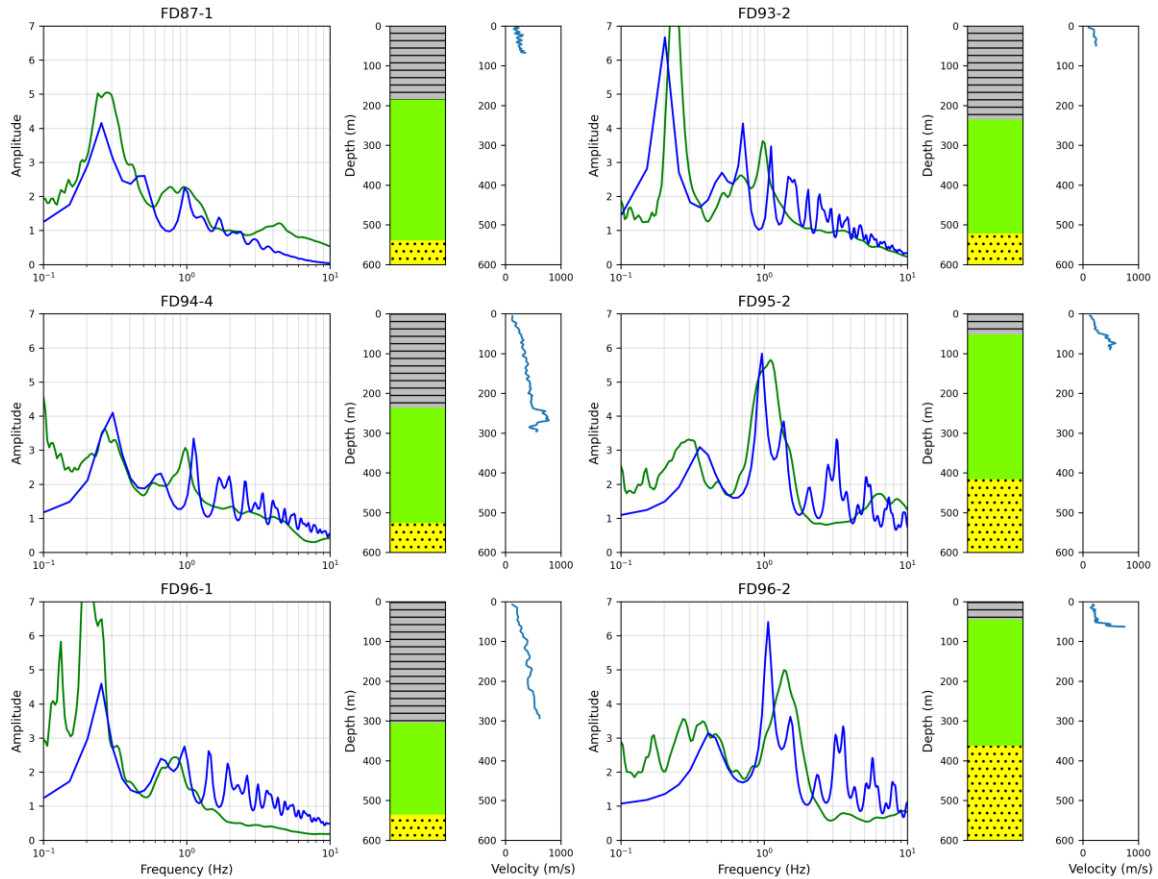


Figure 5-3. Amplification spectrum of empirical mHVSr response (green line) compared to the theoretical SH wave transfer function (blue line) predicted from the 1-D model (soil column and Vs depth profile are shown) for the six sites in the FR delta.

5.3 Clustering mHVSr Curves

Ghofrani and Atkinson (2014) considered grouping sites based on their H/V characteristics and determining standard amplification curves. They proposed that V_{s30} may not be a good proxy for sites with deeper deposits (i.e., large depth to bedrock). For these cases, the peak frequency of the H/V spectrum may be a better site variable as it conveys information from depths > 30 m. They assume that the H/V spectra is an accurate representation of the amplification resulting from near surface sediments. They noticed that H/V spectra grouped by peak frequency have a stable behaviour with very similar shapes. To model the

variation of A_{peakHV} with f_{peakHV} they fit a quadratic equation to the peaks, in this manner, determining region specific ‘standard curves’.

Applying a similar methodology, Braganza *et al.* (2016) developed a suite of amplification functions derived from ground-motion recordings collected at seismograph sites in southwestern Ontario. To determine the amplification function for a site, only the type of surficial geology and the site period are required. Farrugia *et al.* (2018) developed generalized amplification functions for surficial geology types in Alberta. For sand, silt or clay sites, and muskeg sites they fit a Gaussian model to the empirical data, whereas for rock sites they fit a power function to show amplification at higher frequencies. Using these models in conjunction with known surficial geologic conditions and f_{peakHV} at a site, the amplification spectrum for a site can be estimated.

Building on the preliminary investigation in section 5.2.1 which demonstrates correspondence between the measured mHVSR in the Metro Vancouver area and the modelled SH transfer function, a cluster analysis was completed to group together mHVSR responses with similar spectral shape and then interpret what the general subsurface soil conditions (number of layers, type of sediments, etc.) are for each class of measurement. This analysis was completed to define a set of standard mHVSR response types in the Metro Vancouver region, which then has the potential to allow rapid site condition interpretation of future mHVSR measurements through comparison with these existing types. The variation in subsurface ground conditions and thereby the stratigraphic profile at any given location throughout Metro Vancouver is considerable but should reduce to a select set of amplification response types. The number and morphology of amplification response types throughout Metro Vancouver is of significant interest and importance to understanding site effects and achieving microzonation mapping in the region.

Laouami *et al.* (2018) proposed four target mHVSR curves based on four soil classes (SC-A, SC-B, SC-C and SC-D). Through calculation of the correlation coefficient, the similarity between the target mHVSR and the mHVSR from each time window is determined. In this way they can assign site class based on determining which target mHVSR and thereby soil class the current measurement is most like, based on the highest

number of individual time windows that are assigned to a particular class. It is possible to designate mHVSRs for a single site to two site classes based on results of correlation analysis. This application of assigning soil classes based on correlation of newly acquired mHVSR data with target mHVSR curves is similar to the intentions in this Chapter.

Using a database of processed mHVSR results from the Metro Vancouver region, MhVSR response types with similar or repetitive morphology were produced using a clustering algorithm. The procedure was adapted from more conventional time series clustering. Clustering time series data (or in this case, spectral ordinate data) is challenging because each data point is an ordered sequence meaning that,

- The order in which the data occurs is important;
- The sequences may have patterns that are not aligned;
- The sequences may be of variable length.

For ease of implementing the clustering algorithm, the input data vectors are all the same length; 200 log-spaced samples, defining the mHVSR from 0.1 to 50 Hz. K-means clustering was used to form clusters of similar mHVSR response. K-means clustering is one of the simplest machine learning algorithms. K-means clustering functions by identifying K centroids in a dataset and grouping each 'data point' into its nearest cluster, while keeping the centroids as small as possible (Steinley, 2006).

For the present work, the target number of clusters for K-means clustering was 16 and the Euclidean distance was used as a measure of similarity. The number of expected clusters was overestimated so that the resultant clusters could be checked and removed/merged if manual inspection suggested to do so. Of the 16 initial mHVSR clusters identified from 2000 mHVSR sites, 9 were retained for further analysis (Figure 5-4). Through manual inspection of these 9 clusters, 3 unique types of response were identified (Figure 5-5) and will be related to subsurface geological conditions. When the clusters were merged and the representative spectra defined, the x-axis (frequency) of each measurement was normalized by the f_{0HV} of each measurement.

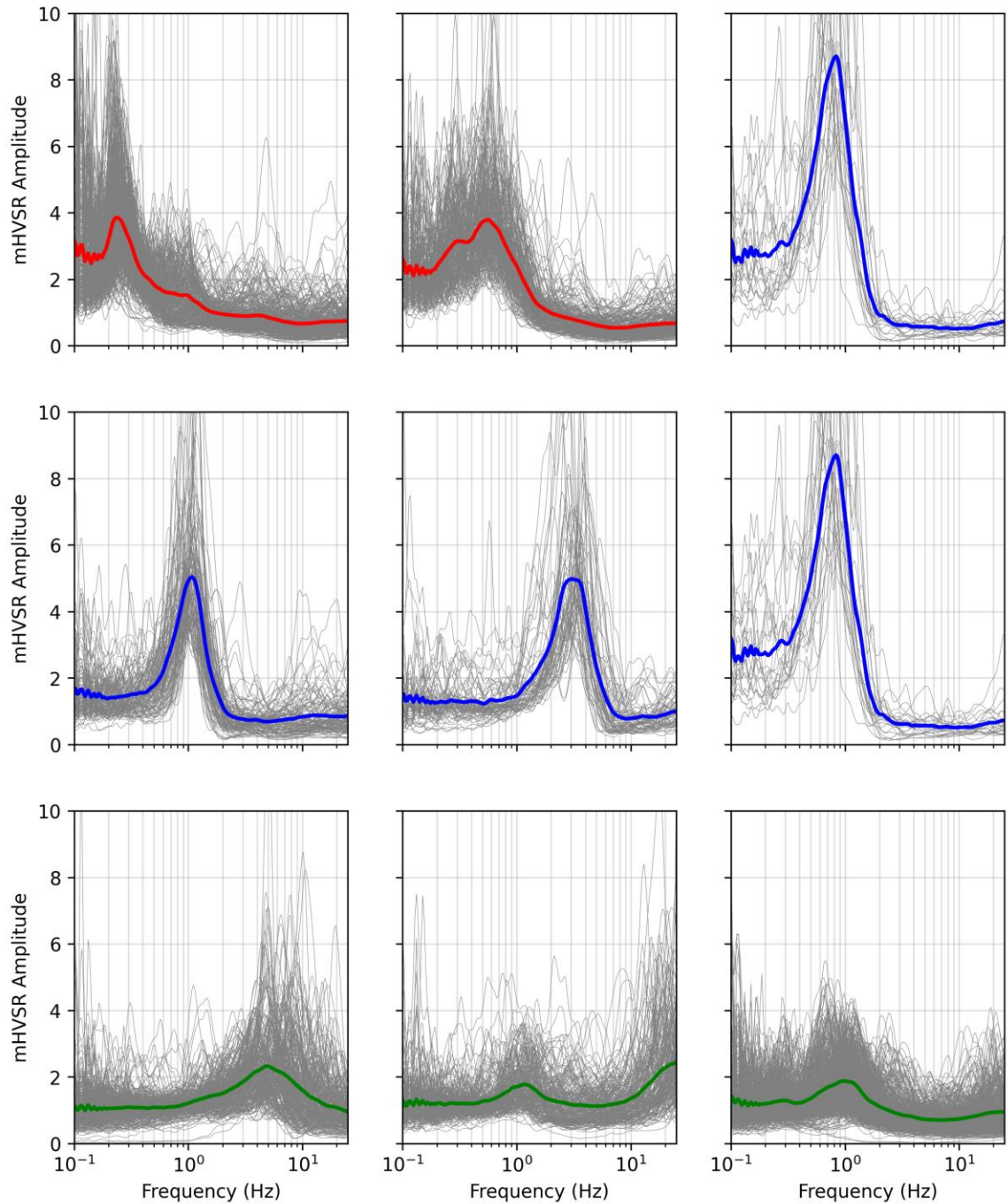


Figure 5-4. Groups of valid clusters identified from K-means clustering of more than 2000 mHVSr curves. Colored according to which representative curve they were assigned to in Figure 5-5.

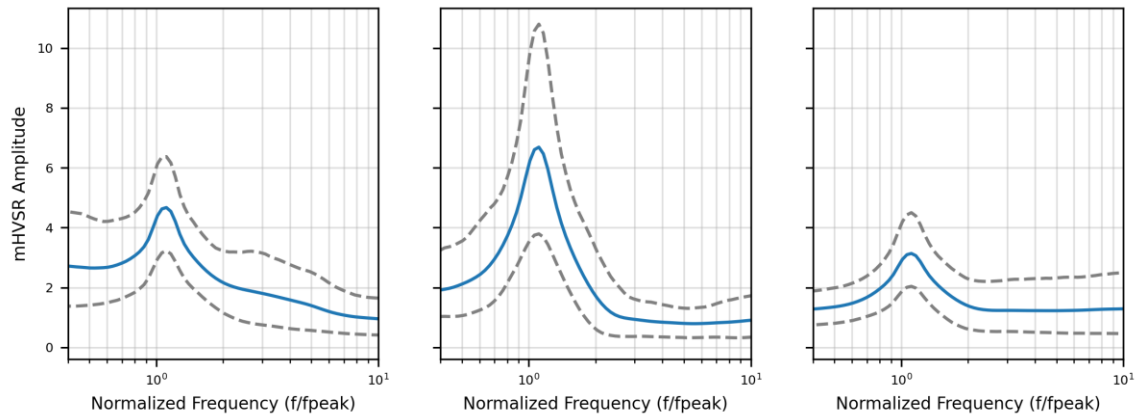


Figure 5-5. Three standard mHVSR response types defined for the Metro Vancouver region through cluster analysis. Solid line is the mean and grey dashed lines are 10th and 90th percentile.

A map showing the spatial distribution of three clustered mHVSR response types within Metro Vancouver is provided in Figure 5-6. A total of 538 mHVSR measurements were used to define cluster I (left - Figure 5-5), 225 mHVSRs were used to define cluster II (middle -Figure 5-5), and 1009 mHVSRs were used to define cluster III (right - Figure 5-5). The low frequency, broad response of response type I relates to very thick till sites (UBC, Surrey) and the deepest parts of the FR delta. This response type includes double peak responses resulting from addition of a second layer in the stratigraphic profile. The relatively high amplitude, clear peak response of response type II correlates with the softest, thinnest sediment deposits. For these sites, the thickness of the sedimentary package overlying bedrock is quite thin, but the impedance contrast at the interface is significant, resulting in the high amplitude of the peaks observed at these sites. These measurements are concentrated at the edges of the FR delta, stream edges, False Creek (fills) and the Burnaby Lake area. The low amplitude, broad peak of response type III correlates with areas that have till deposits. The single-soil layer stratigraphy with a more moderate impedance contrast is typical of Vancouver and at mid-elevations (Capilano/colluvial deposits) along the North Shore, primarily occurring up-slope of shorelines and at the transition zones between shorelines and hills. The surficial geology for response type I is primarily Capilano, Fraser and Salish sediments, type II measurements are concentrated in areas with Capilano, Salish and Vashon Drift/Capilano

sediments. Type III measurements primarily occur in areas where the surficial geology in Vashon Drift/Capilano sediments (Figure 5-7).

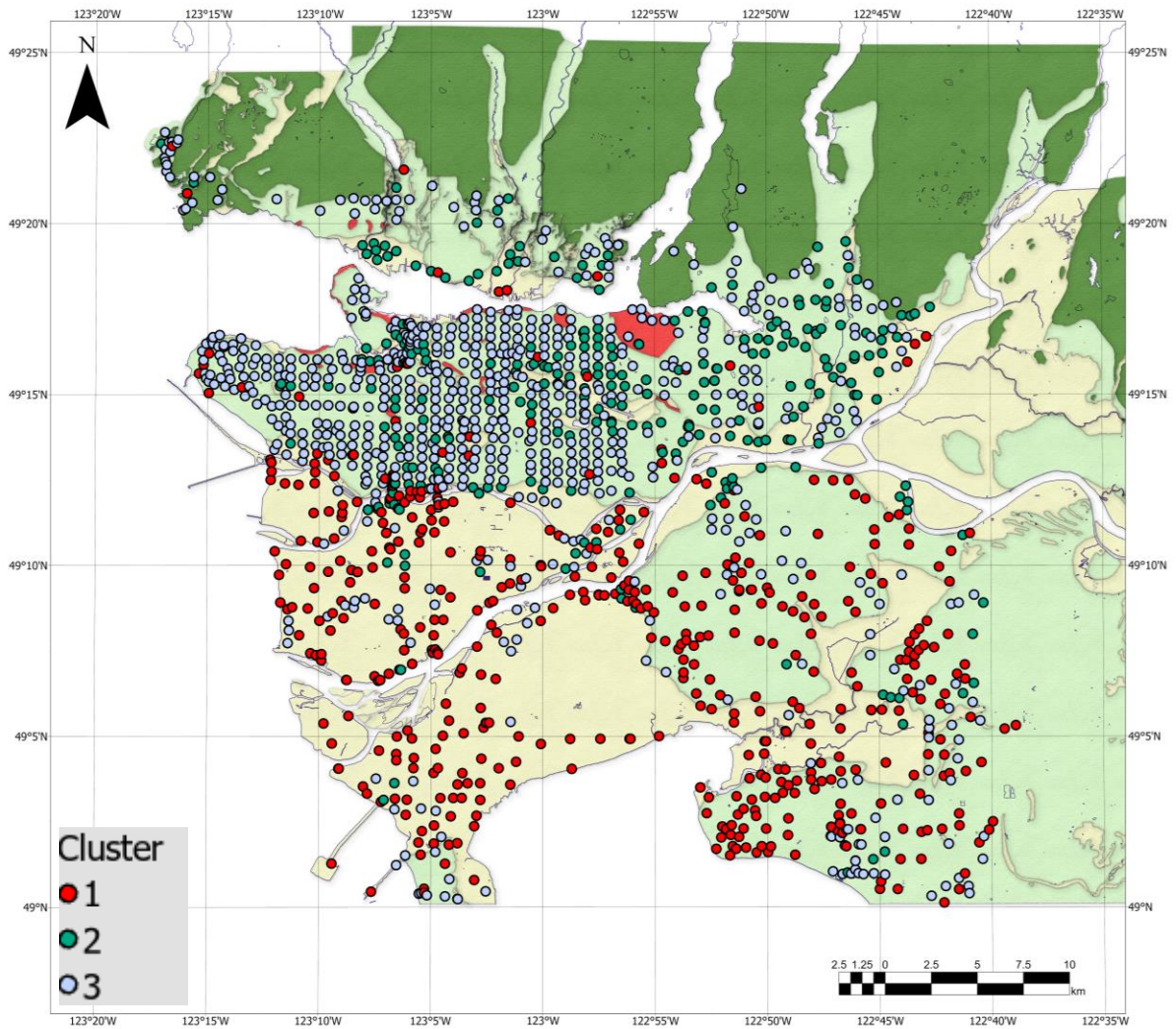


Figure 5-6. Map demonstrating spatial distribution of measurements included in each cluster. Background map is of simplified surficial geology, same as Figure 5-1.

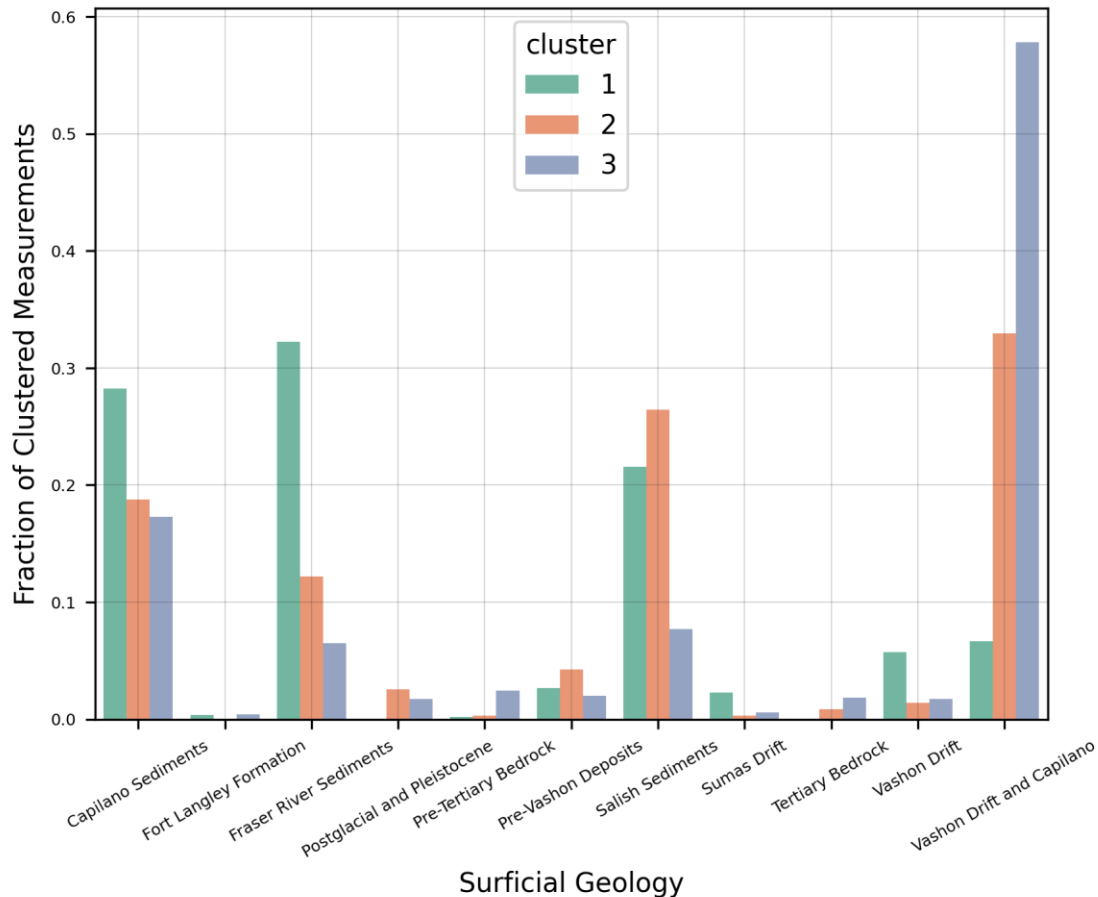


Figure 5-7. Surficial geologic conditions of ~2000 mHVSRs categorized by clustered mHVSR response type.

5.4 Discussion

Interpretation of the mHVSR is severely limited by the ambiguity regarding the composition of the microtremor wavefield. In recent times, many studies have aimed to clarify this, but work remains to be done. Lunedei and Malischewsky (2015) provide a detailed description of the theoretical models developed in the last several decades to explain the mHVSR. There are two main lines of microtremor wavefield interpretation: (1) aims to describe the mHVSR by taking into account the complete wavefield and all seismic phases, and (2) as only Rayleigh wave ellipticity. The microtremor wavefield is almost certainly comprised of all seismic phases and the actual proportion of body waves to surface waves is likely to be dependent on the particular site, time of day, etc. Sanchez-Sesma *et al.* (2001) and Garcia-Jerez (2013) propose that the microtremor wavefield is a

diffuse field containing all types of body (P and S) and surface (Rayleigh and Love) waves. With regards to the second interpretation area, techniques have been developed to extract the Rayleigh wave ellipticity from the total wavefield recorded (HVFTA, Poggi and Fah, 2001; RayDec, Hobiger *et al.*, 2009). Regardless of the uncertainty regarding the wavefield composition, there is a consensus that peaks in the mHVSR are related to resonant frequencies of the soil column, and by extension related to the thickness and stiffness of sediments overlying engineering bedrock. The short investigation into the theoretical site response modelling in the FR delta demonstrated this last point.

Defining new soil/site classification schemes based on mHVSR and/or its peak frequencies is challenging because the number of desired classes is ~ 5 and definitely < 10 , however, the optimal number of classes can be difficult to pre-define for a region or worldwide. For example, current HVSR amplification classification schemes relegate multi-peak response into ‘poorly or not understood’ categories; that which is not yet understood is hidden. In contrast, more than half of the mHVSR database for Metro Vancouver consists of multi-peak response and therefore these current frequency-dependent classification schemes are not applicable. A region-specific amplification classification for Metro Vancouver is necessary.

Using 2000 single-station microtremor data throughout the Metro Vancouver region, mHVSR with similar spectral shapes were therefore grouped together through application of spectral clustering. Analysis of the cluster analysis yielded three distinct types of amplification response observed throughout the Metro Vancouver region. It should be noted that sites with a flat response were omitted from this analysis, however, this would certainly constitute another response type in the region, primarily concentrated in areas with exposed Tertiary or Pre-Tertiary bedrock. The work presented here is preliminary, and further investigations will serve to refine the classification scheme and provide more detailed information about the soil profile configuration (number of layers) as well as material properties, so that an mHVSR response anywhere in the region can be assigned to a typical 1D stratigraphy that may then be used for preliminary ground response analysis and site-specific seismic hazard assessment.

Several previous studies have defined standard (earthquake or microtremor) amplification response types through fitting functional forms to the empirical spectrum. We opted to use a different approach and through definition of clusters of similar mHVSr response, normalizing the independent ordinate of each measurement by the frequency at which its lowest peak occurs at, and then computing the average of these normalized curves, defined the three standard response types of the Metro Vancouver region. The clustering algorithm used to group similar amplification spectra together is the most important aspect of this process, and in the future work can be applied and improved upon that presently implemented. K-means clustering has several limitations including if the initially randomly placed clusters are in bad locations, then K-means won't assign a proper centroid and will provide poor clustering. Not unique to K-means clustering, using the Euclidean distance as a measure of similarity can be misleading. The challenge with clustering the mHVSr responses across the Metro Vancouver region was that our objective was to group together response types that demonstrated similarity in terms of their overall shape, regardless of the frequency at which the peak occurs in the measurement. Dynamic time warping is a method for measuring the similarity between two temporal sequences that is perhaps better suited to clustering of mHVSrs. Using dynamic time warping instead of the Euclidean distance may provide improved response type results. Another possible improvement to our procedure would involve not normalizing the spectral ordinate of each measurement by the frequency of its lowest peak and computing the arithmetic average to define the shape of each cluster, rather Dynamic Time Warping Barycenter Averaging could be used.

5.5 References

- Arai, H., & Tokimatsu, K. (2004). S-wave velocity profiling by inversion of microtremor H/V spectrum. *Bulletin of the Seismological Society of America*, 94(1), 53–63. <https://doi.org/10.1785/0120030028>
- Armstrong, J. E. (1981). *Post-Vashon Wisconsin Glaciation, Fraser Lowland, British Columbia*. <https://doi.org/10.4095/109532>
- Armstrong, J. E. (1984). *Environmental and engineering applications of the Surficial geology of the Fraser Lowland, British Columbia*. <https://doi.org/10.4095/119727>

- Bodin, P., Smith, K., Horton, S., & Hwang, H. (2001). Microtremor observations of deep sediment resonance in metropolitan Memphis, Tennessee. *Engineering Geology*, 62(1–3), 159–168. [https://doi.org/10.1016/S0013-7952\(01\)00058-8](https://doi.org/10.1016/S0013-7952(01)00058-8)
- Boore, D. M., & Joyner, W. B. (1997). Site amplifications for generic rock sites. *Bulletin of the seismological society of America*, 87(2), 327-341.
- Braganza, S., Atkinson, G. M., Ghofrani, H., Hassani, B., Chouinard, L., Rosset, P., Motazedian, D., & Hunter, J. (2016). Modeling site amplification in eastern Canada on a regional scale. *Seismological Research Letters*, 87(4), 1008–1021.
- Cassidy, J. F., & Molnar, S. (2009). *Recent Earthquake Site Response Studies in Canada*. 257–279. https://doi.org/10.1007/978-1-4020-9196-4_19
- Castellaro, S. (2016). The complementarity of H/V and dispersion curves. *Geophysics*, 81(6), T323-T338.
- Clague, J. J. (1994). *Quaternary stratigraphy and history of south-coastal British Columbia*. <https://doi.org/10.4095/203249>
- Clague, J. J., Luternauer, J. L., & Mosher, D. C. (1998). *Geology and natural hazards of the Fraser River Delta, British Columbia*. <https://doi.org/10.4095/210031>
- Faccioli, E. Z. I. O., Vanini, M., & Frassinetti, L. (2002, September). Complex site effects in earthquake ground motion, including topography. In 12th European conference on earthquake engineering (Vol. 844). Barbican Centre London, UK.
- Fäh, D., Kind, F., & Giardini, D. (2001). A theoretical investigation of average HIV ratios. *Geophysical Journal International*, 145(2), 535–549. <https://doi.org/10.1046/J.0956-540X.2001.01406.X>
- Farrugia, J. J., Atkinson, G. M., & Molnar, S. (2018). Validation of 1D earthquake site characterization methods with observed earthquake site amplification in Alberta, Canada. *Bulletin of the Seismological Society of America*, 108(1), 291–308.
- García-Fernández, M., & Jiménez, M. J. (2012). Site characterization in the Vega Baja, SE Spain, using ambient-noise H/V analysis. *Bulletin of Earthquake Engineering* 2012 10:4, 10(4), 1163–1191. <https://doi.org/10.1007/S10518-012-9351-1>
- Goetz, R. P. (2009). *Study of the horizontal-to-vertical spectral ratio (HVSR) method for characterization of deep soils in the Mississippi embayment*. University of Missouri-Columbia.
- Guéguen, P., Chatelain, J. L., Guillier, B., & Yepes, H. (2000). An indication of the soil topmost layer response in Quito (Ecuador) using noise H/V spectral ratio. *Soil Dynamics and Earthquake Engineering*, 19(2), 127–133. [https://doi.org/10.1016/S0267-7261\(99\)00035-4](https://doi.org/10.1016/S0267-7261(99)00035-4)

- Hunter, J. A. (1995). Shear wave velocities of Holocene sediments, Fraser River delta, British Columbia. *Current Research 1995-A Cordillera and Pacific Margin*.
- Hunter, J. A., Burns, R. A., Good, R. L., & Pelletier, C. F. (1998). *A compilation of shear wave velocities and borehole geophysics logs in unconsolidated sediments of the Fraser River Delta, British Columbia*. <https://doi.org/10.4095/209974>
- Hunter, J., Christian, H., Harris, J., R. Britton, J., & L. Luternauer, J. (1999). Mapping shear wave velocity structure beneath the Fraser River delta sediments - Preliminary results. *8th Canadian Conference on Earthquake Engineering*.
- Laouami, N., Hadid, M., & Mezouar, N. (2018). Proposal of an empirical site classification method based on target simulated horizontal over vertical spectral ratio. *Bulletin of Earthquake Engineering*, 16(12), 5843–5874.
- LeBrun, B., Duval, A. M., Bard, P. Y., Monge, O., Bour, M., Vidal, S., & Fabriol, H. (2004). Seismic microzonation: a comparison between geotechnical and seismological approaches in Pointe-à-Pitre (French West Indies). *Bulletin of Earthquake Engineering*, 2(1), 27-50.
- Lermo Samaniego, J., & J Chavez- Garcia, F. (1994). Are microtremors useful in site response evaluation? *Bulletin of the Seismological Society of America*, 84, 1350–1364.
- Lunedei, E., & Albarello, D. (2010). Theoretical HVSR curves from full wavefield modelling of ambient vibrations in a weakly dissipative layered Earth. *Geophysical Journal International*, 181(2), 1093–1108.
- Luternauer, J. L., Barrie, J. v, & Conway, K. W. (1988). *Surficial geology and geohazards on the continental shelf off western Canada*. <https://doi.org/10.4095/122722>
- Luternauer, J. L., & Finn, W. D. L. (1983). Stability of the Fraser River Delta front. *Canadian Geotechnical Journal*, 20(4), 603–616. <https://doi.org/10.1139/t83-070>
- Luternauer, J. L., & Hunter, J. A. (1996). Mapping Pleistocene deposits beneath the Fraser River delta: preliminary geological and geophysical results. *Current Research 1996-E*, 41–48.
- Luternauer, J., Linden, R., Westrheim, S., & Thomson, R. (1986). Sedimentology of amphitrite bank, a commercially exploited groundfish habitat—Southwestern continental shelf, British Columbia, Canada. *Environmental Geology*, 8, 107–121. <https://doi.org/10.1007/BF02509897>
- Macau, A., Benjumea, B., Gabàs, A., Figueras, S., & Vilà, M. (2014). The Effect of Shallow Quaternary Deposits on the Shape of the H/V Spectral Ratio. *Surveys in Geophysics 2014 36:1*, 36(1), 185–208. <https://doi.org/10.1007/S10712-014-9305-Z>

- Malischewsky, P. G., & Scherbaum, F. (2004). Love's formula and H/V-ratio (ellipticity) of Rayleigh waves. *Wave Motion*, 40(1), 57–67.
<https://doi.org/10.1016/J.WAVEMOTI.2003.12.015>
- Nasmith, H. W., Buck, G. F., Karrow, P. R., & White, O. (1998). The engineering geology of the Greater Victoria area. *Urban Geology of Canadian Cities*, 21–38.
- Oubaiche, E. H., Chatelain, J. L., Hellel, M., Wathélet, M., MacHane, D., Bensalem, R., & Bouguern, A. (2016). The Relationship between Ambient Vibration H/V and SH Transfer Function: Some Experimental Results. *Seismological Research Letters*, 87(5), 1112–1119. <https://doi.org/10.1785/0220160113>
- Poggi, V., & Fäh, D. (2010). Estimating Rayleigh wave particle motion from three-component array analysis of ambient vibrations. *Geophysical Journal International*, 180(1), 251–267.
- Rahimi, S., Wood, C. M., & Bernhardt-Barry, M. (2021). The MHVSR technique as a rapid, cost-effective, and noninvasive method for landslide investigation: case studies of Sand Gap and Ozark, AR, USA. *Landslides* 2021 18:8, 18(8), 2705–2720.
<https://doi.org/10.1007/S10346-021-01677-7>
- Rohmer, O., Bertrand, E., Mercerat, E. D., Régnier, J., Pernoud, M., Langlaude, P., & Alvarez, M. (2020). Combining borehole log-stratigraphies and ambient vibration data to build a 3D Model of the Lower Var Valley, Nice (France). *Engineering Geology*, 270, 105588.
<https://doi.org/10.1016/J.ENGCEO.2020.105588>
- Sánchez-Sesma, F. J., Rodríguez, M., Iturrarán-Viveros, U., Luzón, F., Campillo, M., Margerin, L., García-Jerez, A., Suarez, M., Santoyo, M. A., & Rodríguez-Castellanos, A. (2011). A theory for microtremor H/V spectral ratio: application for a layered medium. *Geophysical Journal International*, 186(1), 221–225. <https://doi.org/10.1111/J.1365-246X.2011.05064.X>
- Steidl, J. H., Tumarkin, A. G., & Archuleta, R. J. (1996). What is a reference site?. *Bulletin of the Seismological Society of America*, 86(6), 1733-1748.
- Steinley, D. (2006). K-means clustering: a half-century synthesis. *British Journal of Mathematical and Statistical Psychology*, 59(1), 1-34.
- Teague, D. P., Cox, B. R., & Rathje, E. M. (2018). Measured vs. predicted site response at the Garner Valley Downhole Array considering shear wave velocity uncertainty from borehole and surface wave methods. *Soil Dynamics and Earthquake Engineering*, 113, 339–355. <https://doi.org/10.1016/J.SOILDYN.2018.05.031>
- Tucker, B. E., King, J. L., Hatzfeld, D., & Nersesov, I. L. (1984). Observations of hard-rock site effects. *Bulletin of the Seismological Society of America*, 74(1), 121-136.
- Tran, T., Scherbaum, F., & Malischewsky, P. (2011). On the relationship of peaks and troughs of the ellipticity (H/V) of Rayleigh waves and the transmission response of single layer

over half-space models. *Geophysical Journal International*, 184, 793–800.
<https://doi.org/10.1111/j.1365-246X.2010.04863.x>

van der Baan, M. (2009). The origin of SH-wave resonance frequencies in sedimentary layers. *Geophysical Journal International*, 178(3), 1587–1596.

Wotherspoon, L. M., Munro, J., Bradley, B. A., Wood, C., Thomson, E., Deschenes, M., & Cox, B. R. (2018). *Site Period Characteristics across the Canterbury Region of New Zealand*. 599–607. <https://doi.org/10.1061/9780784481462.058>

Chapter 6

6 Conclusions

The results presented in this thesis aim to demonstrate the utility of the mHVSr method to assist in understanding the variability in site effects observed throughout the Metro Vancouver region. A replicable procedure to process three-component microtremor data to compute the mHVSr at a site was developed in this thesis, particularly in the case of large databases (100's to 1000's). The potential of the mHVSr method for site characterization remains underrealized and continued use will require standardization in mHVSr acquisition and processing so that mHVSr spectra generated over multiple years by different practitioners and/or in different regions around the world can be reliably produced and directly compared.

In Chapter 3 a review of the existing recommendations regarding mHVSr data acquisition and processing was provided. Using a large dataset of mHVSr data from the Metro Vancouver region, these recommendations were revisited and updated as necessary based on parameter sensitivity analyses of selected acquisition and processing choices. In addition, through assimilation of many previously proposed ideas regarding mHVSr processing, a processing workflow was developed specifically to streamline processing of large mHVSr datasets and allow for replicable results regardless of the practitioner. The primary difference of the processing workflow developed here is implementation of frequency-domain clustering algorithm for window selection as opposed to more traditional time-domain window rejection criteria implemented in much of the currently available mHVSr processing software. Future work will aim to implement the developed workflow into an open-source software package which can be used for mHVSr processing (most likely through Python).

In Chapter 4 a comprehensive mHVSr peak-picking methodology was introduced. In Metro Vancouver it is very common to have multiple peaks and as such a peak identification algorithm was developed to consider this and to provide statistics about each peak present in a mHVSr spectrum. In addition, understanding that simply reporting the amplitude and frequency at which a peak occurs does not provide important information

regarding the peak shape which is related to site characterization information (e.g., subsurface geometry, depth and strength of impedance contrasts). The comprehensive peak picking methodology therefore also includes determination of parameters that convey peak shape as well as the parameters of fitting a Gaussian function to the peak, where possible. In this manner, we can effectively communicate both the presence of multiple peaks in measurements and the shape of peaks. From these interpreted peaks, we developed a map of f_{0HV} to demonstrate the variability of the parameter throughout Metro Vancouver.

The ultimate applications of processed mHVSR data include development of a map demonstrating the spatial variability of f_{0HV} (lowest frequency peak) or f_{peak} (peak with highest amplitude) in a region, developing a relationship to relate frequency with impedance contrast depth, calibration of the mHVSR response with existing eHVSR or SSR results, and potentially even inverting the mHVSR spectrum on its own or jointly with surface wave array data to obtain a model of the subsurface soil column. To this end, it is important to retain in a final mHVSR database sufficient information to perform any of these applications. Considering our own experience and working closely from the example of Wang *et al.* (2022), we are preparing a database of mHVSRs for Metro Vancouver for public dissemination based on the database structure we introduced in Chapter 4 which contains both final interpreted results, but also all of the intermediate data to allow a user to accomplish any of the aforementioned objectives. To facilitate ease of testing new mHVSR processing routines, we provide the raw microtremor time series recordings, the Fourier amplitude spectra computed for each defined time window and component of motion, and the calculated spectral ratios for each time window. All data included is provided in a consistent format and each measurement has an associated file with relevant meta-data. This meta-data as well as the interpreted results are also provided summarized in an Excel Spreadsheet. An ArcGIS-platform OpenData repository for the Metro Vancouver microzonation project's databases, including the mHVSR database of this thesis, are planned to be hosted online via Western Libraries' geospatial hub (<https://western-libraries-geospatial-hub-westernu.hub.arcgis.com/>).

In Chapter 5, through application of a K-means clustering algorithm, we defined nine consistent or repetitive mHVSR amplification spectra amongst the 2000 mHVSRs which

are simplified to three main response types that are mapped in comparison to the regional geology in Metro Vancouver. To our knowledge, our map demonstrating the spatial distribution of mHVSr response types is one of the first ever produced or novel. Going forward, further work will develop soil profiles with parameter ranges for each type of mHVSr response using available borehole geotechnical data for calibration. The ultimate or long-term objective is to allow rapid assessment of 1D soil profiles in future from a measured mHVSr response (the lowest cost site predictor variable) for use with ground response analysis and site-specific seismic hazard assessment.

The key outcomes of this work include:

- Updating or verifying the guidelines previously published regarding mHVSr data processing and acquisition (Chapter 3)
- Development of an mHVSr processing methodology suited for batch processing of large mHVSr datasets in a consistent and repeatable manner (Chapter 3)
- Development of a peak picking algorithm that can identify and compute a comprehensive suite of parameters and their statistics of multiple mHVSr peaks, including peak frequency, amplitude, broadness, and also attempt to fit a multi-peak Gaussian curve (Chapter 4)
- Production of both a point map and an interpolated map of f_{0HV} for the Metro Vancouver region (Chapter 4)
- Definition of three standard mHVSr response types for the Metro Vancouver region through clustering of the spectral mHVSr data and creating a map demonstrating the spatial distribution of these response types (Chapter 5)

Overall, our mapping of f_{0HV} and the three mHVSr amplification response types within Metro Vancouver is an improvement in regional amplification hazard mapping, based on a dense grid of *in situ* data that have previously been calibrated as equivalent to linear earthquake site amplification rather than predicted from subsurface stratigraphy (e.g., $f_0 = V_{Save}/4h$) or average material properties (e.g., V_{S30}). Numerical site response and wave

propagation modelling is ongoing by other Metro Vancouver microzonation project personnel to predict amplification due to 2D and 3D effects as well as shaking intensity and thereby degree of soil nonlinearity to implement into final amplification hazard mapping products for Metro Vancouver. The f_{0HV} and three mHVSR amplification response types mapping for Metro Vancouver generated in this thesis are demonstrations of empirically-driven 1D amplification mapping that will not be improved upon in the near future due to: (1) the extreme effort and cost over two decades in acquiring and consistently processing the mHVSR results to date, (2) a greater density of mHVSR data acquisition would only elucidate smaller-scale variations not present in the current data but the overall regional 1D site effect has been established here, and (3) the paucity of earthquake recordings even as seismic networking and instrumentation has grown exponentially (less than a dozen to ~200) over the same two decades.

7 Curriculum Vitae

Name:	Aamna Sirohey
Post-secondary Education and Degrees:	The University of Western Ontario London, Ontario, Canada 2013-2018 B.Sc.
Honours and Awards	Western Scholarship of Excellence 2014-2015 J.P. Bickell Mining Foundation Scholarship 2017-2018 Charles Carmichael Prize in Earth Sciences 2017-2018 Western Gold Medal – Geophysics 2017-2018 J.B. Bancroft Medal & Prize 2017-2018
Related Work Experience	NSERC Undergraduate Summer Research Award The University of Western Ontario May 2016 – August 2016 NSERC Undergraduate Summer Research Award The University of Western Ontario May 2018 – August 2018

Peer-Reviewed Journal Articles

- J. Assaf, S. Molnar, H. El Naggar, A. Sirohey, 2022. Seismic site characterization in Fraser River delta in Metropolitan Vancouver, *Soil Dynamics and Earthquake Engineering*, 161, 107384, <https://doi.org/10.1016/j.soildyn.2022.107384>.
- S. Molnar, A. Sirohey, J. Assaf, S. Castellaro, C. Cornou, B. Cox, B. Guillier, B. Hassani, H. Kawase, S. Matsushima, F.J. Sánchez-Sesma, A. Yong, 2022. A review of the microtremor horizontal-to-vertical spectral ratio (MHVSR) method. *Journal of Seismology*, <https://doi.org/10.1007/s10950-021-10062-9>.
- S. Molnar, J. Assaf, A. Sirohey, S. R. Adhikari, 2020. Overview of local site effects and seismic microzonation mapping in Metropolitan Vancouver, British Columbia, Canada. *Engineering Geology*, 270, 105568, <https://doi.org/10.1016/j.enggeo.2020.105568>.

Peer-Reviewed Conference Papers

J. Assaf, S. Molnar, H. El Naggar, A. Sirohey, 2019. Seismic Site Characterization at Strong Motion Stations in Metro Vancouver, 15th Canadian Conference on Earthquake Engineering, June 17-20 2019, Quebec City, 8 pg.

Technical Reports

J. Assaf, A. Sirohey, H. Ghofrani, S. Molnar, 2022. Compilation and systematic processing of earthquake and microtremor HVSr amplification at Metro Vancouver strong-motion stations, Report MVSMP-22-05, ISSN 2816-6027, 38 p, https://metrovanmicromap.ca/wp-content/uploads/2022/05/MVSMP-22-01_CompilationHVSrAmplificationStrongmotionStations.pdf.

Conference Presentations

A. Sirohey, S. Molnar, 2021. MHVSR 'Big Data' to outline standard procedures for data acquisition, processing, interpretation and presentation, SSA annual meeting, 19-23 April 2021, virtual poster presentation.